GEOTECHNICAL ASPECTS OF LANDFILL DESIGN AND CONSTRUCTION

Xuede Qian
Geotechnical Engineering Specialist
Michigan Department of Environmental Quality

Robert M. Koerner
H. L. Bowman Professor of Civil Engineering, Drexel University
Director, Geosynthetic Research Institute

Donald H. Gray
Professor of Civil and Environmental Engineering
The University of Michigan

PRENTICE HALL
Upper Saddle River, New Jersey 07458

Contents

180

ste

211

FIGURE 2.5 Recommended Procedure for Preparation of a Compaction Test Specimen Using Variable Compactive Energy for Each Trial (USEPA, 1993b)

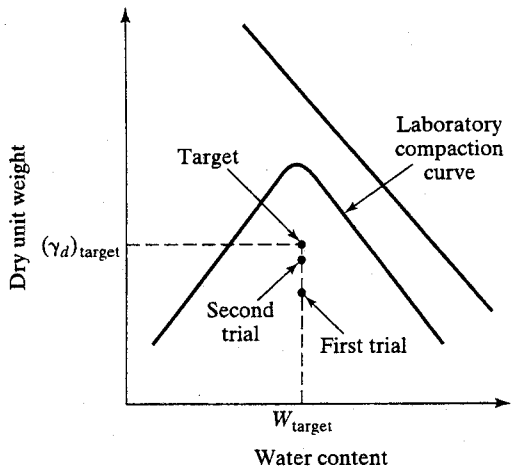

2.7.5 Shear Strength

Strength tests are performed on Shelby tubes of cohesive soils collected from the proposed excavation area of the landfill. Strength tests are conducted to develop shear strength parameters to be used in the sideslope and foundation stability analyses. These shear strength tests consist of unconfined compression tests and consolidated-undrained triaxial tests with pore pressure measurements. The results of the unconfined compression tests are used to develop total-strength parameters for the short-term or undrained condition, which is representative of the conditions immediately after excavation. These tests are performed in accordance with ASTM D2166. The results of the consolidated-undrained triaxial tests with pore pressure measurements are used to develop effective-strength parameters for the long-term or drained condition. These tests are performed in accordance with ASTM D2850.

2.7.6 Compressibility

Consolidation tests should be performed on undisturbed samples. These tests are conducted to obtain compression parameters of the foundation soils for landfill foundation settlement analysis. These analyses are performed in accordance with ASTM D2435.

Recommended minimum values for the frequency of testing are shown in Table 2.3. The tests listed in Table 2.3 are normally performed prior to construction as part of the characterization of the borrow source. However, if time or circumstances do not permit characterization of the borrow source prior to construction, the samples for testing are obtained during excavation or delivery of the soil materials.

The common soil laboratory and field tests used for landfill site investigation, design and construction are listed as follows:

Unified Soil Classification System (ASTM D2487)
AASHTO Soil Classification System (ASTM D3282)

TABLE 2.3 Recommended Minimum Testing Frequencies for Investigation of Borrow Source (USEPA, 1993b)

Parameter	Frequency
Water Content	1 Test per 2,000 m^3 or Each Change in Material Type
Atterberg Limits	1 Test per 5,000 m^3 or Each Change in Material Type
Percentage Fines	1 Test per 5,000 m^3 or Each Change in Material Type
Percentage Gravel	1 Test per 5,000 m^3 or Each Change in Material Type
Compaction Curve	1 Test per 5,000 m^3 or Each Change in Material Type
Hydraulic Conductivity	1 Test per 10,000 m^3 or Each Change in Material Type

Note: 1 $yard^3$ = 0.76 m^3

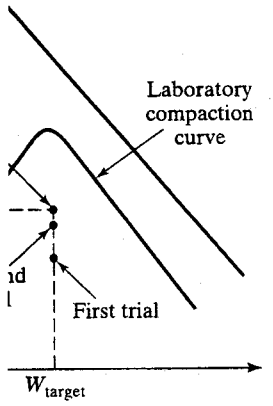

Moisture Content (ASTM D2216)
Specific Gravity (ASTM D854)
Atterberg Limits (Plastic and Liquid Limits) (ASTM D4318)
Sieve Analysis (ASTM D421)
Hydrometer Analysis (ASTM D422)
Shrinkage Limit (ASTM D427)
Standard Proctor Compaction (ASTM D698)
Modified Proctor Compaction (ASTM D1557)
Permeability of Granular Soil (ASTM D2434)
Consolidation (ASTM D2435)
Unconfined Compression (ASTM D2166)
Direct Shear (Granular Soil) (ASTM D3080)
Triaxial Compression (ASTM D2850)
Flexible Wall Permeability Test (ASTM D5084)
Sealed Double-Ring Infiltrometer (ASTM D5093)
Field Density by Nuclear Method (ASTM D3017)
Field Density by Sand Cone (ASTM D1556)
Field Density by Rubber Balloon (ASTM D2167)

PROBLEMS

2.1 What factors must be considered in evaluating potential landfill sites?

2.2 Describe what locational criteria or restrictions must be considered for landfill siting according to the RCRA Subtitle D rules.

2.3 List important geologic and hydrogeologic conditions that must be considered when selecting a landfill site.

2.4 Explain what the 100-year floodplain means.

2.5 What is the definition of a seismic impact zone for landfill design in the RCRA Subtitle D rules?

(iii) Sludges and indigenous materials, and
(iv) Reusable geosynthetics (geotextiles or geomembranes).

Perhaps the greatest uncertainties regarding shear strength determinations of municipal solid waste have to do with fundamental principles; namely, is the linear Mohr-Coulomb theory appropriate for use with the waste? Municipal solid waste can under go large deformations without failing. If so, at what strains are the strength data relevant? Failure is conventionally defined as either sudden rupture with all loss of strength or alternatively by increasing strain without limit at essentially constant stress. At what strain should failure be declared?

Singh and Murphy (1990) reported triaxial testing of municipal solid waste performed on Shelby tube samples. After undergoing strains greater than 30%, the stress continued to increase with no indication of reaching an asymptotic value. During load tests conducted in Monterey Park, California, a surcharged landfill slope underwent large deformations but no failure plane was apparent (Singh and Murphy, 1990). Based on this and other information, Singh and Murphy concluded that a Mohr-Coulomb characterization of the waste strength may be inappropriate and that slope failure (through the waste material) may not be a critical aspect of landfill design. This situation could differ drastically when liquids are involved. Koerner and Soong (2000) present case histories of 10 massive landfill failures. All were associated with liquids either within the waste mass, between liner materials, or in the foundation soils beneath the waste. Failure surfaces were generally partially within the waste mass.

In general, however, landfills tend to involve slippage along interfaces within the liner system or within weak underlying soils. Therefore, while it is necessary to estimate the strength properties of waste when conducting stability analyses, it is more important (Fassett et al., 1994) to evaluate weak interfaces and/or poor foundation materials properly, as well as strain compatibility between dissimilar materials.

6.8 COMPRESSIBILITY OF MUNICIPAL SOLID WASTE

The compressibility of municipal solid waste has been studied for several decades. Early work focussed on the behavior and suitability of landfills for future construction sites. As the practice of sanitary landfilling increased and landfill sites became more scarce the focus shifted to improving the efficiency of waste placement to improve unit waste volume (Fassett et al., 1994). The general findings of earlier research can be summarized as follows:

(i) The majority of the settlement occurred quickly;
(ii) Increased compaction can reduce total settlement; and
(iii) Settlement under loads decreases with age and depth of municipal solid waste (Fassett et al., 1994).

Two main factors affect settlement of municipal solid waste, namely, the initial density of the waste and compaction effort at placement (which affect mechanical compression); and the moisture content, depth, waste composition, pH, and temperature, which affect physico-chemical and biochemical alteration of the waste (Wallis, 1991).

Traditional soil mechanics theories of compressibility have been applied to municipal solid waste. Therefore, the same considerations and parameters have been used. Note, however, that these theories are based on fully saturated soils and not on partially saturated (i.e., $S \ll 100\%$) MSW materials. Settlement is generally considered to consist of three components:

$$\Delta H_{total} = \Delta H_i + \Delta H_c + \Delta H_\alpha \tag{6.11}$$

Where ΔH_{total} = total settlement;
ΔH_i = immediate settlement;
ΔH_c = consolidation settlement; and
ΔH_α = secondary compression, or creep.

Initial settlement of municipal solid waste resulting from increased loads occurs typically within the first three months (Bjarngard and Edgers, 1990). Waste settlement is similar to that of peat soil in which, after rapid immediate and consolidation settlement, additional settlement is accompanied by little or no excess pore pressure buildup and is primarily due to long-term secondary compression (Sowers, 1973). Because the consolidation phase is completed so rapidly, it is generally lumped together with the immediate settlement and called "primary settlement" (Lukas, 1992). However, unlike peat deposits, the secondary compression of municipal solid waste includes an important decomposition component.

The parameters commonly used to estimate the primary settlement of municipal solid waste resulting from an increase in vertical stress include the primary compression index (C_c) and the modified primary compression index (C'_c). These parameters have been defined by Fassett et al. (1994) and are written as

$$C_c = \frac{\Delta e}{\log(\sigma_1/\sigma_0)} \tag{6.12}$$

and

$$C'_c = \frac{\Delta H}{H_0 \cdot \log(\sigma_1/\sigma_0)} = \frac{C_c}{1 + e_0} \tag{6.13}$$

where Δe = change in void ratio;
e_0 = initial void ratio;
σ_0 = initial vertical effective stress;
σ_1 = final vertical effective stress;
H_0 = original thickness of waste layer; and
ΔH = change in thickness of waste layer.

There are several problems with this approach (Edil et al., 1990). First, the initial void ratio (e_0) or initial height of waste (H_0), especially for old landfills, is often not known. Second, the effective stress is a function of MSW unit weight (and level of leachate in the landfill) which is generally not accurately known. Third, the e-log(σ)

relationship is often not linear; therefore, C_c and C'_c vary with the initial stresses within the landfill and as these stresses change with time.

The secondary compression index (C_α) or the modified secondary compression index (C'_α) are used to estimate the settlement that occurs after completion of the primary settlement (Fassett et al., 1994). This usually occurs while the waste is subjected to a constant load. The indexes are

$$C_\alpha = \frac{\Delta e}{\log(t_2/t_1)} \tag{6.14}$$

and

$$C'_\alpha = \frac{\Delta H}{H_0 \cdot \log(t_2/t_1)} = \frac{C_\alpha}{1 + e_0} \tag{6.15}$$

where t_1 = starting time of secondary settlement; and
t_2 = ending time of secondary settlement.

These parameters tend to change during creep deformation and with chemical or biogradation of the waste. The most important cause of secondary settlement is most likely volume reduction due to decomposition of organic matter. This view is not substantiated, however, by field evidence and test results at this time.

In order to measure the compressibility resulting from an increase in load, plate load tests (Landva et al., 1984), pressuremeters (Steinberg and Lucas, 1984), and odometers (Bjarngard and Edgers, 1990; Chen et al., 1977; Landva et al., 1984; Oakley, 1990) have been used in various investigations. To measure the rate of settlement under constant load, surveying methods have been widely used. Techniques include aerial photo comparisons over time (Druschel and Wardwell, 1991), benchmark surveys on the landfill surface (Steinberg and Lucas, 1984; Dodt et al., 1987; Wallis, 1991; Druschel and Wardwell, 1991), and settlement platforms placed below earth embankments constructed on landfills (Sheurs and Khera, 1980). An additional technique utilizes telescoping inclinometers (Siegel et al., 1990; Galante et al., 1991). These devices allow measurements of settlement at various depths under both increases in load and constant load. Frequent readings during landfilling are needed (Fassett et al., 1994) to back-calculate separate values of C_c and C_α.

The high compressibility of waste fill is evident from Figure 6.9, where consolidation results from five locations are plotted (Landva and Clark, 1990). These tests were all done in a 470-mm diameter apparatus. The samples were placed in the container in about 50-mm lifts and lightly compacted. The gradient of the log pressure versus strain is the modified primary compression index (C'_c). The range of C'_c in Figure 6.9 is 0.2 to 0.5. This value is high in comparison with soils, even with organic soils. Keene (1977) installed nine settlement platforms at various elevations of a sanitary landfill to investigate the landfill settlement for five years. The settlement readings indicated that the primary compression was about 3% and occurred rapidly. Primary settlement essentially ended at one-half to one month after completion of filling. Sowers (1973) pointed out that the compression index, C_c, is related to the initial void ratio, e_0, as shown in Figure 6.10. There is a considerable variation in C_c for any value of e. The higher values are for fills containing large amounts of garbage, wood, brush, and tin

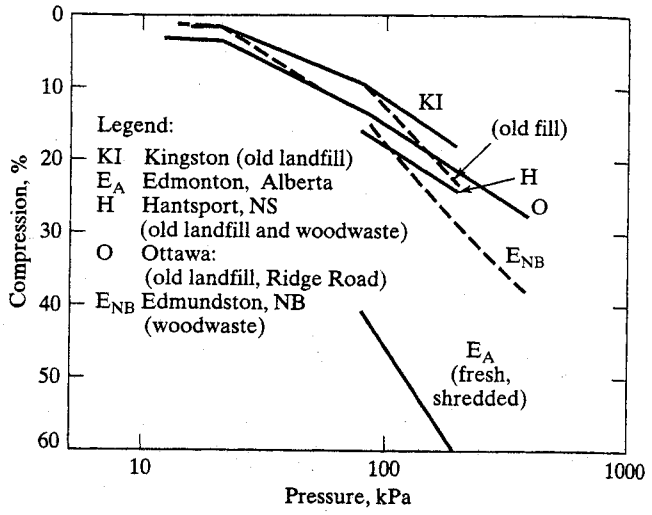

FIGURE 6.9 Compressive Strain versus Log Pressure for Various Landfills in Canada (Landva and Clark, 1990)

KI: $C_C' = 0.17$ ($p = 20 - 200$ kPa) O: $C_C' = 0.21$ ($p = 100 - 400$ kPa)
E_A: $C_C' = 0.35$ ($p = 80 - 200$ kPa) E_{NB}: $C_C' = 0.36$ ($p = 100 - 400$ kPa)
H: $C_C' = 0.22$ ($p = 80 - 200$ kPa)

cans; the lower values are for the less resilient materials. The maximum C_c for peat is about one-third greater than the maximum observed for waste fills.

Landva and Clark (1990) found that the coefficient of secondary consolidation, C_α, (the gradient of the compression versus log time relationship) was in the range 0.2 to 3.0 percent per log cycle time, depending on the type of waste involved. Field testing results using a settlement platform (Keene, 1977) showed that the coefficient of secondary consolidation, C_α, varies between 0.014 and 0.034. Too few tests have been carried out for any firm relationship to be established between the value of C_α and the type of waste, but it does appear that C_α increases with increasing organic content. Sowers (1973) pointed that the coefficient of secondary consolidation, C_α, is also a

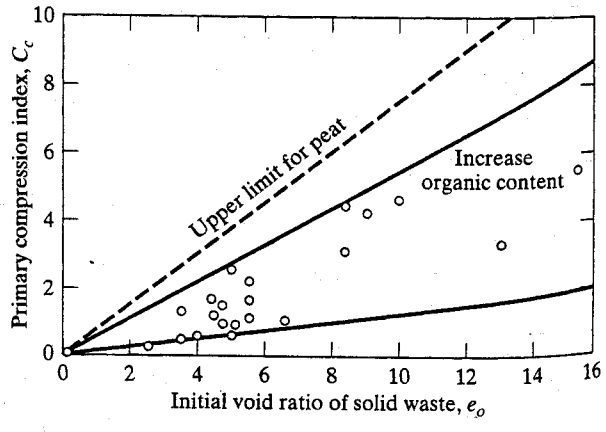

FIGURE 6.10 Compressibility of MSW Landfills (Sowers, 1973)

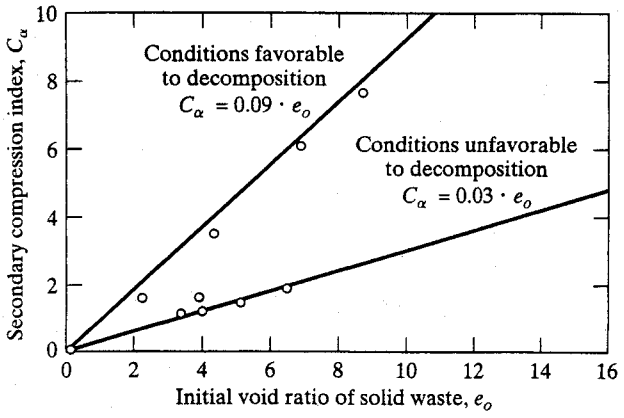

FIGURE 6.11 Secondary Compression of MSW Landfills (Sowers, 1973)

function of the void ratio, as shown in Figure 6.11. For any given void ratio, there is a large range in C_α, related to the potential for physico-chemical and bio-chemical decay. The value is high if the organic content subject to decay is large and the environment is favorable: namely, warm, moist, with fluctuating water table that pumps fresh air into the fill. The value is low for more inert materials and an unfavorable environment. More research and data are necessary before this relationship can be defined more closely.

The most widely reported compressibility parameter is the modified secondary compression index (C'_α). The reported values of C'_α range from 0.001 to 0.59. The lowest value represents the compressibility of a landfill that had been subjected to dynamic compaction. For typical landfills the lower limit of C'_α is generally around 0.01 to 0.03. This compares to 0.005 to 0.02 for common clays (Holtz and Kovacs, 1981). Fasset et al. (1994) observed that the typical upper limit of C'_α appears to be approximately 0.1.

According to Yen and Scanlon (1975), the settlement rate of waste increases with depth, hence larger values of C'_α should be associated with thicker fills. They observed that this effect leveled off at about 90 ft. and suggested that conditions within the landfill at great depths limit the biological activity to anaerobic decomposition, which is much slower than the aerobic decomposition believed to occur in shallower fills.

The values of C_α and C'_α, like C_c and C'_c, are dependent on the values used for e_0 or H_0. The value of C'_α is also dependent on stress level, time, and on how the origin of time is selected. The waste placement or filling period for landfills is often long and should be taken into consideration for settlement rate analyses (Yen and Scanlon, 1975). The zero time selection has a large impact on C'_α particularly during earlier phases of a landfill (Fassett et al., 1994)

An additional problem with determining C'_α is the fact that this parameter is generally not constant. Edgers (1992) presents settlement log-time data from 22 case histories (shown in Figure 6.12). The majority of the curves show a relatively flat slope (i.e. low C'_α values) at small times, but at larger times the slope greatly increases (Figure 6.13). They attributed the higher slopes in the later stages of compression to increasing decomposition, but it may simply be an artifact of the log-time scale. It is

FIGURE 6.12 Landfill Settlement versus Log Time (Bjarnagard and Edgers, 1990)

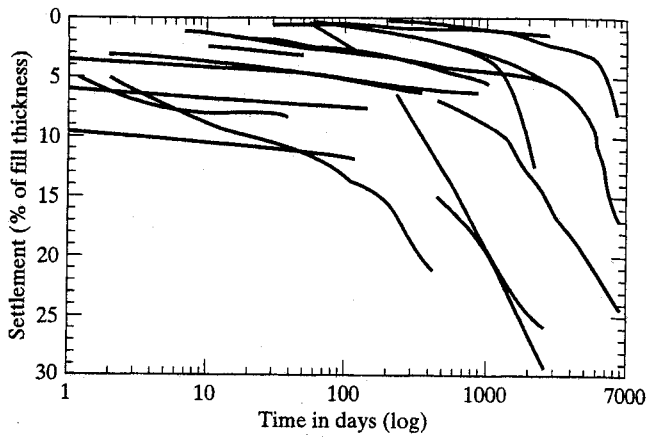

highly likely that decomposition of municipal solid waste will affect its compressibility. Fassett et al. (1994) have concluded that the relative contribution of mechanical compression, thermal effects, and biological decomposition to the total settlement has not been adequately addressed. What is critical to note in Figure 6.12 is that the settlement of MSW landfills can be enormous. Thirty (30) percent of total height settlement has huge implications in cover soil design and related landfill planning. This issue will be revisited in subsequent chapters of the book.

FIGURE 6.13 Idealized Plot of Landfill Settlement versus Log Time (Bjarnagard and Edgers, 1990)

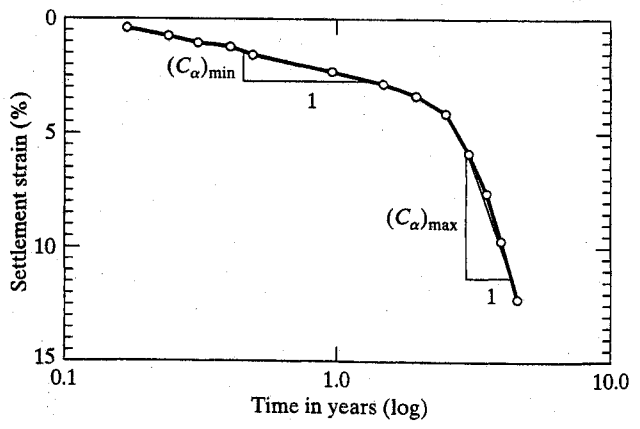

PROBLEMS

6.1 Explain why it is difficult to determine the engineering properties of municipal solid waste.

6.2 Which waste property or parameter is the most useful in landfill design and performance?

6.3 List the factors that influence the unit weight of solid waste.

CHAPTER 12

Landfill Settlement

Settlement is an important concern in the management of municipal solid waste landfills. Landfill settlement continues over an extended period of time, with a final settlement that can approach 30% of the initial fill height as shown in Figure 12.1 from Spikula (1997). From an operator's viewpoint, landfill capacity will increase if most of the settlement occurs during the initial or early filling stages. Accordingly, waste placement or management strategies that maximize the rate/amount of early settlement are desirable from an economic standpoint. On the other hand, a large postclosure settlement is undesirable from a maintenance point of view, since it may lead to surface ponding, development of cracks in soil materials (such as compacted clay liners), tearing of the geomembrane, and damage to the geocomposite drainage layer. In addition, ancillary landfill facilities, such as gas collection and drainage pipes and leachate injection pipes (as in bioreactor landfills), may be damaged as a result of large differential postclosure settlement.

12.1 MECHANISM OF SOLID WASTE SETTLEMENT

The settlement of landfills affects the design of protection systems such as covers, barriers, and drains. Landfill storage capacity, and the cost and feasibility of using the underlying refuse for the support of buildings, pavements, and utilities will also be affected. Excessive settlements may cause ponding and even fracture of covers and

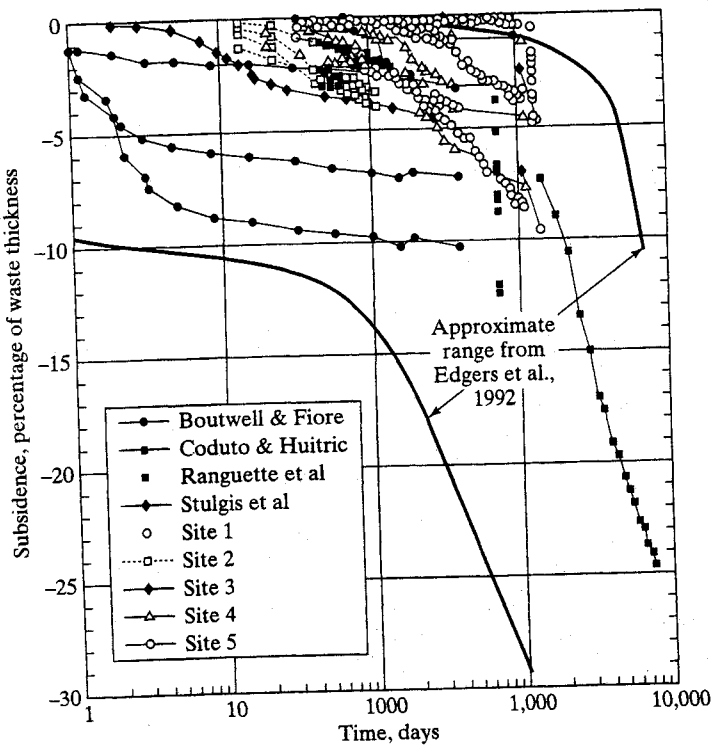

FIGURE 12.1 Landfill Subsidence, New and Previously Published Data (after Spikula, 1997)

drains. The latter outcome may increase the amount of moisture entering the landfill, which, in turn, will produce more leachate.

Settlement of municipal solid waste often begins rapidly as load is placed and continues to occur for long periods thereafter. The mechanisms of refuse settlement are complex, even more so than for soil, because of the extreme heterogeneity of waste fill and the presence of large voids. The main mechanisms involved in waste settlement are the following (Sowers, 1973; Murphy and Gilbert, 1985; Edil et al., 1990; Edgers et al., 1992):

(i) *Mechanical Compression:* Densification, distortion, bending, crushing, and reorientation; similar to consolidation of organic soils. Compression caused by the self-weight of the landfill and imposed loads, occurs in the from of initial, and/or primary consolidation, and/or secondary (delayed) compression.

(ii) *Raveling:* The movement of finer particles into larger voids or cavities within the fill. It is usually difficult to distinguish this mechanism from others.

(iii) *Physical-Chemical Change:* The deterioration and volume loss of waste products by corrosion, oxidation, and combustion.

(iv) *Bio-Chemical Decomposition:* The reduction of waste mass by fermentation and decay, both aerobic and anaerobic processes. This mechanism will be discussed at length in Chapter 15 on bioreactor landfills.

Many factors affect the magnitude of the settlement, and several of them are interrelated: (i) initial density or void ratio of the solid waste, including the types and amount of daily cover used; (ii) waste compaction effort and placement sequence; (iii) content of the decomposable materials in the waste; (iv) overburden pressure and stress history, such as conducting vertical expansion to overfill over an old landfill; (v) leachate level and fluctuations in landfills; (vi) landfill operation methods, such as leachate recirculation can accelerate waste biodegradation; and (vii) environmental factors, such as moisture content, oxygen which reaches the waste, temperature within the landfill, and gases present or generated within the landfill (Edil et al., 1990).

Settlement can occur jointly with evolution and release of large quantities of landfill gas. A detailed geotechnical mechanism or explanation for settlement caused by or associated with gas generation is not available at present. Similarly, the role of moisture equilibration (Noble et al, 1989) and hydrodynamic effects in the compression of partially saturated materials also is not well understood.

It should be noted that waste settles substantially both under its own weight and under the weight of a new load (for example, the placement of new waste over existing waste as in vertical expansions, which will be covered in Chapter 14). The introduction of cover soil to or on top of the waste fill complicates the computation of stresses due to these weights. As a result, two types of waste unit weight can be defined: (i) Actual waste unit weight (weight of refuse per unit volume of refuse); and (ii) Effective waste unit weight (weight of waste plus cover per unit volume of landfill) (Ham, et al., 1978). Waste unit weights are highly erratic, typically varying within a landfill from 32 to 70 lb/ft^3 (5 to 11 kN/m^3). Moisture contents typically range from 10 to 50% on a dry-weight basis (Sowers, 1968, 1973; Ham et al., 1978).

Settlement of waste fill is characteristically irregular. Initially, there is a large settlement within one or two months after completing construction, followed by a substantial amount of secondary compression over an extended period of time (recall Figure 12.1). The magnitude of settlement decreases over time and with increasing depth below the surface of the landfill. Waste settlement under its own weight typically ranges from 5 to 30% of the original thickness, with most of the settlement occurring in the first year or first two years (Edil et al., 1990).

12.2 EFFECT OF DAILY COVER

Complications arising from the settlement behavior of the daily cover itself are normally ignored when estimating landfill settlement. Placement of a daily cover of inorganic soil over waste fill is standard practice at most landfill sites; it is done to keep waste from blowing away, to restrict access to rodents, birds, and insects, and to provide additional overburden pressure. Typical procedures consist of placing 2 feet (0.60 m) of compacted waste and 6 inches (0.15 m) of soil cover. A simple settlement analysis assumes that this intermediate zone of soil material would settle as an independent layer between the much thicker layers of waste, while remaining largely intact and undergoing some consolidation settlement of its own.

This conceptual model of cover soil behavior does not accurately simulate actual behavior. Although the inert soil component initially occupies approximately 20% of

12.4.2 Settlement of Existing Solid Waste

The following equations can be used to calculate the settlement of an existing solid waste landfill caused by vertical expansion (Chapter 14) or other additional extra loading, such as a light structure on a raft foundation.

The *primary settlement* is obtained by

$$\Delta H_c = C_c \cdot \frac{H_o}{1 + e_o} \cdot \log \frac{\sigma_o + \Delta\sigma}{\sigma_o} \tag{12.8}$$

or

$$\Delta H_c = C_c' \cdot H_o \cdot \log \frac{\sigma_o + \Delta\sigma}{\sigma_o} \tag{12.9}$$

where ΔH_c = primary settlement;
e_o = initial void ratio of the waste layer before settlement;
H_o = initial thickness of the waste layer of the existing landfill;
C_c = primary compression index;
C_c' = modified primary compression index, $C_c' = 0.17 \sim 0.36$;
σ_o = existing overburden pressure acting at the mid level of the waste layer;
$\Delta\sigma$ = increment of overburden pressure due to vertical expansion or other extra load.

The *long-term secondary settlement* is given by

$$\Delta H_\alpha = C_\alpha \cdot \frac{H_o}{1 + e_o} \cdot \log \frac{t_2}{t_1} \tag{12.10}$$

or

$$\Delta H_\alpha = C_\alpha' \cdot H_o \cdot \log \frac{t_2}{t_1} \tag{12.11}$$

where ΔH_α = secondary settlement;
e_o = initial void ratio of the waste layer before starting secondary settlement;
H_o = initial thickness of the waste layer before starting secondary settlement;
C_α = secondary compression index;
C_α' = modified secondary compression index, $C_\alpha' = 0.03 \sim 0.1$;
t_1 = starting time of the secondary settlement. It is assumed to be equal to the age of the existing landfill for vertical expansion project;
t_2 = ending time of the secondary settlement.

(e.g., temperature within landfill and oxygen reaching the waste) still is not entirely clear. These functions should be used with caution in engineering practice and should be supported by additional testing data and research.

12.7 ESTIMATION OF LANDFILL FOUNDATION SETTLEMENT

If the landfill is underlain by a soil layer, particularly a thick layer of soft, fine-grained soil, consolidation settlements may be large. In these cases, design analyses should consider settlement of the foundation clay layer. Both primary consolidation and long-term secondary settlement should be considered. Calculations are performed using conventional equations from soil mechanics theory and a time frame at least equal to the active life and postclosure care period of the landfill.

Excessive settlement of an underlying foundation clay layer will affect the performance of a landfill liner and leachate collection system. The purposes of analyzing the settlement of a foundation clay layer and overlying landfill liner and leachate collection/removal system are as follows:

(i) Tensile strain induced in the liner system and leachate collection and removal system must be limited to a minimum allowable tensile strain for the components of these two systems. The compacted clay liner usually has the smallest allowable tensile strain value between 0.1% and 1.0% and an average allowable tensile strain of 0.5%.

(ii) Post-settlement grades of the landfill cell subbase and the leachate collection pipes must be sufficient to maintain leachate performance to prevent grade reversal and leachate ponding in accordance with the rule requirements.

12.7.1 Total Settlement of Landfill Foundation

The total settlement of landfill foundation soil can be divided into three portions: elastic settlement, primary consolidation settlement, and secondary consolidation settlement. The settlement of sandy soils includes only elastic settlement. The settlement of clayey soils includes all three types of settlements. The total settlement of clayey soil is equal to the sum of the elastic settlement and the primary and secondary settlements. Because the permeability of clay is quite low, it takes a long time to complete the whole process of consolidation settlement. The settlement of clayey soil is usually much larger than the settlement of sandy soils.

Because the settlement of sandy soils includes only elastic settlement, the settlement of sand layer can be calculated from the Elastic Settlement equation, which is

$$Z_e = (\Delta\sigma/M_s)H_o \tag{12.20}$$

where Z_e = elastic settlement of soil layer, ft or m;
H_o = initial thickness of soil layer, ft or m;
$\Delta\sigma$ = increment of vertical effective stress, lb/ft^2 or kN/m^2;
M_s = constrained modulus of soil, lb/ft^2 or kN/m^2.

The constrained modulus is given by

$$M_s = \frac{E_s \cdot (1 - v_s)}{(1 + v_s)(1 - 2 \cdot v_s)} \tag{12.21}$$

where M_s = constrained modulus of soil, lb/ft^2 or kN/m^2;
E_s = elastic modulus of soil, see Table 9.5, lb/ft^2 or kN/m^2;
v_s = Poisson's ratio of soil, see Table 9.5.

The *primary consolidation settlement* is given by

$$Z_c = C_r \cdot \frac{H_{oi}}{1 + e_{oi}} \cdot \log \frac{p_c}{\sigma_o} + C_c \cdot \frac{H_o}{1 + e_{oi}} \cdot \log \frac{\sigma_o + \Delta\sigma}{p_c} \tag{12.22}$$

where Z_c = primary consolidation settlement of clay layer, ft or m;
H_o = initial thickness of clay layer, ft or m;
e_{oi} = initial void ratio of clay layer;
C_r = recompression index;
C_c = primary compression index.
σ_o = initial vertical effective stress, lb/ft^2 or kN/m^2;
p_c = preconsolidation pressure, lb/ft^2 or kN/m^2;
$\Delta\sigma$ = increment of vertical effective stress, lb/ft^2 or kN/m^2.

The *secondary compression settlement* is given by

$$Z_\alpha = C_\alpha \cdot \frac{H_{os}}{1 + e_{os}} \cdot \log \frac{t_2}{t_1} \tag{12.23}$$

where Z_α = long-term secondary compression settlement, ft or m;
e_{os} = initial void ratio of clay layer before starting secondary consolidation settlement;
C_α = secondary consolidation compression index;
H_{os} = initial thickness of clay layer before starting secondary consolidation settlement, ft or m;
t_1 = starting time of the time period for which long-term settlement of the layer is desired;
t_2 = ending time of the time period for which long-term settlement of the layer is desired.

The total settlement of clay layer includes three portions: elastic settlement, primary consolidation settlement, and secondary consolidation settlement. These three types of settlement for clayey soil layers can be calculated from Equations 12.20, 12.22, and 12.23, respectively. The total settlement of clayey soil at point *i* can be determined from the equation

$$Z_i = (Z_e)_i + (Z_c)_i + (Z_\alpha)_i \tag{12.24}$$

where Z_i = total settlement of points *i*;
$(Z_e)_i$ = elastic settlement of point *i*;
$(Z_c)_i$ = primary consolidation settlement of point *i*;
$(Z_\alpha)_i$ = secondary consolidation settlement of point *i*.

The preceding settlement equations (Equations 12.20 through 12.24) provide a framework and means to account for different types of settlement. Not all foundations on soil settle exactly in the manner previously described. In addition to soil type, the amount of settlement in each category also depends on the degree of saturation, load duration, and load distribution.

The settlement calculations should be performed at discrete points along several selected settlement lines, such as Lines 1, 2, 3, and 4 for a municipal solid waste landfill as shown in Figure 12.16. The following principles should guide the arrangement of the settlement lines for landfill foundation settlement calculations:

(i) Some settlement lines should be set along the leachate collection pipelines (usually 1% slope) to check the grade changes and tensile strains of the leachate collection pipes due to settlement.

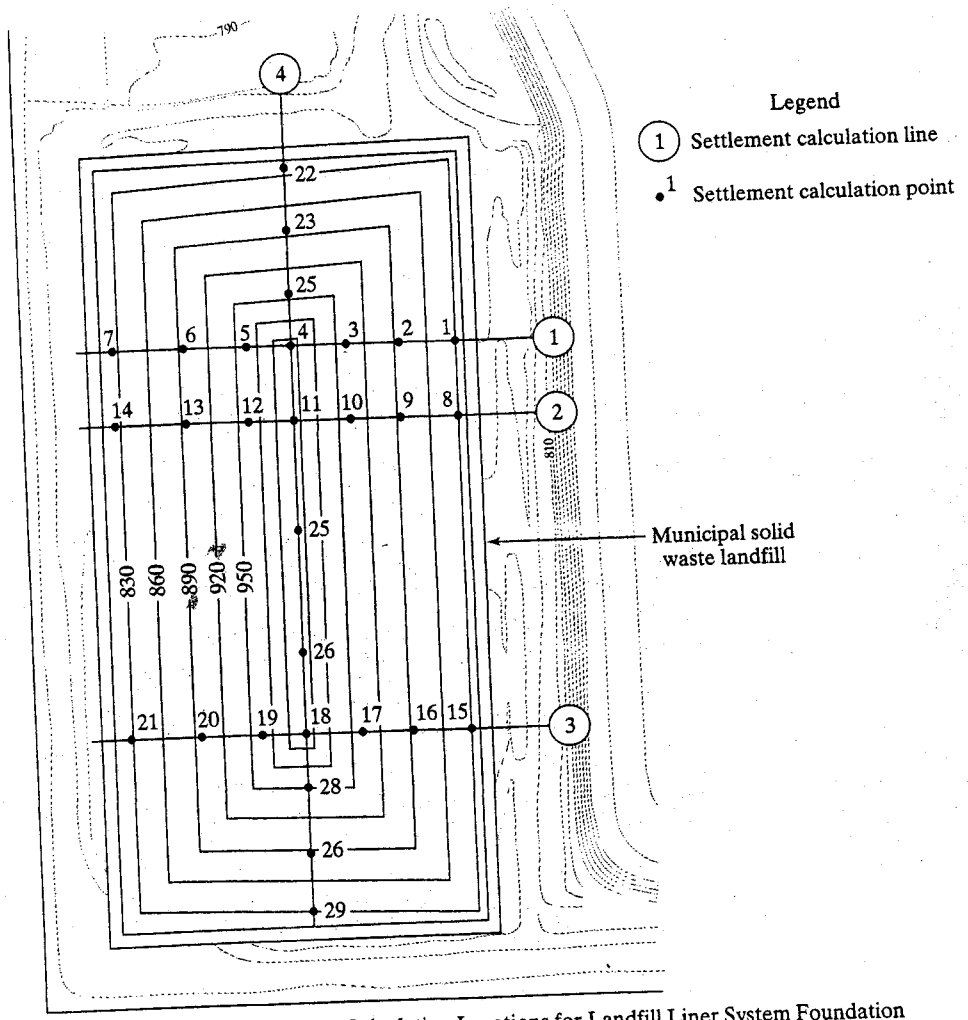

FIGURE 12.16 Settlement Calculation Locations for Landfill Liner System Foundation

(ii) Some settlement lines should be set perpendicular to the leachate collection pipes (i.e., along the direction of leachate flow in the leachate drainage layer—usually 2% slope), to check the slope change of leachate drainage layer.

(iii) Settlement lines are usually set locations where there are the large changes of overburden pressures, which may cause large differential settlements of the subgrade.

At each settlement point shown in Figure 12.16 (i.e., Point 1 to Point 29), the thickness of the various soil units at each point and the thickness of the waste to be placed (i.e., overburden pressure) can be estimated from the engineering plans or cross-sections for the specific projects. The value of the total settlement at each point depends on both the engineering properties of soils and the load due to the waste fill.

12.7.2 Differential Settlement of Landfill Foundation

The differential settlements, tensile strains of liner system materials and leachate collection pipes, and changes of final grades between adjacent settlement points after settlement can be evaluated from the calculated values of the total settlements at various settlement points along each settlement line ranged on the landfill subgrade.

The differential settlement between adjacent points can be calculated using the equation

$$\Delta Z_{i,i+1} = Z_{i+1} - Z_i \tag{12.25}$$

where $\Delta Z_{i,i+1}$ = differential settlement between points i and $i + 1$;
Z_i = total settlement of point i;
Z_{i+1} = total settlement of point $i + 1$.

The final slope angle between adjacent points after settlement can be calculated using the equation

$$\tan\beta_{Fnl} = \frac{X_{i,i+1} \cdot \tan\beta_{Int} - \Delta Z_{i,i+1}}{X_{i,i+1}} \tag{12.26}$$

where $X_{i,i+1}$ = horizontal distance between points i and $i + 1$;
$\Delta Z_{i,i+1}$ = differential settlement between points i and $i + 1$;
β_{Int} = initial slope angle between points i and $i + 1$;
β_{Fnl} = final slope angle between points i and $i + 1$ after settlement.

The landfill subgrade changes along each settlement line due to different settlement can be calculated from the Equation 12.26. Figure 12.17 presents the slope changes due to differential settlement along a settlement line. The differential settlement will result in grade reversal between points 3 and 4 as shown in Figure 12.17. As a result, leachate will pond on the liner at this area.

The tensile strains of a liner system and a leachate collection system resulting from the settlements can be estimated using the equation

$$\varepsilon_{i,i+1} = \frac{(L_{i,i+1})_{Fnl} - (L_{i,i+1})_{Int}}{(L_{i,i+1})_{Int}} \times 100\% \tag{12.27}$$

where $\varepsilon_{i,i+1}$ = tensile strain in liner system between points i and $i + 1$;

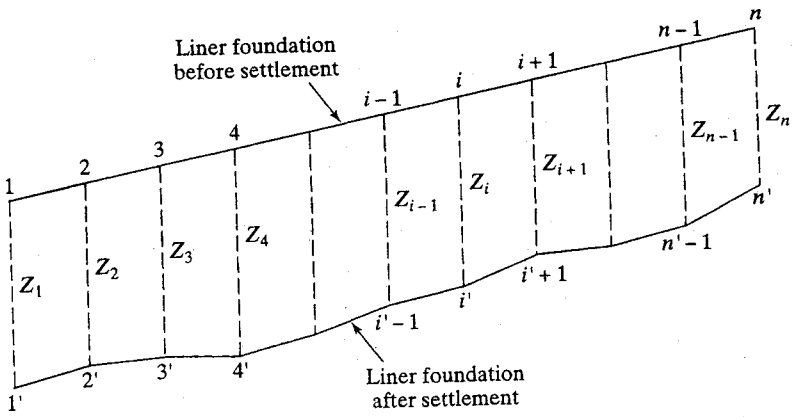

FIGURE 12.17 Subgrade Changes along a Settlement Line due to Differential Settlement

$(L_{i,i+1})_{Int}$ = distance between points i and $i + 1$ in their initial positions;
$(L_{i,i+1})_{Fnl}$ = distance between points i and $i + 1$ in their post-settlement positions.

The distance between points i and $i + 1$ in their initial positions can be calculated using the equation

$$(L_{i,i+1})_{Int} = [(X_{i,i+1})^2 + (X_{i,i+1} \cdot \tan\beta_{Int})^2]^{1/2} \quad (12.28)$$

The distance between points i and $i + 1$ in their post-settlement positions can be calculated using the equation

$$(L_{i,i+1})_{Fnl} = [(X_{i,i+1})^2 + (X_{i,i+1} \cdot \tan\beta_{Int} - \Delta Z_{i,i+1})^2]^{1/2} \quad (12.29)$$

The maximum acceptable tensile strains (i.e., the elongations at yield) of various liner system and leachate collection system components must be obtained from material specific laboratory testing.

PROBLEMS

12.1 What benefit does a landfill operation gain from some settlement in the landfill waste?

12.2 Describe the impact of landfill settlement on landfill design and performance.

12.3 What are the main mechanisms of solid waste settlement?

12.4 List the main factors that influence the amount of landfill settlement.

12.5 What are the main differences of the settlement of solid waste compared with the settlement of clay?

12.6 What are the main advantages and disadvantages of the calculation method for landfill settlement described in Section 12.4?

CHAPTER 13

Landfill Stability Analysis

Modern solid waste landfills serve a variety of functions, including maximization of waste storage per unit area, isolation of waste from the surrounding environment, and conversion opportunities to useable land areas after closure. Until recently, attention related to the design, construction, filling, and post-closure monitoring and maintenance of new landfills has focused mainly on the prevention of unacceptable levels of leakage in the surrounding groundwater. Closure plans for old landfills have likewise centered on similar concerns of gas emissions that are fully warranted. However,

stability is an issue that has sometimes been overlooked. Several huge failures along liner slopes—through landfill foundations and within the waste mass itself—have occurred.

Along lined slopes, two stability situations can be readily identified: (i) the leachate collection layer along the base liner before waste is placed, and (ii) the final cover system above the waste. While instability of these relatively thin layers can be classified as failures, their impact is usually localized and repairs can sometimes be made at a reasonable cost. They are often referred to as *veneer* failures.

Foundation failures beneath the waste and failures of the waste mass itself are in completely different categories in that implications are generally severe. For example, the 1988 failure of 490,000 m^3 of hazardous waste was very significant due to its repair cost and legal implications, which required a thorough post-failure analysis (Mitchell et al., 1990; Seed et al. 1990; Byrne et al. 1992). This failure was very significant in that it stimulated (i) the introduction of textured geomembranes, (ii) consideration of post-peak soil shear strengths, and (iii) concern over low shear strengths of compacted clay liners placed beneath geomembranes. In addition, waste placement and closure plans for landfills on very soft foundations can be seriously affected by the potential for stability failures.

Consequently, the mass stability of landfills is now a major concern in their design, construction, filling, and closure. The situation is further heightened when bioreactor landfills (with large amounts of liquids) are being considered. (See Chapter 15.) This chapter includes a discussion of potential failure mechanisms, evaluation of relevant material properties, description of stability methods, factor of safety calculations, and description of a number of case histories involving landfill failures.

13.1 TYPES OF LANDFILL FAILURES

Landfills can fail in several ways—during cell excavation, during liner system construction, during waste filling, and after landfill closure. An important feature in the identification and assessment of potential failure mode is the fact that both covers and liners for modern landfills are typically multi-layer composites composed of both soil and geosynthetic materials. A schematic diagram of a typical double composite liner system used for a municipal solid waste landfill was shown in Figure 1.10. The liner system shown in Figure 1.10 contains several interfaces whose resistance against interface shear stresses may be low, and thus act as possible failure surfaces. Additionally, all classical geotechnical failure modes are possible depending upon site-specific conditions (usually involving saturated fine-grained soils) and the placement and geometry of the waste mass. Potential failure modes are summarized schematically in Figure 13.1. A brief description of each situation follows.

13.1.1 Sliding Failure of Leachate Collection System

As seen in Figure 13.1(a), the leachate collection system can slide on the underlying liner system if the slope is too steep or too long. This type of veneer failure has often occurred during heavy rains. It is remedied by pushing the sand or gravel back onto the lined slope. However, if the failure surface is within the liner system, the

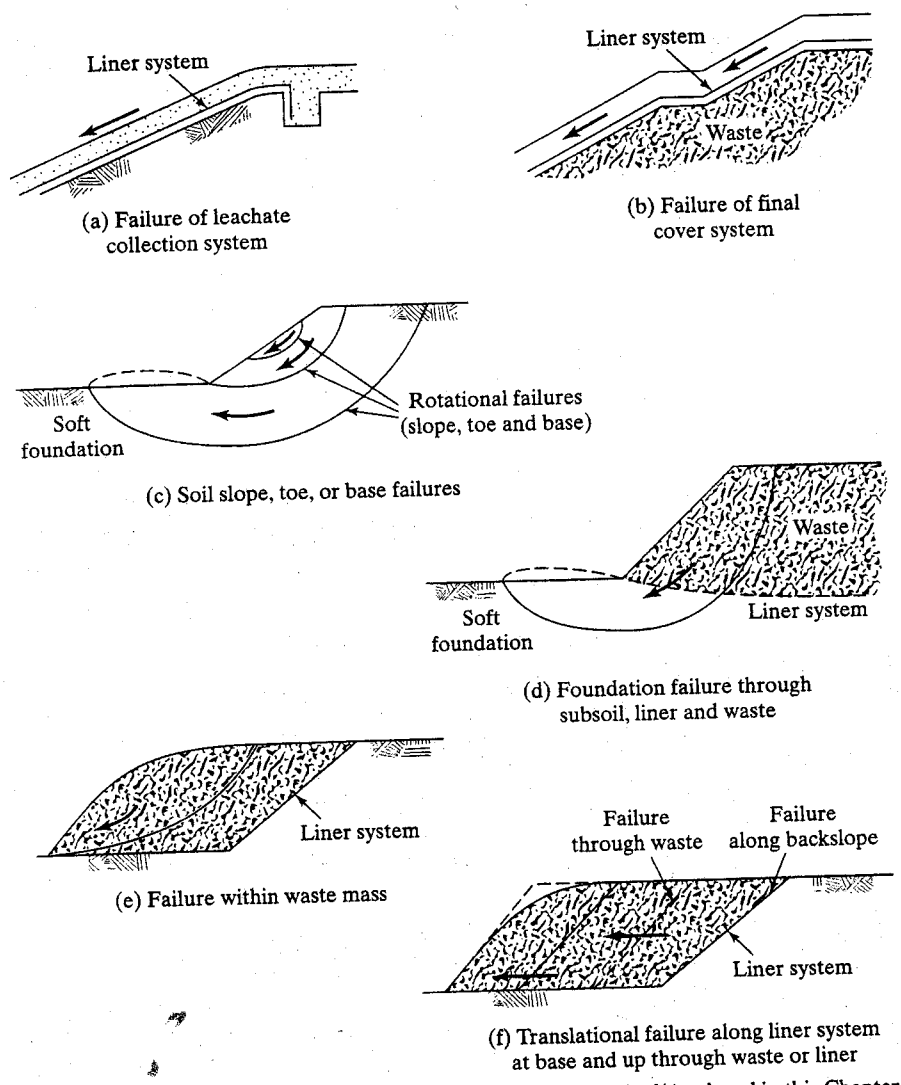

(a) Failure of leachate collection system

(b) Failure of final cover system

(c) Soil slope, toe, or base failures

(d) Foundation failure through subsoil, liner and waste

(e) Failure within waste mass

(f) Translational failure along liner system at base and up through waste or liner

FIGURE 13.1 Various Types of Landfill Failures to be Described/Analyzed in this Chapter

reconstruction will require more effort and cost. Leachate collection soil sliding above or within the liner system is not an uncommon situation.

13.1.2 Sliding Failure of Final Cover System

As seen in Figure 13.1(b), the final cover system (topsoil and protection soil) can slide on the liner system if the slope is too steep or too long. This type of veneer failure often occurs during a heavy rain, and should also be investigated for seismic stability

depending on site-specific conditions. If only soil is displaced, the remedy is to replace the soil. However, the question of long-term stability remains. If the failure surface is within the liner system, the implications are more severe. Cover soil failures of this type above the waste mass are not uncommon.

13.1.3 Rotational Failure of Sidewall Slope or Base

As seen in Figure 13.1(c), the soil mass behind the waste repository or beneath the site could be unstable and fail. Failure is usually rotational, emerging along the slope, at the toe, or within the foundation. This is completely a geotechnical problem (i.e., geosynthetics are not included) and applies to steep side slopes and/or soft foundation soils. It is obviously site specific and does not involve liner systems or waste properties. Nevertheless, such situations should be investigated.

13.1.4 Rotational Foundation Failure Through Waste, Liner, and Subsoil

As seen in Figure 13.1(d), a rotational failure can be initiated in a soft foundation soil that can propagate up through the waste mass. If a liner system is present, it offers only negligible resistance and should be discounted in the analysis. Such failures have occurred (in both unlined and lined sites) and a few have been massive (e.g., up to 500,000 m^3).

13.1.5 Rotational Failure within the Waste Mass

As seen in Figure 13.1(e), failure can occur within the waste mass, completely independent of the liner system. It is handled exactly as the geotechnical failures illustrated in Figure 13.1(c), except that the material is solid waste (municipal or hazardous) instead of soil. Such failures are prompted by steep waste slopes, high liquid content, and lack of placement (operations) control.

13.1.6 Translational Failure by Movement along the Liner System

As seen in Figure 13.1(f), a lateral translational failure can occur with the solid waste sliding above, within, or beneath the liner system at the base of the waste mass. The extension of the failure plane back from the toe can propagate up through the waste, or continue in the liner system along the back slope. Such failures have occurred at both clay-lined sites and at geosynthetically-lined sites. They have resulted in the largest failures to date, two of which involved over 1,000,000 m^3 of waste.

13.2 FACTORS INFLUENCING LANDFILL STABILITY

The stability of a landfill is influenced by many variables and considerations in addition to those present in conventional geotechnical analyses. A landfill is a complex

system with multiple locations and interfaces, which constitute possible loci for failure. The factors influencing landfill stability can be summarized as follows:

(i) Interface shear strengths between various geosynthetic materials;
(ii) Interface shear strengths between geosynthetics and soil materials;
(iii) Internal shear strengths of compacted clay liners (CCLs);
(iv) Internal shear strength of solid waste;
(v) Internal shear strength of subbase and side slope soils;
(vi) Slope and height of excavated side slopes;
(vii) Waste filling slope and height;
(viii) Landfill subbase slopes;
(ix) Normal stresses;
(x) Pore water pressures acting on base liner;
(xi) Subbase geological profiles;
(xii) Groundwater level;
(xiii) Local site hydrology;
(xiv) Freeze-thaw conditions;
(xv) Construction placement and operations equipment; and
(xvi) Dynamic and/or seismic stresses.

13.3 SELECTION OF APPROPRIATE PROPERTIES

The three types of materials usually encountered in failures of the types addressed in this chapter are geosynthetics, solid wastes, and natural soils. Each will be addressed. However, failures sometimes happen in materials other than the above—for example, one failure occurred within a layer of leachate-saturated wood bark chips. Thus, the situation is ever-evolving and the lessons learned from these unfortunate incidences are important for future projects and their respective designs.

13.3.1 Geosynthetic Materials Properties

Within a multilayer liner system, there are numerous materials of concern with regard to low interface shear strengths. The following lists some of them, along with the current method of lessening the concern:

(i) Low-friction, smooth-geomembrane surfaces, the shear strength of which is greatly enhanced by *texturing*. Recall Section 4.2.4.
(ii) Geotextile-to-geonet surfaces; the shear strength concern of this material is essentially eliminated by thermal bonding in the factory.
(iii) Bentonite containing GCLs; the shear strength of this material is enhanced by needle punching, stitch bonding, or encasement between two geomembranes.
(iv) Bentonite extruding from GCLs; the shear susceptibility of this material is avoided by using nonwoven geotextiles on both surfaces of the GCL.
(v) Geomembrane-to-compacted clay liners; the shear strength of this material is lessened by proper moisture content control when placing the compacted clay.

For all of the listed interfaces, and others as well, the project-specific materials evaluated under site-specific conditions are necessary. By project-specific materials, we mean replicates of the candidate geosynthetics to be used at the site, as well as the associated soils at their targeted density and moisture conditions. By site-specific conditions, we mean normal stresses, strain rates, peak or residual shear strengths, and temperature extremes (high and/or low). Moisture content is also important and anticipated conditions (often saturated) are necessary. Water is usually used, although in some cases, site-specific leachates are required. Note that it is completely inappropriate to use values of interface shear strengths from the literature for final design.

The test for the assessment of shear strength of interfaces involving geosynthetics is the direct shear test that has been utilized in geotechnical engineering for many years. The procedure to follow is ASTM D5321, and a special adaptation when GCLs are involved, namely, ASTM D6243.

In conducting a direct shear test on a specific interface, one typically performs three replicate tests with the only variable being different values of normal stress. The middle value is usually targeted to the anticipated site-specific condition, with a lower and higher value of normal stress covering the range of possible values. The results of these three tests yield a set of shear displacement versus shear stress curves. (See Figure 13.2(a).) From each curve, a peak shear strength (τ_p) and a residual shear strength (τ_r) are obtained. As a next step, these shear-strength values, together with their respective normal stress values, are plotted on Mohr-Coulomb stress space to obtain the shear-strength parameters of friction and adhesion. (See Figure 13.2(b).)

The points are then connected (usually with a straight line), and the two fundamental shear-strength parameters are obtained. These shear-strength parameters are as follows:

δ = the angle of shearing resistance, peak and/or residual, of the two opposing surfaces (often called the interface friction angle); and

c_a = the adhesion of the two opposing surfaces, peak and/or residual (the compliment of cohesion when testing fine-grained soils against one another).

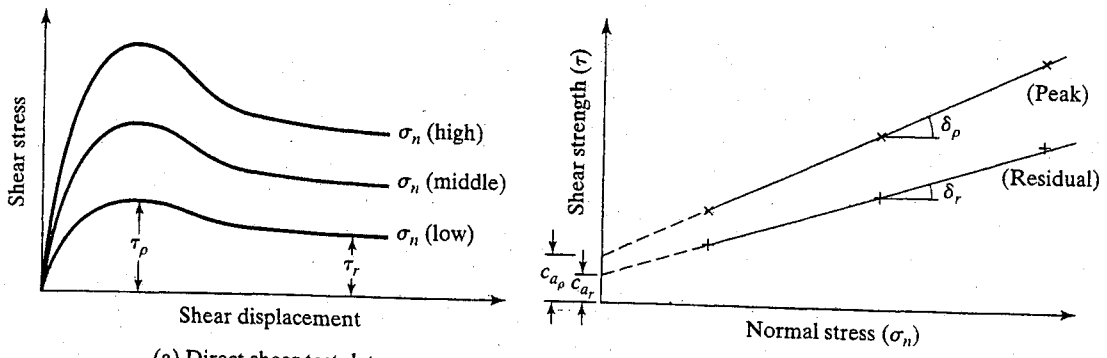

(a) Direct shear test data (b) Mohr-Coulomb stress space

FIGURE 13.2 Direct Shear Test Results and Method of Analysis to Obtain Shear Strength Parameters

Each set of parameters constitutes the equation of a straight line that is the Mohr-Coulomb failure criterion common to geotechnical engineering. The concept is readily adaptable to geosynthetic materials in the following forms:

$$\tau_p = c_{ap} + \sigma_n \cdot \tan\delta_p \tag{13.1}$$

$$\tau_r = c_{ar} + \sigma_n \cdot \tan\delta_r \tag{13.2}$$

The upper limit of δ when soil is involved as one of the interfaces is ϕ, the angle of shearing resistance of the soil component. The upper limit of the c_a-value is c, the cohesion of the soil component. In the slope stability analyses to follow, the c_a term will be included for the sake of completeness, but then it will be neglected (as being a conservative assumption) in the design graphs and numeric examples. To utilize an adhesion value, there must be a clear physical justification for use of such values when geosynthetics are involved. Only unique situations such as textured geomembranes with physical interlocking of soils having cohesion or the needle-punched fibers of a GCL are valid reasons for including such a term.

Note that residual strengths are always equal to, or lower than, peak strengths. The amount of difference is very dependent on the material and no general guidelines can be given. Clearly, material-specific and site-specific direct shear tests must be performed to determine the appropriate values. Further, each direct shear test must be conducted to a relatively large displacement to determine the residual (or, at least, large displacement) behavior (see Stark and Poeppel, 1994). The decision as to the use of peak, large displacement, or residual strengths in the subsequent analysis is a very subjective one. It is both a materials-specific and site-specific issue that is left up to the designer and/or regulator. Even further, the combination of use of peak values at the crest of a slope, and large displacement or residual values at the toe may be justified. As such, the analyses to follow will use an interface δ-value with no subscript, thereby concentrating on the computational procedures, rather than this particular detail. However, the importance of appropriate and accurate δ-values to be used in the analysis cannot be stressed enough.

Due to the manufactured structure of many geosynthetics, the size of the recommended shear box is quite large. It must be at least 300 mm by 300 mm unless it can be shown that data generated by a smaller device contains no scale or edge effects—that is, that no bias exists when using a smaller shear box. The implications of such a large shear box should not be taken lightly. The following issues should receive particular attention:

(i) Unless it can be justified otherwise, the interface will usually be tested in a saturated state. Thus, complete and uniform saturation over the entire specimen area must be achieved. This is particularly important for CCLs and GCLs (Daniel et al., 1993). Hydration takes relatively long in comparison to soils in conventional (smaller) testing shear boxes.

(ii) Consolidation of soils (including CCLs and GCLs) in larger shear boxes is similarly effected.

(iii) Uniformity of normal stress over the entire area must be maintained during consolidation and shearing to prevent stress concentrations from occurring. This is particularly important when testing at high normal stresses.

(iv) The application of relatively low normal stresses (e.g., 1 to 3 psi or 7 to 20 kPa) simulating typical cover soil thicknesses, challenges the accuracy of some commercially available shear box setups and monitoring systems, especially pressure gages.

(v) Shear rates necessary to attain drained conditions (if this is the desired situation) are extremely slow, requiring long testing times.

(vi) Deformations necessary to attain residual strengths require large relative movement of the two respective halves of the shear box. To prevent travel over the edges of the opposing shear box sections, devices should have the lower shear box significantly longer than 12 inches (300 mm). However, with a lower shear box longer than the upper traveling section, new surface is constantly being added to the shearing plane. This influence is not clear in the material's response or in the subsequent behavior.

(vii) The attainment of a true residual strength is difficult to achieve. ASTM D5321 states that one should "run the test until the applied shear force remains constant with increasing displacement". Many commercially available shear boxes have insufficient travel to reach this condition, and thus most report large-displacement values.

(viii) The ring torsion shearing apparatus is an alternative device that can be used to determine true residual strength values. However, this device has its own problems that are caused by inherent large deformations. See Stark and Poeppel (1994) for information and data using this alternative test method.

13.3.2 Solid Waste Properties

The shear strength of solid waste of all types is high. Indeed near vertical cuts have been made in municipal solid waste with no indications of instability. Hazardous waste, which is either particulate or contains large amounts of soil, is also quite stable. The shear strength of municipal solid waste was studied by Singh and Murphy (1990) and their results were presented in Figure 6.7. The data is felt to be quite conservative and, even so, represents a material with considerable shear strength (i.e., a relatively high c- and/or ϕ-value). In spite of the high shear strength of waste materials, waste materials can (and have) failed because of related situations, the most common of which are the following:

(i) Weak subsoils beneath the waste mass [recall Figures 13.1(c) and (d)], which initially fail within the foundation and then continue progressively up through the waste mass.

(ii) High leachate levels in the waste create hydrostatic pressure, which decreases the effective stresses at the base. This, in turn, decreases the shear strength of an otherwise stable material.

(iii) Leachate injection into landfills, (see Chapter 15) has the same effect of decreasing effective stresses and the shear strength of the waste materials.

Thus, the shear strength of solid waste is an important issue, and the reader is referred to the appropriate sections in Chapter 6.

13.3.3 In-Situ Soil Slope and Subsoil Properties

A thorough geotechnical investigation in parallel with a hydrogeological study to reliably identify soil and site stratigraphy is necessary. During the investigation, information such as Standard Penetration Test (SPT) blow counts, visual description of soil samples, depth to groundwater, etc., should be recorded. Undisturbed samples are to be collected for laboratory analysis. Laboratory or in-situ tests are then conducted to evaluate the engineering properties of the soils. These properties primarily include the short- and long-term shear parameters, unit weight, and moisture content (Hassini, 1992).

"Short term" usually refers to the elapsed time up to the end of construction (i.e., the excavation time). Short-term failure is generally due to excessively steep slopes and may occur within a relatively short time after excavation. For saturated clays, excavation causes a rapid change of stress condition within the slope. In the zone of potential failure (i.e., high induced shear stress and/or low shear strength), a slight positive excess pore water pressure may initially result, which will cause a reduction in the effective shear strength, and hence increase the likelihood of failure.

"Long term" generally refers to long duration, post-construction times. As deformation along a potential failure zone increases beyond a critical limit, significant negative excess pore pressure begins to develop, which temporarily increases the strength in the potential failure zone (Humphrey and Leonards, 1986). The dissipation of this negative excess pore pressure can trigger failure of inadequately designed slopes. The rate of dissipation of negative excess pore pressure depends primarily on the coefficient of consolidation of the clay and the average depth to the potential failure zone. Drained shear strength conditions are attained at approximately the same time the excess pressure dissipates. Using Terzaghi's theory of consolidation (Terzaghi, 1943), it is possible to estimate the time for negative pore pressure release. For instance, let the characteristics of the slope be as follows:

Consolidation coefficient, $c_v = 0.11$ ft^2/day (0.01 m^2/day);
Depth to potential failure zone, $H = 16.5$ ft (5.0 m); and
Time factor for 90% consolidation, $T_v = 0.95$.

The time for pore water pressure release by substituting these values into the time-for-consolidation formulation of Equation 13.2 is about 6 years. The relevant equation is

$$t = \frac{T_v \cdot H^2}{C_v} \tag{13.3}$$

The critical factor of safety for slope stability analysis usually extends to the end of dissipation of the excess negative pore pressure. It is necessary to perform stability analysis for the following two conditions (Hassini, 1992):

(i) Immediately after excavation: The undrained shear parameters are used with a correction taking into account the rapid, but temporary, slight increase in pore pressure.

(ii) After a period corresponding to dissipation of negative excess pore pressure: The drained shear parameters are used. The effect of the reduction in confining stress (causing swelling or expansion) on shear parameters should be included.

For landfill covers, long-term conditions are most likely to be critical. Effective stress analysis is to be used. Drained shear parameters are determined from consolidated-drained tests or consolidated-undrained tests with pore pressure measurements. The pore pressure should be determined in the field from flow-net or seepage analysis. For the stability analysis, a factor of safety of 1.5 is recommended (Hassini, 1992).

Representative soil samples should be tested in the laboratory to determine soil parameters necessary for the appropriate calculations. The testing should include natural moisture contents, in-situ dry densities, grain size distributions, Atterberg Limits, unconfined compressive strengths, triaxial tests, and one-dimensional consolidation tests.

Consolidated-undrained (CU) triaxial tests with pore water pressure measurements and unconsolidated-undrained (UU) triaxial tests should be performed on selected Shelby tube samples. In general, the triaxial test consists of two stages. The first stage consists of the application of an all-around cell confining pressure. The second stage consists of the application of a principal stress to the top of the sample to induce shear stresses and eventual failure.

In the CU triaxial test, the sample is allowed to fully consolidate (i.e., all excess pore water pressures are dissipated) during the first stage. During the second stage, the sample fails slowly, at a strain rate of 0.002 in/min (0.05 mm/min), generating excess negative or positive pore water pressures. During the CU test, the pore water pressure is constantly measured during the second phase to allow a determination of the parameters necessary for an evaluation of the shear strength of the soils using an effective stress analysis. The effective stress analysis treats the soil as an essentially frictional material and is normally used for the evaluation of the long-term shear strength of cohesive soils. A three-point consolidated-undrained (CU) triaxial test is run using selected Shelby tube samples. Three consolidation pressures are selected to approximate the different confining pressures of the in-situ samples.

An unconsolidated-undrained (UU) triaxial test is performed to verify the short-term strength of the soil. In the UU triaxial test, the sample is not allowed to consolidate during the application of the cell pressure. The results of the UU test simulate the behavior of cohesive soils that fail in rapid shear over a short period of time (i.e., at a strain rate of approximately 1.4 mm/min). The results are therefore considered applicable to short-term slope stability analyses.

In order to determine average soil parameters for the slope stability analyses, the following parameters are to be plotted with respect to the site-specific stratigraphy: natural moisture content, in-place dry density, "N" values from the Standard Penetration Test, and unconfined compressive strength. The plots of these parameters versus depth are used in conjunction with the results from the triaxial tests to develop design parameters for the different soil strata defined in each critical cross section. The typical liner cross section and total unit weights and shear-strength values for these soil strata are then presented on individual cross sections to be used for the slope stability analyses.

13.4 VENEER SLOPE STABILITY ANALYSES

This section treats the standard veneer slope stability problem [as shown in Figure 13.1(a) and (b)] and then superimposes upon it a number of situations, all which tend to destabilize slopes. Included are gravitational, construction equipment, seepage and seismic forces, respectively. Each will be illustrated by a design graph and a numeric example.

13.4.1 Cover Soil (Gravitational) Forces

Figure 13.3 illustrates the common situation of a finite-length, uniformly-thick cover soil placed over a liner material at a slope angle β. It includes a passive wedge at the toe and has a tension crack on the crest. The analysis that follows is from Koerner and Soong (1998), but it is similar to Koerner and Hwu (1991). Comparable analyses are also available from Giroud and Beech (1989), McKelvey and Deutsch (1991), and others.

The symbols used in Figure 13.3 are defined a follows:

W_A = total weight of the active wedge
W_P = total weight of the passive wedge
N_A = effective force normal to the failure plane of the active wedge
N_P = effective force normal to the failure plane of the passive wedge
γ = unit weight of the cover soil
h = thickness of the cover soil
L = length of slope measured along the geomembrane
β = soil slope angle beneath the geomembrane

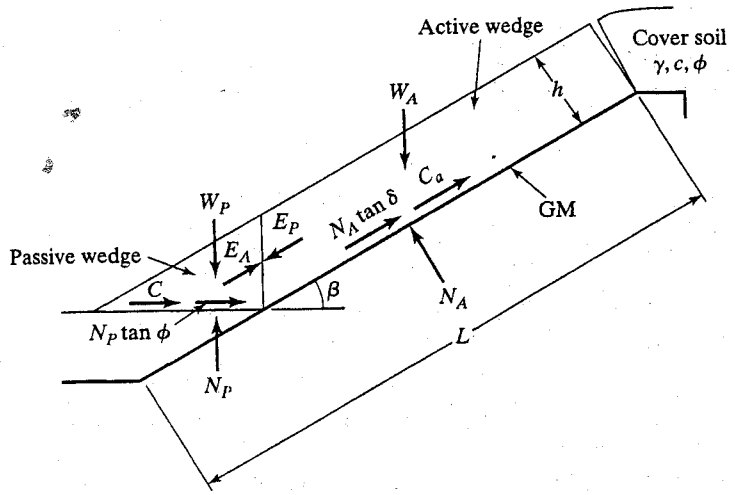

FIGURE 13.3 Limit Equilibrium Forces Involved in a Finite Length Slope Analysis for a Uniformly Thick Cover Soil

ϕ = friction angle of the cover soil
δ = interface friction angle between cover soil and geomembrane
C_a = adhesive force between cover soil of the active wedge and the geomembrane
c_a = adhesion between cover soil of the active wedge and the geomembrane
C = cohesive force along the failure plane of the passive wedge
c = cohesion of the cover soil
E_A = interwedge force acting on the active wedge from the passive wedge
E_p = interwedge force acting on the passive wedge from the active wedge
FS = factor of safety against cover soil sliding on the geomembrane.

The expression for determining the factor of safety can be derived as follows:

Considering the active wedge, the forces acting on it are

$$W_A = \gamma \cdot h^2 \cdot (L/h - 1/\sin\beta - \tan\beta/2) \tag{13.4}$$

$$N_A = W_A \cdot \cos\beta \tag{13.5}$$

$$C_a = c_a \cdot (L - h/\sin\beta) \tag{13.6}$$

By balancing the forces in the vertical direction, the following formulation results:

$$E_A \cdot \sin\beta = W_A - N_A \cdot \cos\beta - \frac{N_A \cdot \tan\delta + C_a}{FS}$$

Hence, the interwedge force acting on the active wedge is

$$E_A = \frac{(FS)(W_A - N_A \cdot \cos\beta) - (N_A \cdot \tan\delta + C_a) \cdot \sin\beta}{\sin\beta \cdot (FS)} \tag{13.7}$$

The passive wedge can be considered in a similar manner:

$$W_P = \frac{\gamma \cdot h^2}{\sin 2\beta}$$

$$N_P = W_P + E_P \cdot \sin\beta$$

$$C = \frac{c \cdot h}{\sin\beta} \tag{13.8}$$

By balancing the forces in the horizontal direction, the following formulation results:

$$E_P \cdot \cos\beta = \frac{C + N_P \cdot \tan\phi}{FS}$$

Hence, the interwedge force acting on the passive wedge is

$$E_P = \frac{C + W_P \cdot \tan\phi}{\cos\beta \cdot (FS) - \sin\beta \cdot \tan\phi}$$

By setting $E_A = E_P$, the resulting equation can be arranged in the form of the quadratic equation $ax^2 + bx + c = 0$, which in this case, using *FS*-values, results in

$$a \cdot FS^2 + b \cdot FS + c = 0$$

The resulting *FS*-value is then obtained from the conventional solution of the quadratic equation, which gives

$$FS = \frac{-b \pm (b^2 - 4 \cdot a \cdot c)^{0.5}}{2 \cdot a} \tag{13.9}$$

where
$$a = (W_A - N_A \cdot \cos\beta) \cdot \cos\beta$$
$$b = -[(W_A - N_A \cdot \cos\beta) \cdot \sin\beta \cdot \tan\phi + (N_A \cdot \tan\delta + C_a) \cdot \sin\beta \cdot \cos\beta + (C + W_P \cdot \tan\phi) \cdot \sin\beta]$$
$$c = (N_A \cdot \tan\delta + C_a) \cdot \sin^2\beta \cdot \tan\phi$$

When the calculated *FS*-value falls below 1.0, sliding of the cover soil on the geomembrane is to be anticipated. Thus, a value of greater than 1.0 must be targeted as being the minimum factor of safety. How much greater than 1.0 the *FS*-value should be, is a design and/or regulatory issue. Recommendations for minimum allowable *FS*-values under different conditions are available in Koerner and Soong (1998). In order to better illustrate the implications of Equations 13.9, typical design curves for various *FS*-values as a function of slope angle and interface friction angle are given in Figure 13.4. Note that the curves are developed specifically for the variables stated in the legend of the figure. Example 13.1 illustrates the use of the analytic development and the

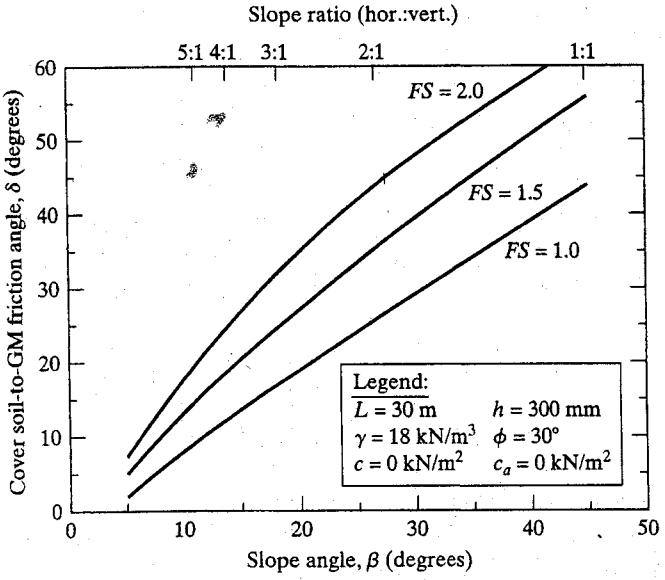

FIGURE 13.4 Design Curves for Stability of Uniform-Thickness Cohesionless Cover Soils on Linear Failure Planes for Various Global Factors of Safety

resulting design curves in what will be the standard example to which other examples will be considered as compared.

EXAMPLE 13.1

The following are given: a 30-m slope with a uniformly thick 300-mm-deep cover soil at a unit weight of 18 kN/m^3. The soil has a friction angle of 30° and zero cohesion (i.e., it is a sand). The cover soil is placed directly on a geomembrane as shown in Figure 13.3. Direct shear testing has resulted in an interface friction angle between the cover soil and geomembrane of 22° with zero adhesion. What is the *FS*-value at a slope angle of 3(H)-to-1(V) (i.e., 18.4°)?

Solution Using Equation 13.9 to solve for the *FS*-value results in a value of 1.25, which is seen to be in agreement with the curves of Figure 13.4:

$$a = 14.7 \text{ kN/m}$$
$$b = -21.3 \text{ kN/m}$$
$$c = 3.5 \text{ kN/m}$$

Thus, $FS = 1.25$

This value can be confirmed using Figure 13.4.

Comment In general, this is too low of a value for a final cover soil factor-of-safety and a redesign is necessary. There are many possible options to increase the value (e.g., changing the geometry of the situation, the use of toe berms, tapered cover soil thickness, and veneer reinforcement, see Koerner and Soong, 1998). Nevertheless, this general problem will be used throughout this section for comparison with other cover soil slope stability situations.

13.4.2 Tracked Construction Equipment Forces

The placement of cover soil on a slope with a relatively low shear strength interface (like a geomembrane) should always start at the toe and move upward to the crest. Figure 13.5(a) shows the recommended method. In doing so, the gravitational forces of the cover soil and live load of the construction equipment are compacting previously placed soil and working with an ever-present passive wedge and a stable lower portion beneath the active wedge. While it is necessary to specify low ground pressure equipment to place the soil, the reduction in the *FS*-value for this situation of equipment working up the slope will be seen to be relatively small.

For soil placement down the slope, however, a stability analysis cannot rely on toe buttressing and also a dynamic stress should be included in the calculation. These conditions decrease the *FS*-value—in some cases, to a great extent. Figure 13.5(b) shows this procedure. Unless absolutely necessary, it is not recommended that cover soil be placed on a slope in this manner. If it is necessary, the design must consider the unsupported soil mass and the possible dynamic force of the specific type of construction equipment and its manner of operation.

For the *first case* of a bulldozer pushing cover soil up from the toe of the slope to the crest, the analysis uses the free body diagram of Figure 13.6(a). The analysis uses a

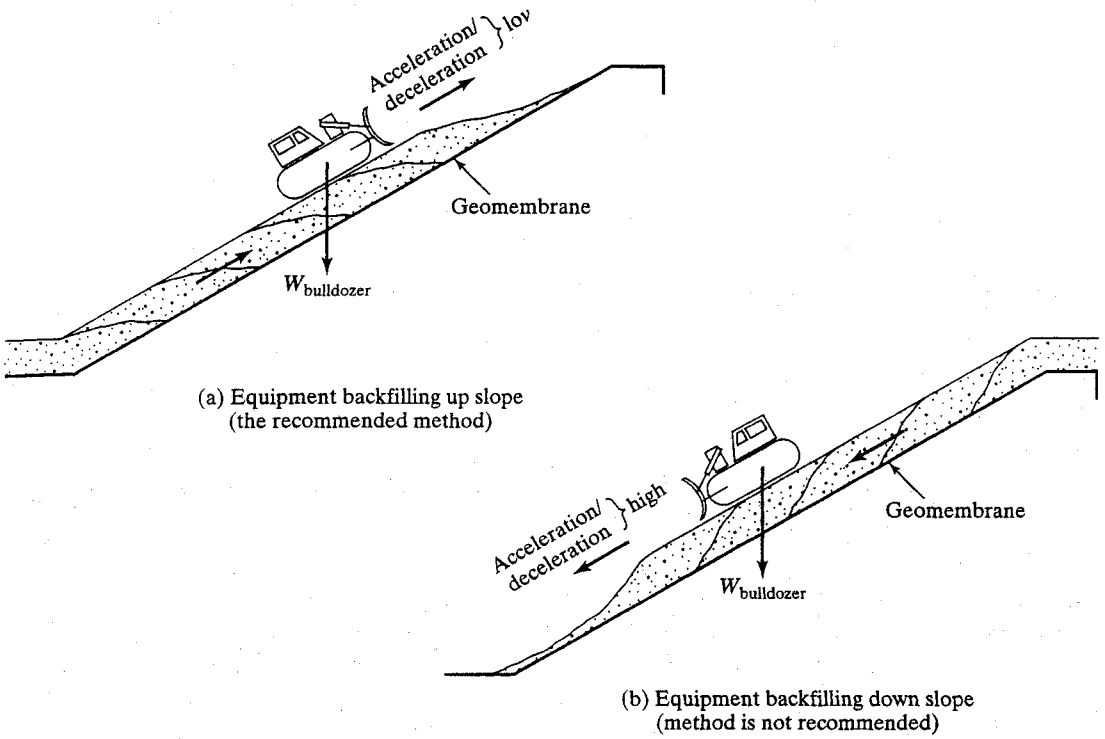

FIGURE 13.5 Construction Equipment Placing Cover Soil on Slopes Containing Geosynthetics

known type of construction equipment (such as a bulldozer characterized by its ground contact pressure) and dissipates this force or stress through the cover soil thickness to the surface of the geomembrane. A Boussinesq analysis is used (see Poulos and Davis, 1974). This results in an equipment force per unit width of

$$W_e = q \cdot w \cdot I \tag{13.10}$$

where W_e = equivalent equipment force per unit width at the geomembrane interface;
$q = W_b/(2 \cdot w \cdot b)$;
W_b = actual weight of equipment (e.g., a bulldozer);
w = length of equipment track;
b = width of equipment track;
I = influence factor at the geomembrane interface (see Figure 13.7).

Upon determining the additional equipment force at the cover soil-to-geomembrane interface, the analysis proceeds as described in Section 13.3.1 for gravitational forces only. In essence, the equipment moving up the slope adds an additional term (W_e) to the W_A-force in Equation 13.4. Note, however, that this involves the generation of a resisting force as well. Thus, the net effect of increasing the driving force as well as the resisting force is somewhat neutralized insofar as the resulting *FS*-value is

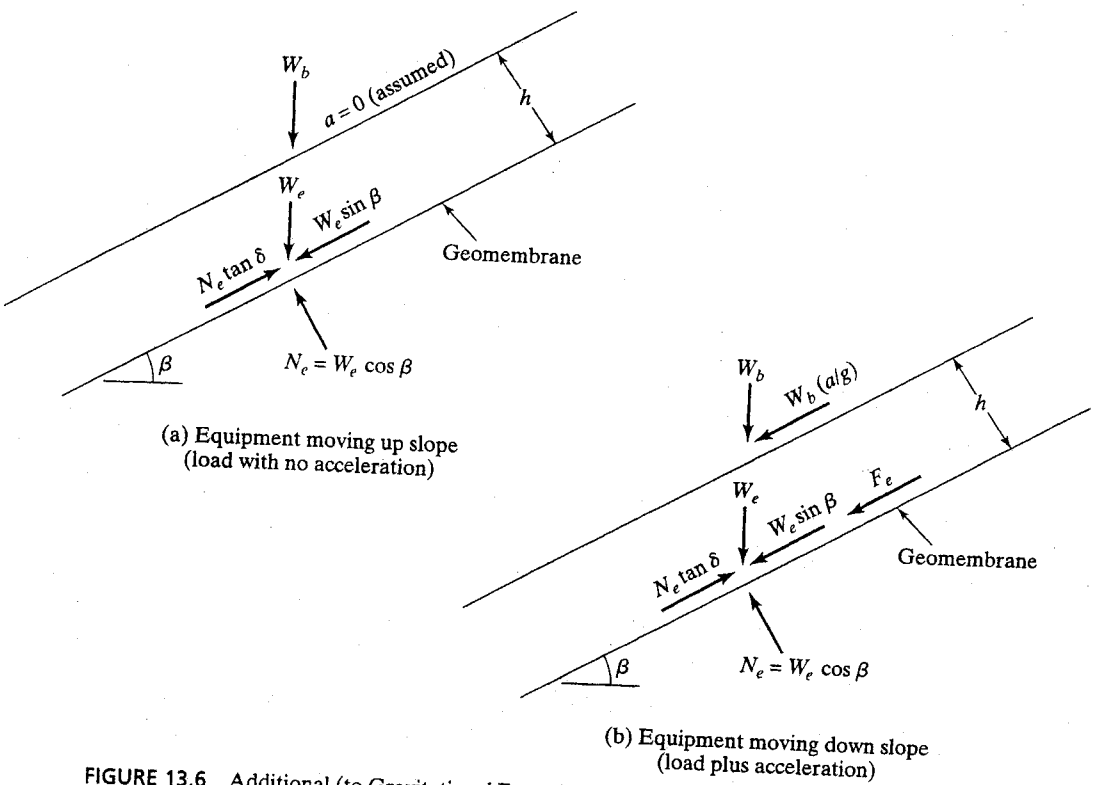

FIGURE 13.6 Additional (to Gravitational Forces) Limit Equilibrium Forces due to Construction Equipment Moving on Cover Soil (see Figure 13.3 for the gravitational soil force to which the above forces are added).

concerned. It should also be noted that no acceleration/deceleration forces are included in this analysis, which is somewhat idealistic. Using these concepts (the same equations used in Section 13.3.1 are used here), typical design curves for various *FS*-values as a function of equivalent ground contact equipment pressures and cover soil thicknesses are given in Figure 13.8. Note that the curves are developed specifically for the variables stated in the legend. Example 13.2 illustrates the use of the formulation.

EXAMPLE 13.2

The following are given: a 30-m-long slope with uniform cover soil of 300 mm thickness at a unit weight of 18 kN/m^3. The soil has a friction angle of 30° and zero cohesion (i.e., it is a sand). It is placed on the slope using a bulldozer moving from the toe of the slope up to the crest. The bulldozer has a ground pressure of 30 kN/m^2 and tracks that are 3.0 m long and 0.6 m wide. The cover soil to geomembrane friction angle is 22° with zero adhesion. What is the *FS*-value at a slope angle 3(H)-to-1(V)(i.e., 18.4°)?

Solution This problem follows Example 13.1 exactly except for the addition of the bulldozer moving up the slope. Using the additional equipment load, Equation 13.10 substituted into Equation 13.9 results in the following:

$$a = 73.1 \text{ kN/m}$$
$$b = -104.3 \text{ kN/m}$$
$$c = 17.0 \text{ kN/m}$$

Thus, $FS = 1.24$

This value can be confirmed using Figure 13.8.

Comment While the resulting *FS*-value is still low, the result is important to assess by comparing it with Example 13.1 (i.e., the same problem except without the bulldozer). It is seen that the *FS*-value has only decreased from 1.25 to 1.24. Thus, in general, a low ground contact pressure bulldozer placing cover soil up the slope with negligible acceleration/deceleration forces does not significantly decrease the factor-of-safety.

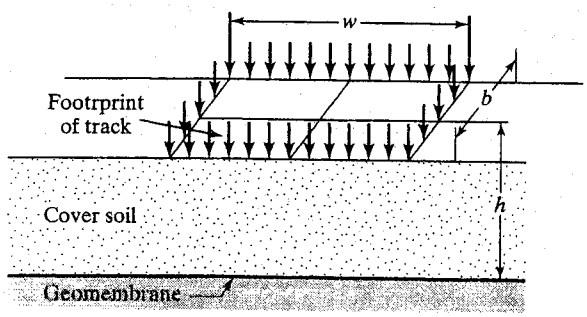

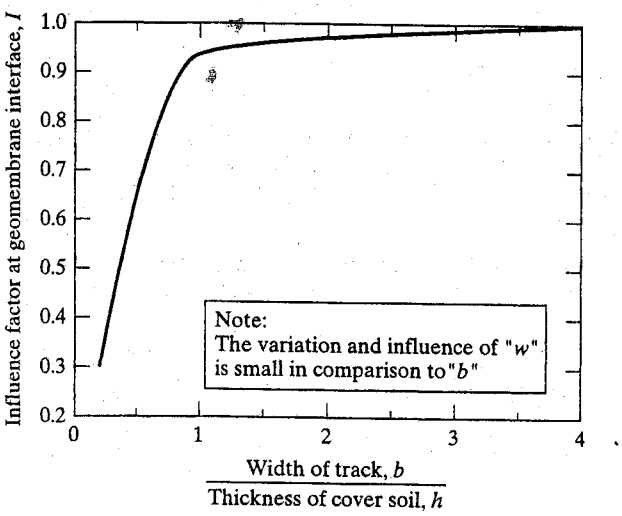

FIGURE 13.7 Values of Influence Factor, "I", for Use in Equation 13.10 to Dissipate Surface Force through the Cover Soil to the Geomembrane Interface (after Soong and Koerner, 1996)

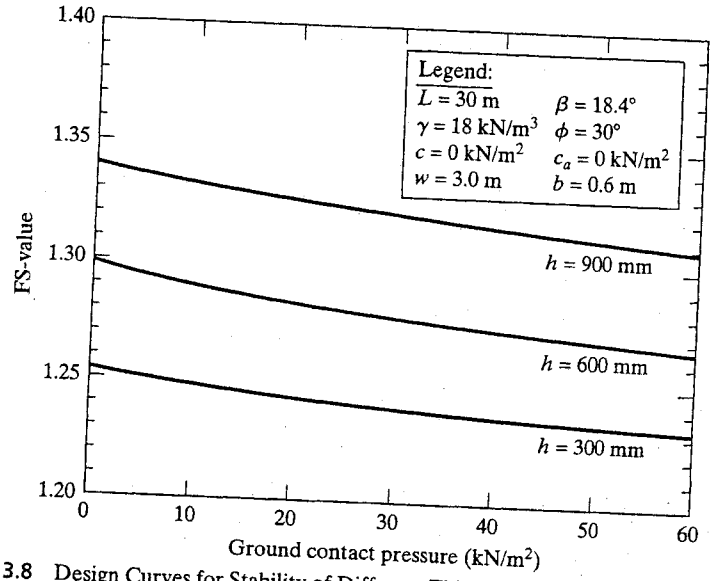

FIGURE 13.8 Design Curves for Stability of Different Thickness of Cover Soil for Various Construction Equipment Ground Contact Pressure

For the *second case* of a bulldozer pushing cover soil down from the crest of the slope to the toe as shown in Figure 13.5b, the analysis uses the force diagram of Figure 13.6(b). While the weight of the equipment is treated as just described, the lack of a passive wedge along with an additional force due to acceleration (or deceleration) of the equipment significantly decreases the resulting *FS*-values. This analysis again uses a specific piece of construction equipment operated in a specific manner. It produces a force parallel to the slope equivalent to $W_b \cdot (a/g)$, where W_b = the weight of the bulldozer, a = acceleration of the bulldozer, and g = acceleration due to gravity. Its magnitude is equipment operator dependent and related to both the equipment speed and time to reach such a speed (see Figure 13.9).

The acceleration of the bulldozer, coupled with an influence factor I from Figure 13.7, results in the dynamic force per unit width at the cover soil to geomembrane interface F_e. The relationship is given by

$$F_e = W_e \cdot (a/g) \tag{13.11}$$

where F_e = dynamic force per unit width parallel to the slope at the geomembrane interface;
W_e = equivalent equipment (e.g., bulldozer) force per unit width at geomembrane interface, recall Equation 13.10;
β = soil slope angle beneath geomembrane;
a = acceleration of the construction equipment;
g = acceleration due to gravity.

Using these concepts, the new force parallel to the cover soil surface is dissipated through the thickness of the cover soil to the interface of the geomembrane. Again, a

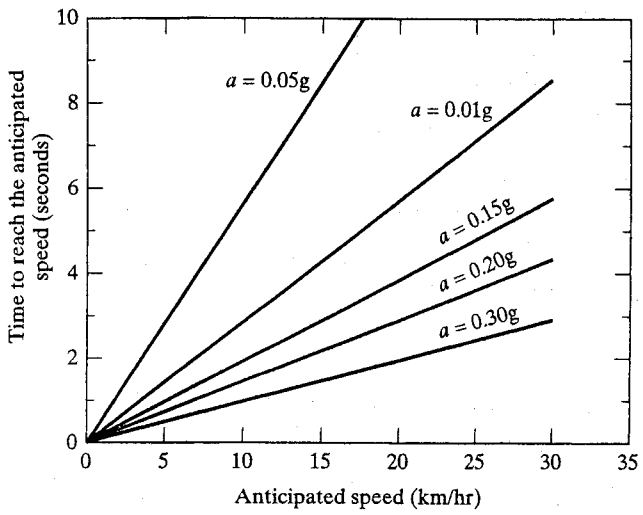

FIGURE 13.9 Graphic Relationship of Construction Equipment Speed and Rise Time to Obtain Equipment Acceleration.

Boussinesq analysis is used (see Poulos and Davis, 1974). The expression for determining the *FS*-value is derived next.

Considering the active wedge and balancing the forces in the direction parallel to the slope, the resulting formulation is

$$E_A + \frac{(N_e + N_A)\cdot\tan\delta + C_a}{FS} = (W_A + W_e)\cdot\sin\beta + F_e$$

where

N_e = effective equipment force normal to the failure plane of the active wedge.

$$N_e = W_E\cdot\cos\beta \tag{13.12}$$

Note that all the other symbols have been previously defined.

The interwedge force acting on the active wedge can now be expressed as

$$E_A = \frac{(FS)[(W_A + W_e)\cdot\sin\beta + F_e]}{FS} - \frac{[(N_A + N_e)\cdot\tan\delta + C_a]}{FS}$$

The passive wedge can be treated in a similar manner. The following formulation of the interwedge force acting on the passive wedge results:

$$E_P = \frac{C + W_P\cdot\tan\phi}{\cos\beta\cdot(FS) - \sin\beta\cdot\tan\phi}$$

By setting $E_A = E_P$, the resulting equation can be arranged in the form of the quadratic equation $ax^2 + bx + c = 0$ which in this case, using *FS*-values, is

$$a\cdot FS^2 + b\cdot FS + c = 0$$

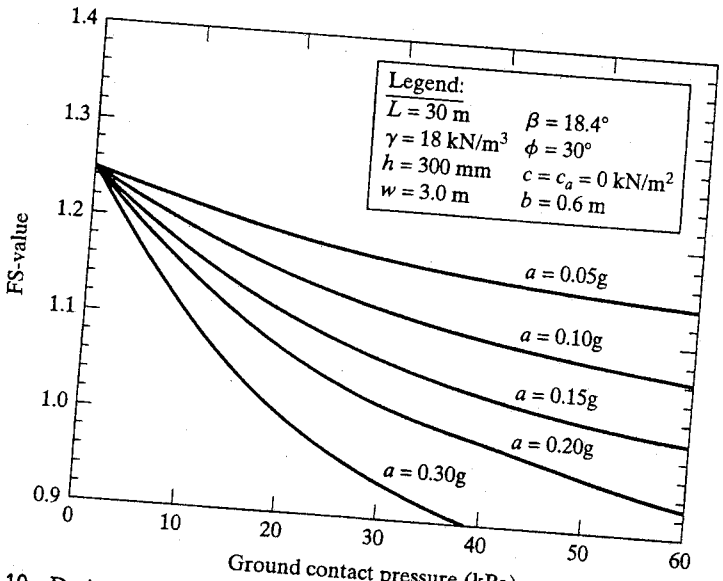

FIGURE 13.10 Design Curves for Stability of Different Construction Equipment Ground Contact Pressure for Various Equipment Accelerations

The resulting *FS*-value is then obtained from the conventional solution of the quadratic equation

$$FS = \frac{-b \pm (b^2 - 4 \cdot a \cdot c)^{0.5}}{2 \cdot a} \tag{13.13}$$

where
$$a = [(W_A + W_e) \cdot \sin\beta + F_e] \cdot \cos\beta$$
$$b = -\{[(N_A + N_e) \cdot \tan\delta + C_a] \cdot \cos\beta + [(W_A + W_e) \cdot \sin\beta + F_e] \cdot \sin\beta \cdot \tan\phi + (C + W_P \cdot \tan\phi)\}$$
$$c = [(N_A + N_e) \cdot \tan\delta + C_a] \cdot \sin\beta \cdot \tan\phi$$

Using these concepts, typical design curves for various *FS*-values as a function of equipment ground contact pressure and equipment acceleration can be developed (see Figure 13.10). Note that the curves are developed specifically for the variables stated in the legend. Example 13.3 illustrates the use of the formulation.

EXAMPLE 13.3

The following are given: a 30-m-long slope with uniform cover soil of 300-mm thickness at a unit weight of 18 kN/m^3. The soil has a friction angle of 30° and zero cohesion (i.e., it is a sand). It is placed on the slope using a bulldozer moving from the crest of the slope down to the toe. The bulldozer has a ground contact pressure of 30 kN/m^2 and tracks that are 3.0 m long and 0.6 m wide. The estimated equipment speed is 20 km/hr, and the time to reach this speed is 3.0 seconds. The cover soil to geomembrane friction angle is 22 degrees with zero adhesion. What is the *FS*-value at a slope angle of 3(H)-to-1(V) (i.e., 18.4°)?

Solution Using the design curves of Figure 13.10 along with Equation 13.13, the solution can be obtained.

- From Figure 13.9, at 20 km/hr and 3.0 seconds, the bulldozer's acceleration is 0.19g.
- From Equation 13.13,

$$a = 88.8 \text{ kN/m}$$
$$b = -107.3 \text{ kN/m}$$
$$c = 17.0 \text{ kN/m}$$

Thus, $FS = 1.03$

This value can be confirmed using Figure 13.10.

Comment This problem solution can now be compared with those of the previous two examples:

Example 13.1.	Cover soil along with no bulldozer loading:	$FS = 1.25$
Example 13.2.	Cover soil plus bulldozer moving up slope:	$FS = 1.24$
Example 13.3.	Cover soil plus bulldozer moving down slope:	$FS = 1.03$

The inherent danger of a bulldozer moving down the slope is readily apparent. Note, that the same result comes about by the bulldozer decelerating instead of accelerating. The sharp breaking action of the bulldozer is arguably the more severe condition, due to the extremely short times involved when stopping forward motion. Clearly, only in unavoidable situations should the cover soil placement equipment be allowed to work down the slope. If it is unavoidable, an analysis should be made of the specific stability situation and the construction specifications should reflect the precise conditions made in the design. The maximum weight and ground contact pressure of the equipment should be stated along with suggested operator movement of the cover soil placement operations. Truck traffic on the slopes can also give stresses as high or even higher than illustrated here and should be avoided in all circumstances.

13.4.3 Inclusion of Seepage Forces

The previous sections presented the general problem of slope stability analysis of cover soils placed on slopes under different conditions. The tacit assumption throughout was that either permeable soil or a drainage layer was placed above the barrier layer with adequate flow capacity to efficiently and safely remove permeating water away from the cross section. The amount of water to be removed is obviously a site-specific situation. Note that, in extremely arid areas, or with very low permeability cover soils, drainage may not be required, although this is generally the exception.

Unfortunately, adequate drainage of final covers has sometimes not been available and seepage-induced slope stability problems have occurred. Figure 13.11 shows a final cover slope failure during a heavy raining. The following situations have resulted in seepage-induced slides:

- Drainage soils with hydraulic conductivity (permeability) too low for site-specific conditions.
- Inadequate drainage capacity at the toe of long slopes, where seepage quantities accumulate and are at their maximum.
- Fines from quarried drainage stone either clogging the drainage layer or accumulating at the toe of the slope, thereby decreasing the as-constructed permeability over time.

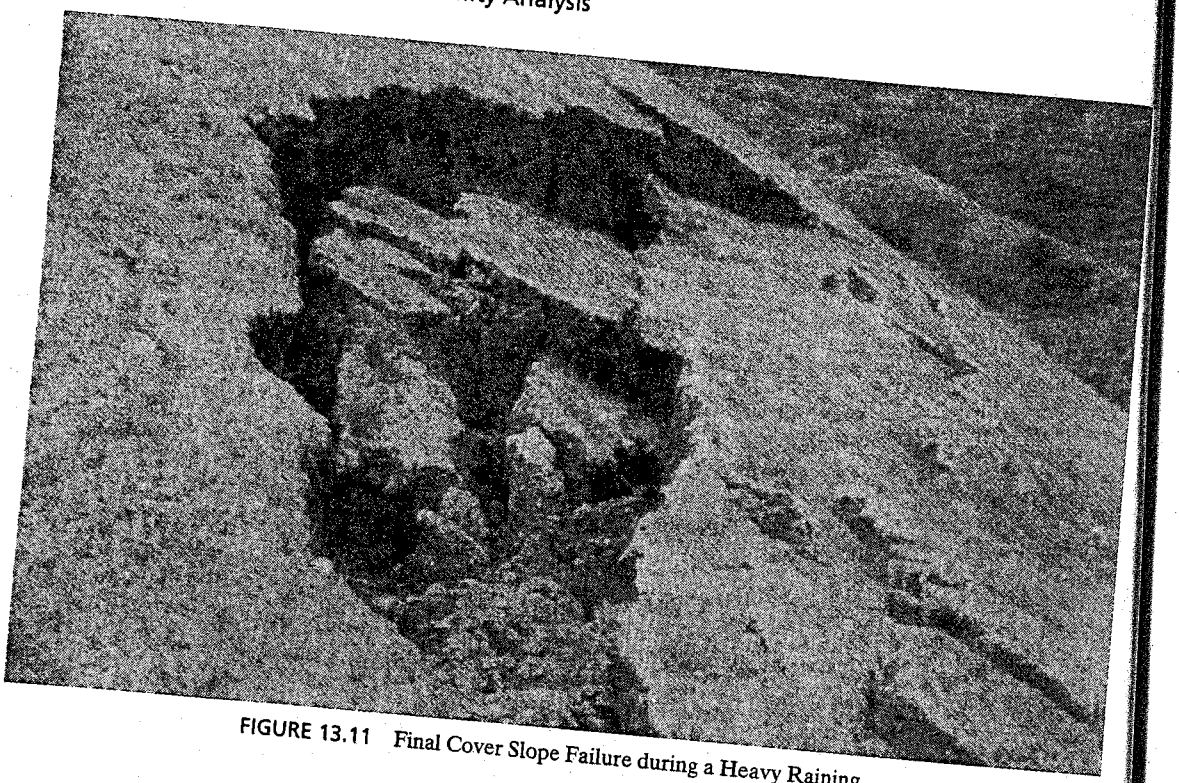

FIGURE 13.11 Final Cover Slope Failure during a Heavy Raining

- Fine, cohesionless, cover soil particles migrating through the filter (if one is present) either clogging the drainage layer, or accumulating at the toe of the slope, thereby decreasing the as-constructed outlet permeability over time.
- Freezing of the outlet drainage at the toe of the slope, while the top of the slope thaws, thereby mobilizing seepage forces against the ice wedge at the toe.

If seepage forces of the types described occur, a variation in slope stability design methodology is required. Such an analysis is the focus of this subsection. (See Koerner and Soong, 1998; and Qian, 1997; also, Thiel and Stewart, 1993; and Soong and Koerner, 1996.)

Consider a cover soil of uniform thickness placed directly above a geomembrane at a slope angle of β, as shown in Figure 13.12. What is different from previous examples, however, is that within the cover soil there can exist a saturated soil zone for part or all of the thickness. The saturated boundary is shown as two possibly different phreatic surface orientations. This is because seepage can be built up in the cover soil in two different ways: a horizontal buildup from the toe upward, or a parallel-to-slope buildup outward. These two hypotheses are defined and quantified as a horizontal submergence ratio (HSR) and a parallel submergence ratio (PSR). The dimensional definitions of both ratios are given in Figure 13.12.

When analyzing the stability of slopes using the limit equilibrium method, free-body diagrams of the passive and active wedges are taken with the appropriate forces

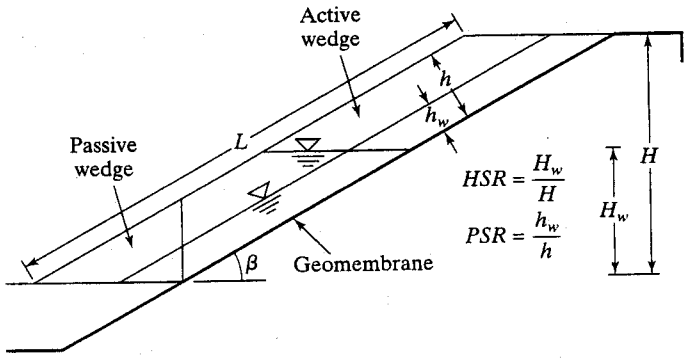

FIGURE 13.12 Cross Section of a Uniform Thickness Cover Soil on a Geomembrane Illustrating Different Submergence Assumptions and Related Definitions (Soong and Koerner, 1996)

being applied (now including pore water pressures). The formulation for the resulting factor of safety for horizontal seepage buildup and also for parallel-to-slope seepage buildup is described next.

13.4.3.1 The Case of the Horizontal Seepage Buildup. Figure 13.13 shows the free-body diagram of both the active and passive wedge assuming horizontal seepage building. Horizontal seepage buildup can occur when toe blockage occurs due to inadequate outlet capacity, contamination or physical blocking of outlets, or freezing conditions at the outlets.

All symbols used in Figure 13.13 were previously defined except the following:

γ_{sat} = saturated unit weight of the cover soil
γ_t = dry unit weight of the cover soil
γ_w = unit weight of water
H = vertical height of the slope measured from the toe
H_w = vertical height of the free water surface measured from the toe
U_h = resultant of the pore pressures acting on the interwedge surfaces
U_n = resultant of the pore pressures acting perpendicular to the slope
U_v = resultant of the vertical pore pressures acting on the passive wedge

The expression for determining the factor of safety can be derived as follows:

Considering the active wedge,

$$W_A = \frac{\gamma_{sat} \cdot h \cdot (2 \cdot H_w \cdot \cos\beta - h)}{\sin 2\beta} + \frac{\gamma_{dry} \cdot h \cdot (H - H_w)}{\sin\beta} \tag{13.14}$$

$$U_n = \frac{\gamma_w \cdot h \cdot \cos\beta \cdot (2 \cdot H_w \cdot \cos\beta - h)}{\sin 2\beta} \tag{13.15}$$

$$U_h = 0.5 \cdot \gamma_w \cdot h^2 \tag{13.16}$$

$$N_A = W_A \cdot \cos\beta + U_h \cdot \sin\beta - U_n \tag{13.17}$$

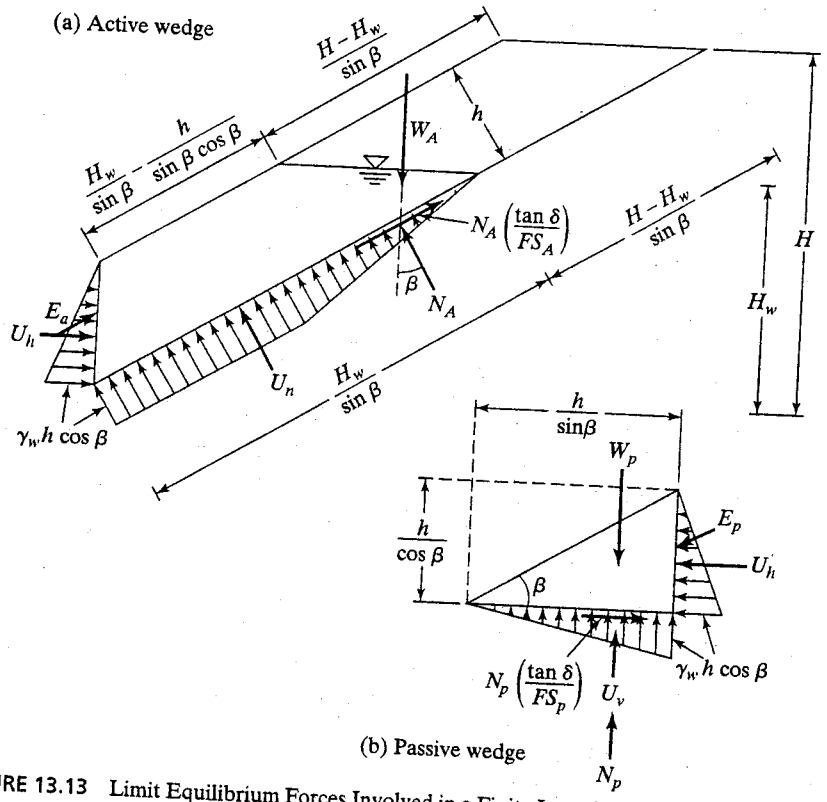

FIGURE 13.13 Limit Equilibrium Forces Involved in a Finite Length Slope of Uniform Cover Soil with Horizontal Seepage Buildup

The interwedge force acting on the active wedge can then be expressed as

$$E_A = W_A \cdot \sin\beta + U_h \cdot \cos\beta - \frac{N_A \cdot \tan\delta}{FS}$$

The passive wedge can be considered in a similar manner and the following expressions result:

$$W_P = \frac{\gamma_{sat} \cdot h^2}{\sin 2\beta} \tag{13.18}$$

$$U_v = U_h \cdot \cot\beta \tag{13.19}$$

The interwedge force acting on the passive wedge can then be expressed as

$$E_P = \frac{U_h \cdot (FS) - (W_P - U_v) \cdot \tan\phi}{\sin\beta \cdot \tan\phi - \cos\beta \cdot (FS)}$$

By setting $E_A = E_P$, the following equation can be arranged in the form of $ax^2 + bx + c = 0$, which in this case is

$$a \cdot FS^2 + b \cdot FS + c = 0$$

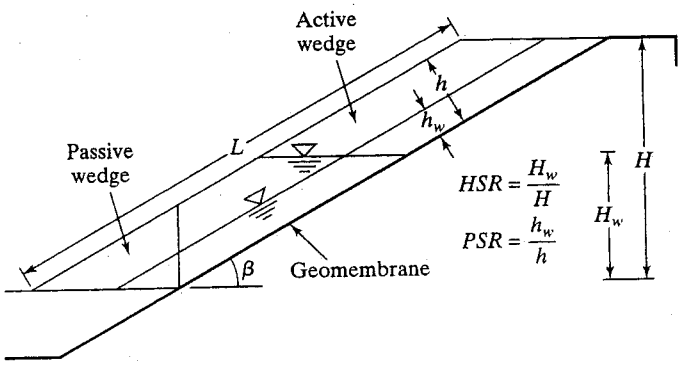

FIGURE 13.12 Cross Section of a Uniform Thickness Cover Soil on a Geomembrane Illustrating Different Submergence Assumptions and Related Definitions (Soong and Koerner, 1996)

being applied (now including pore water pressures). The formulation for the resulting factor of safety for horizontal seepage buildup and also for parallel-to-slope seepage buildup is described next.

13.4.3.1 The Case of the Horizontal Seepage Buildup. Figure 13.13 shows the free-body diagram of both the active and passive wedge assuming horizontal seepage building. Horizontal seepage buildup can occur when toe blockage occurs due to inadequate outlet capacity, contamination or physical blocking of outlets, or freezing conditions at the outlets.

All symbols used in Figure 13.13 were previously defined except the following:

γ_{sat} = saturated unit weight of the cover soil
γ_t = dry unit weight of the cover soil
γ_w = unit weight of water
H = vertical height of the slope measured from the toe
H_w = vertical height of the free water surface measured from the toe
U_h = resultant of the pore pressures acting on the interwedge surfaces
U_n = resultant of the pore pressures acting perpendicular to the slope
U_v = resultant of the vertical pore pressures acting on the passive wedge

The expression for determining the factor of safety can be derived as follows:

Considering the active wedge,

$$W_A = \frac{\gamma_{sat} \cdot h \cdot (2 \cdot H_w \cdot \cos\beta - h)}{\sin 2\beta} + \frac{\gamma_{dry} \cdot h \cdot (H - H_w)}{\sin\beta} \tag{13.14}$$

$$U_n = \frac{\gamma_w \cdot h \cdot \cos\beta \cdot (2 \cdot H_w \cdot \cos\beta - h)}{\sin 2\beta} \tag{13.15}$$

$$U_h = 0.5 \cdot \gamma_w \cdot h^2 \tag{13.16}$$

$$N_A = W_A \cdot \cos\beta + U_h \cdot \sin\beta - U_n \tag{13.17}$$

The resulting *FS*-value is then obtained from the conventional solution of the quadratic equation as

$$FS = \frac{-b \pm (b^2 - 4 \cdot a \cdot c)^{0.5}}{2 \cdot a} \tag{13.20}$$

where
$$a = W_A \cdot \sin\beta \cdot \cos\beta - U_h \cdot \cos^2\beta + U_h$$
$$b = -W_A \cdot \sin^2\beta \cdot \tan\phi + U_h \cdot \sin\beta \cdot \cos\beta \cdot \tan\phi - N_A \cdot \cos\beta \cdot \tan\delta - (W_P - U_v) \cdot \tan\phi$$
$$c = N_A \cdot \sin\beta \cdot \tan\delta \cdot \tan\phi$$

13.4.3.2 The Case of Parallel-to-Slope Seepage Buildup. Figure 13.14 shows the free body diagrams of both the active and passive wedges with seepage buildup in the direction parallel to the slope. Parallel seepage buildup can occur when soils placed above a geomembrane are initially too low in their hydraulic conductivity, or become too low due to long-term clogging from overlying soils that are not filtered. The individual forces, friction angles, and slope angles involved in Figure 13.14 are listed as follows:

W_A = weight of the active wedge (area times unit weight), lb/ft or kN/m;
W_P = weight of the passive wedge (area times unit weight), lb/ft or kN/m;
β = angle of the slope, degree;
H = height of the cover soil slope from the toe of the cover soil to the top of the slope (see Figure 13.14), ft or m;
h = thickness of the soil layer (perpendicular to the slope), ft or m;
h_w = depth of seepage water in the soil layer (perpendicular to the slope), ft or m;
γ = moisture unit weight of the soil layer, lb/ft^3 or kN/m^3;
γ_{sat} = saturated unit weight of the soil layer, lb/ft^3 or kN/m^3;
γ_w = unit weight of water, 62.4 lb/ft^3 or 9.81 kN/m^3;
ϕ = friction angle of the cover soil, degree;
δ = interface friction angle between the soil layer and geomembrane, degree;
N_A = normal force acting on bottom of the active wedge, lb/ft or kN/m;
F_A = frictional force acting on bottom of the active wedge, lb/ft;
U_{AN} = resultant of the pore water pressures acting on bottom of the active wedge (perpendicular to the slope), lb/ft or kN/m;
U_{AH} = resultant of the pore water pressures acting on lower lateral side of the active wedge (perpendicular to the interface between the active and passive wedges), lb/ft or kN/m;
E_A = force from passive wedge acting on active wedge (unknown in magnitude but assumed direction parallel to the slope), lb/ft or kN/m;
N_P = normal force acting on the bottom of passive wedge, lb/ft or kN/m;
F_P = frictional force acting on the bottom of passive wedge, lb/ft or kN/m;
U_{PH} = resultant of the pore water pressures acting on lateral side of the passive wedge (perpendicular to the lateral side), lb/ft or kN/m;

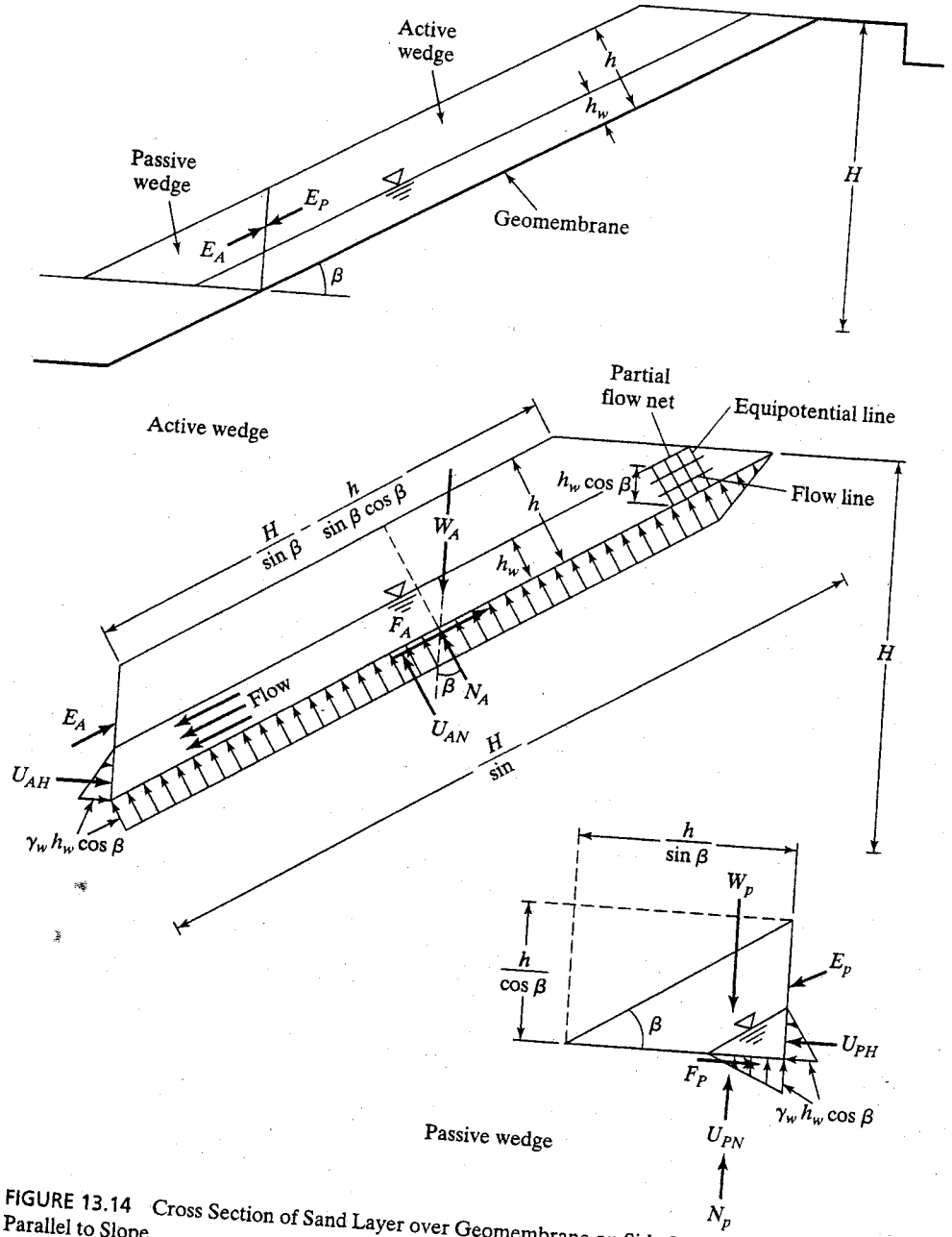

FIGURE 13.14 Cross Section of Sand Layer over Geomembrane on Side Slope with Seepage Parallel to Slope.

U_H = resultant of the pore water pressures acting on lateral side of the active wedge or passive wedge (perpendicular to the lateral side), lb/ft or kN/m, $U_H = U_{AH} = U_{PH}$;

U_{PN} = resultant of the pore water pressures acting on bottom of the passive wedge (perpendicular to bottom of the passive wedge), lb/ft or kN/m;

E_P = force from active wedge acting on passive wedge (unknown in magnitude but assumed direction parallel to the slope), lb/ft or kN/m, $E_A = E_P$;

FS = factor of safety for stability of the cover soil mass.

Considering the force equilibrium of the active wedge (Figure 13.14), we obtain

$\Sigma F_Y = 0$:

$$N_A + U_{AN} = W_A \cdot \cos\beta + U_{AH} \cdot \sin\beta$$

$$N_A = W_A \cdot \cos\beta - U_{AN} + U_{AH} \cdot \sin\beta \tag{13.21}$$

$\Sigma F_X = 0$:

$$F_A + E_A + U_{AH} \cdot \cos\beta = W_A \cdot \sin\beta$$

$$E_A = W_A \cdot \sin\beta - U_{AH} \cdot \cos\beta - F_A \tag{13.22}$$

$$F_A = N_A \cdot \tan\delta / FS \tag{13.23}$$

Substituting Equation 13.21 into Equation 13.23 gives

$$F_A = (W_A \cdot \cos\beta - U_A + U_{AH} \cdot \sin\beta) \cdot \tan\delta / FS \tag{13.24}$$

Substituting Equation 13.24 into Equation 13.22 gives

$$E_A = W_A \cdot \sin\beta - U_{AH} \cdot \cos\beta - (W_A \cdot \cos\beta - U_A + U_{AH} \cdot \sin\beta) \cdot \tan\delta / FS \tag{13.25}$$

Considering the force equilibrium of the passive wedge (Figure 13.14) yields

$$E_P = E_A \tag{13.26}$$

$\Sigma F_Y = 0$:

$$N_P + U_{PN} = W_P + E_P \cdot \sin\beta \tag{13.27}$$

Substituting Equation 13.26 into Equation 13.27 gives

$$N_P = W_P + E_A \cdot \sin\beta - U_{PN} \tag{13.28}$$

Substituting Equation 13.25 into Equation 13.28 gives

$$N_P = W_P + U_{PN} + [W_A \cdot \sin\beta - U_{AH} \cdot \cos\beta - (W_A \cdot \cos\beta - U_A + U_{AH} \cdot \sin\beta) \cdot \tan\delta / FS] \cdot \sin\beta$$

$$N_P = W_P - U_{PN} + W_A \cdot \sin^2\beta - U_{AH} \cdot \sin\beta \cdot \cos\beta - (W_A \cdot \cos\beta - U_A + U_{AH} \cdot \sin\beta) \cdot \sin\beta \cdot \tan\delta / FS \tag{13.29}$$

$\Sigma F_X = 0$:

$$F_P = U_{PH} + E_P \cdot \cos\beta \tag{13.30}$$

Substituting Equation 13.26 into Equation 13.30 gives

$$F_P = U_{PH} + E_A \cdot \cos\beta \tag{13.31}$$

Substituting Equation 13.25 into Equation 13.31 gives

$$F_P = U_{PH} + W_A \cdot \sin\beta \cdot \cos\beta - U_{AH} \cdot \cos^2\beta - (W_A \cdot \cos\beta - U_{AN} + U_{AH} \cdot \sin\beta) \cdot \cos\beta \tag{13.32}$$

$$FS = \frac{N_P \cdot \tan\phi}{F_P} \tag{13.33}$$

Substituting Equations 13.29 and 13.32 into Equation 13.33 gives

$$FS = \frac{(W_P - U_{PN} + W_A \cdot \sin^2\beta - U_{AH} \cdot \sin\beta \cdot \cos\beta) \cdot \tan\phi - (W_A \cdot \cos\beta - U_A + U_{AH} \cdot \sin\beta) \cdot \sin\beta \cdot \tan\delta \cdot \tan\phi / FS}{U_{PH} + W_A \cdot \sin\beta \cdot \cos\beta - U_{AH} \cdot \cos^2\beta - (W_A \cdot \cos\beta - U_{AN} + U_{AH} \cdot \sin\beta) \cdot \cos\beta \cdot \tan\delta / FS}$$

$$(U_{PH} + W_A \cdot \sin\beta \cdot \cos\beta - U_{AH} \cdot \cos^2\beta) \cdot FS - (W_A \cdot \cos\beta - U_{AN} + U_{AH} \cdot \sin\beta) \cdot \cos\beta \cdot \tan\delta = (W_P - U_{PN} + W_A \cdot \sin^2\beta - U_{AH} \cdot \sin\beta \cdot \cos\beta) \cdot \tan\phi - (W_A \cdot \cos\beta - U_A + U_{AH} \cdot \sin\beta) \cdot \sin\beta \cdot \tan\delta \cdot \tan\phi / FS$$

$$(W_A \cdot \sin\beta \cdot \cos\beta + U_{PH} - U_{AH} \cdot \cos^2\beta) \cdot FS^2 - (W_A \cdot \cos\beta - U_{AN} + U_{AH} \cdot \sin\beta) \cdot \cos\beta \cdot \tan\delta \cdot FS = (W_P - U_{PN} + W_A \cdot \sin^2\beta - U_{AH} \cdot \sin\beta \cdot \cos\beta) \cdot \tan\phi \cdot FS - (W_A \cdot \cos\beta - U_A + U_{AH} \cdot \sin\beta) \cdot \sin\beta \cdot \tan\delta \cdot \tan\phi$$

$$(W_A \cdot \sin\beta \cdot \cos\beta + U_{PH} - U_{AH} \cdot \cos^2\beta) \cdot FS^2 - [W_P \cdot \tan\phi + W_A \cdot (\sin^2\beta \cdot \tan\phi + \cos^2\beta \cdot \tan\delta) - U_{AN} \cdot \cos\beta \cdot \tan\delta - U_{PN} \cdot \tan\phi + U_{AH} \cdot \sin\beta \cdot \cos\beta \cdot (\tan\phi - \tan\delta)] \cdot FS + (W_A \cdot \cos\beta - U_A + U_{AH} \cdot \sin\beta) \cdot \sin\beta \cdot \tan\delta \cdot \tan\phi = 0 \tag{13.34}$$

Because $U_H = U_{PH} = U_{AH}$,

$$[W_A \cdot \sin\beta \cdot \cos\beta + U_H \cdot (1 - \cos^2\beta)] \cdot FS^2 - [W_P \cdot \tan\phi + W_A \cdot (\sin^2\beta \cdot \tan\phi + \cos^2\beta \cdot \tan\delta) - U_{AN} \cdot \cos\beta \cdot \tan\delta - U_{PN} \cdot \tan\phi + U_H \cdot \sin\beta \cdot \cos\beta \cdot (\tan\phi - \tan\delta)] \cdot FS + (W_A \cdot \cos\beta - U_{AN} + U_H \cdot \sin\beta) \cdot \sin\beta \cdot \tan\delta \cdot \tan\phi = 0 \tag{13.35}$$

Using $a \cdot x^2 + b \cdot x + c = 0$

The resulting FS can be expressed as

$$FS = \frac{-b \pm (b^2 - 4 \cdot a \cdot c)^{0.5}}{2 \cdot a} \tag{13.36}$$

where

$$a = W_A \cdot \sin\beta \cdot \cos\beta + U_H \cdot (1 - \cos^2\beta)$$

$$b = -[W_P \cdot \tan\phi + W_A \cdot (\sin^2\beta \cdot \tan\phi + \cos^2\beta \cdot \tan\delta) - U_{AN} \cdot \cos\beta \cdot \tan\delta - U_{PN} \cdot \tan\phi + U_H \cdot \sin\beta \cdot \cos\beta \cdot (\tan\phi - \tan\delta)]$$

$$c = (W_A \cdot \cos\beta - U_{AN} + U_H \cdot \sin\beta) \cdot \sin\beta \cdot \tan\delta \cdot \tan\phi$$

$$U_{AN} = \gamma_w \cdot h_w \cdot (H - 0.5\, h_w \cdot \cos\beta)/\tan\beta \tag{13.37}$$

$$U_H = 0.5 \cdot \gamma_w \cdot h_w^2 \tag{13.38}$$

$$U_{PN} = 0.5 \cdot \gamma_w \cdot h_w^2/\tan\beta \tag{13.39}$$

$$W_A = 0.5 \cdot [\gamma \cdot (h - h_w)(2 \cdot H \cdot \cos\beta - h - h_w) + \gamma_{sat} \cdot h_w \cdot (2 \cdot H \cdot \cos\beta - h_w)]/(\sin\beta \cdot \cos\beta) \tag{13.40}$$

$$W_P = 0.5 \cdot [\gamma \cdot (h^2 - h_w^2) + \gamma_{sat} \cdot h_w^2]/(\sin\beta \cdot \cos\beta) \tag{13.41}$$

EXAMPLE 13.4

A 44-ft (13.2-m) high and 3(H):1(V) slope has cover sand with a uniform thickness of 2 ft (0.6 m) at a unit weight of 110 lb/ft^3 (17.3 kN/m^3). The cover sand has a friction angle of 32 degrees and zero cohesion. Seepage occurs parallel to the slope and the seepage water head in the sand layer is 6 inches (0.15 m). The saturated unit weight of sand is 115 lb/ft^3 (18 kN/m^3). The interface friction angle between sand drainage layer and geomembrane is 22 degrees and zero adhesion. What is the factor of safety at a slope of 3(H)-to-1(V)?

Solution The side slope angle is at 18.4° for a 3(H):1(V) slope. Hence,

$\sin\beta = \sin(18.4°) = 0.316$, $\cos\beta = \cos(18.4°) = 0.949$, $\tan\beta = \tan(18.4°) = 0.333$.

$H = 44$ ft (13.2 m), $h = 2$ ft (0.6 m), $h_w = 0.5$ ft (0.15 m), $\gamma = 110$ lb/ft^3 (17.3 kN/m^3),

$\gamma_{sat} = 115$ lb/ft^3 (18 kN/m^3), $\gamma_w = 62.4$ lb/ft^3 (9.81 kN/m^3), $\phi = 32°$, $\delta = 22°$.

$\tan\phi = \tan(32°) = 0.625$, $\tan\delta = \tan(22°) = 0.404$.

$$U_{AN} = \gamma_w \cdot h_w \cdot (H - 0.5\, h_w \cdot \cos\beta)/\tan\beta \tag{13.37}$$
$$= (62.4)(0.5)[44 - (0.5)(0.5)(0.949)]/(0.333) = 4{,}100.3 \text{ lb/ft (58.02 kN/m)}$$

$$U_H = 0.5 \cdot \gamma_w \cdot h_w^2 \tag{13.38}$$
$$= (0.5)(62.4)(0.5)^2 = 7.8 \text{ lb/ft (0.11 kN/m)}$$

$$U_{PN} = 0.5 \cdot \gamma_w \cdot h_w^2/\tan\beta \tag{13.39}$$
$$= (0.5)(62.4)(0.5)^2/(0.333) = 23.4 \text{ lb/ft (0.33 kN/m)}$$

$$W_A = 0.5 \cdot [\gamma \cdot (h - h_w)(2 \cdot H \cdot \cos\beta - h - h_w) + \gamma_{sat} \cdot h_w \cdot (2 \cdot H \cdot \cos\beta - h_w)]/(\sin\beta \cdot \cos\beta) \tag{13.40}$$
$$= (0.5)\{(110)(2 - 0.5)[(2)(44)(0.949) - 2 - 0.5] + (115)(0.5)[(2)(44)(0.949) - 0.5]\}/[(0.316)(0.949)]$$
$$= (0.5)(13{,}366.98 + 4{,}773.19)/[(0.316)(0.949] = 30{,}245.3 \text{ lb/ft (427.6 kN/m)}$$

$$W_P = 0.5 \cdot [\gamma \cdot (h^2 - h_w^2) + \gamma_{sat} \cdot h_w^2]/(\sin\beta \cdot \cos\beta) \tag{13.41}$$
$$= (0.5)\{(110)[(2)^2 - (0.5)^2] + (115)(0.5)^2\}/[(0.316)(0.949)] = 735.7 \text{ lb/ft (10.4 kN/m)}$$

Using Equation 13.36,

$$a = W_A \cdot \sin\beta \cdot \cos\beta + U_H \cdot (1 - \cos^2\beta)$$
$$= (30{,}245.3)(0.316)(0.949) + (7.8)[1 - (0.949)^2] = 9{,}071 \text{ (128 for SI units)}$$

$$b = -[W_P \cdot \tan\phi + W_A \cdot (\sin^2\beta \cdot \tan\phi + \cos^2\beta \cdot \tan\delta) - U_{AN} \cdot \cos\beta \cdot \tan\delta - U_{PN} \cdot \tan\phi + U_H \cdot \sin\beta \cdot \cos\beta \cdot (\tan\phi - \tan\delta)]$$
$$= -\{(735.7)(0.625) + (30{,}245.3)[(0.316)^2(0.625) + (0.949)^2(0.104)] - (4{,}100.3)(0.949)(0.404) - (23.4)(0.625) + (7.8)(0.316)(0.949)(0.625 - 0.404)\}$$
$$= -(459.8 + 12{,}892.1 - 1{,}572.0 - 14.6 + 0.5) = -11{,}766 \text{ (}-166 \text{ for SI units)}$$

$$c = (W_A \cdot \cos\beta - U_{AN} + U_H \cdot \sin\beta) \cdot \sin\beta \cdot \tan\delta \cdot \tan\phi$$
$$= [(30{,}245.3)(0.949) - 4{,}100.3 + (7.8)(0.316)](0.316)(0.625)(0.404) = 1{,}963 \text{ (28 for SI units)}$$

$$FS = \frac{-b \pm (b^2 - 4 \cdot a \cdot c)^{0.5}}{2 \cdot a} \tag{13.36}$$
$$= \frac{11{,}766 + [(-11{,}766)^2 - (4)(9{,}071)(1{,}963)]^{0.5}}{(2)(9{,}071)}$$

FIGURE 13.15 Sand Layer Failure along Sideslope Caused by Seepage Force

$$= \frac{11{,}766 + 8{,}198}{(2)(9{,}071)}$$

$$= 1.10$$

Comment The seriousness of seepage forces in a slope of this type is immediately obvious. Had the saturation been 100% of the drainage layer thickness, the FS-value would have been still lower. Furthermore, the result using a horizontal assumption of saturated cover soil with the same saturation ratio will give essentially identical low *FS*-values. Clearly, the teaching of this example problem is that adequate long-term drainage above the barrier layer in cover soil slopes must be provided to avoid seepage forces from occurring. Figure 13.15 shows a sand layer sliding failure along sideslope caused by seepage force.

An incremental placement method should be implemented for sideslopes higher than the maximum height that can be built in a single lift with a minimum required factor of safety, such as the previous example. Based on the incremental placement method, the first step is to place the sand drainage layer on the sideslope to the maximum unsupported height. As waste is filled against the sideslope to approximately 2 feet (0.6 m) below the protective layer, the next lift of the layer can proceed. This procedure that is illustrated in Figure 13.16 should be continued until the protective layer reaches the top of the sideslope. The heights of the following lifts of the sand drainage layer should not be higher than the calculated maximum unsupported height minus 2

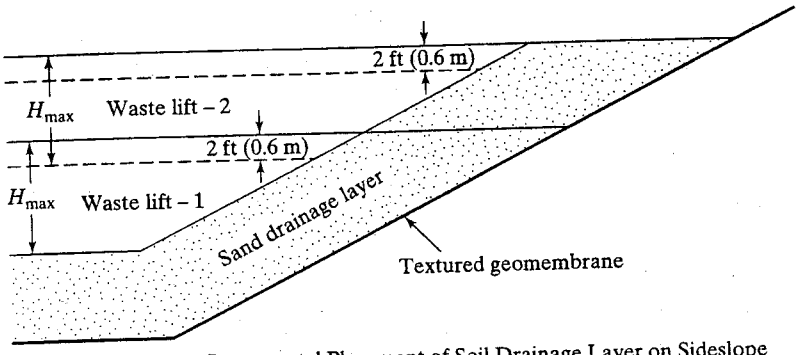

FIGURE 13.16 Incremental Placement of Soil Drainage Layer on Sideslope

feet (0.6 m). The height of the first lift of sand placement can be calculated as shown in the equations that follow (Qian, 1997):

In U.S. units,

$$H = (H_{total} - 2)/n + 2 \tag{13.42}$$

In SI units,

$$H = (H_{total} - 0.6)/n + 0.6 \tag{13.43}$$

where H = height of the first step of sand placement on the sideslope (see Figure 13.14), ft or m;
H_{total} = total height of the cover sand slope from the toe of the cover sand to the top of the slope (see Figure 13.16), ft or m;
n = number of the placement steps.

EXAMPLE 13.5

Continue the calculations of Example 13.4 and use the incremental method to achieve a factor of safety no less than 1.2 for the cover sand resting on the sideslope?

Solution Use the incremental method to place drainage sand on the side slope to achieve a minimum factor of safety of 1.2. Try three steps of sand placement ($n = 3$) on the sideslope.

$$H = (H_{total} - 2)/n + 2 \tag{13.42}$$
$$= (44 - 2)/3 + 2 = 14 + 2 = 16 \text{ ft } (4.8 \text{ m})$$

So,

$H = 16$ ft (4.8 m), $h = 2$ ft (0.6 m), $h_w = 0.5$ ft (0.15 m), $\gamma = 110$ lb/ft^3 (17.3 kN/m^3),
$\gamma_{sat} = 115$ lb/ft^3 (18 kN/m^3), $\gamma_w = 62.4$ lb/ft^3 (9.81 kN/m^3), $\phi = 32°$, $\delta = 22°$.
$\tan\phi = \tan(32°) = 0.625$, $\tan\delta = \tan(22°) = 0.404$,
$\sin\beta = \sin(18.4°) = 0.316$, $\cos\beta = \cos(18.4°) = 0.949$, $\tan\beta = \tan(18.4°) = 0.333$.

$$U_{AN} = \gamma_w \cdot h_w \cdot (H - 0.5\ h_w \cdot \cos\beta)/\tan\beta$$
$$= (62.4)(0.5)[16 - (0.5)(0.5)(0.949)]/(0.333) = 1{,}476.9 \text{ lb/ft } (20.90 \text{ kN/m}) \quad (13.37)$$

$$U_H = 0.5 \cdot \gamma_w \cdot h_w{}^2$$
$$= (0.5)(62.4)(0.5)^2 = 7.8 \text{ lb/ft } (0.11 \text{ kN/m}) \quad (13.38)$$

$$U_{PN} = 0.5 \cdot \gamma_w \cdot h_w{}^2/\tan\beta$$
$$= (0.5)(62.4)(0.5)^2/(0.333) = 23.4 \text{ lb/ft } (0.33 \text{ kN/m}) \quad (13.39)$$

$$W_A = 0.5 \cdot [\gamma \cdot (h - h_w)(2 \cdot H \cdot \cos\beta - h - h_w) + \gamma_{sat} \cdot h_w \cdot (2 \cdot H \cdot \cos\beta - h_w)]/(\sin\beta \cdot \cos\beta)$$
$$= (0.5)\{(110)(2 - 0.5)[(2)(16)(0.949) - 2 - 0.5] + (115)(0.5)[(2)(16)(0.949) - 0.5]\}/[(0.316)(0.949)] \quad (13.40)$$
$$= (0.5)(4{,}598.22 + 1{,}717.41)/[(0.316)(0.949)] = 10{,}530.1 \text{ lb/ft } (148.9 \text{ kN/m})$$

$$W_P = 0.5 \cdot [\gamma \cdot (h^2 - h_w{}^2) + \gamma_{sat} \cdot h_w^2]/(\sin\beta \cdot \cos\beta)$$
$$= (0.5)\{(110)[(2)^2 - (0.5)^2] + (115)(0.5)^2\}/[(0.316)(0.949)] = 735.7 \text{ lb/ft } (10.4 \text{ kN/m}) \quad (13.41)$$

Equation 13.36 yields

$$a = W_A \cdot \sin\beta \cdot \cos\beta + U_H \cdot (1 - \cos^2\beta)$$
$$= (10{,}530.1)(0.316)(0.949) + (7.8)[1 - (0.949)^2] = 3{,}159 \text{ (45 for SI units)}$$

$$b = -[W_P \cdot \tan\phi + W_A \cdot (\sin^2\beta \cdot \tan\phi + \cos^2\beta \cdot \tan\delta) - U_{AN} \cdot \cos\beta \cdot \tan\delta - U_{PN} \cdot \tan\phi + U_H \cdot \sin\beta \cdot \cos\beta \cdot (\tan\phi - \tan\delta)]$$
$$= -\{(735.7)(0.625) + (10{,}530.1)[(0.316)^2(0.625) + (0.949)^2(0.404)] - (1{,}476.9)(0.949)(0.404) - (23.4)(0.625) + (7.8)(0.316)(0.949)(0.625 - 0.404)\}$$
$$= -(459.8 + 4{,}488.5 - 566.2 - 14.6 + 0.5) = -4{,}368 (-62 \text{ for SI units})$$

$$c = (W_A \cdot \cos\beta - U_{AN} + U_H \cdot \sin\beta) \cdot \sin\beta \cdot \tan\delta \cdot \tan\phi$$
$$= [(10{,}530.1)(0.949) - 1{,}476.9 + (7.8)(0.316)](0.316)(0.625)(0.404) = 680 \text{ (10 for SI units)}$$

$$FS = \frac{-b \pm (b^2 - 4 \cdot a \cdot c)^{0.5}}{2 \cdot a} \quad (13.36)$$
$$= \frac{4{,}368 + [(-4{,}368)^2 - (4)(3{,}159)(680)]^{0.5}}{(2)(3{,}159)}$$
$$= \frac{4{,}368 + 3{,}238}{(2)(3{,}159)}$$
$$= 1.20$$

Thus, based on the above calculation, the first step is to place the drainage sand on the sideslope to a height of 16 feet (4.8 m). As waste is filled against the sideslope to approximately 2 feet (0.6 m) below the protective layer, the next lift of 14 feet (4.2 m) can be placed. This procedure should be continued until the protective layer reaches the top of the sideslope.

13.4.4 Inclusion of Seismic Forces

In areas of anticipated earthquake activity, the slope stability analysis of a final cover soil over an engineered landfill, abandoned dump, or remediated site must consider seismic forces. In the United States, the Environmental Protection Agency (EPA)

regulations require such an analysis for sites that have a probability of ≥ 10% of experiencing a 0.10-g peak horizontal acceleration within 250 years. For the continental United States, this includes not only the western states, but major sections of the Midwest and northeast states, as well. If practiced worldwide, such a criterion would have huge implications.

The seismic analysis of cover soils of the type under consideration in this section is a two-part process:

(i) The calculation of a *FS*-value using a pseudostatic analysis via the addition of a horizontal force acting at the centroid of the cover soil cross section.

(ii) If the *FS*-value in the above calculation is less than 1.0, a permanent deformation analysis is required. The calculated deformation is then assessed in light of the potential damage to the cover soil section and is either accepted, or the slope requires an appropriate redesign. The redesign is then analyzed until the situation becomes acceptable.

The *first part* of the analysis is a pseudostatic approach that follows the previous examples except for the addition of a horizontal force at the centroid of the cover soil in proportion to the anticipated seismic activity. It is first necessary to obtain an average seismic coefficient (C_S) from a representative seismic zone map (e.g., as in Algermissen, 1969). Such maps are available on a worldwide basis. The value of C_S is nondimensional and is a ratio of the bedrock acceleration to gravitational acceleration. This value of C_S is modified using available computer codes such as "SHAKE" (see Schnabel et al., 1972) for propagation to the site and then to the landfill cover as shown in Figure 13.17. The computational process within such programs is quite intricate. For detailed discussion, see Seed and Idriss (1982) and Idriss (1990). The analysis is nonetheless similar to those previously presented.

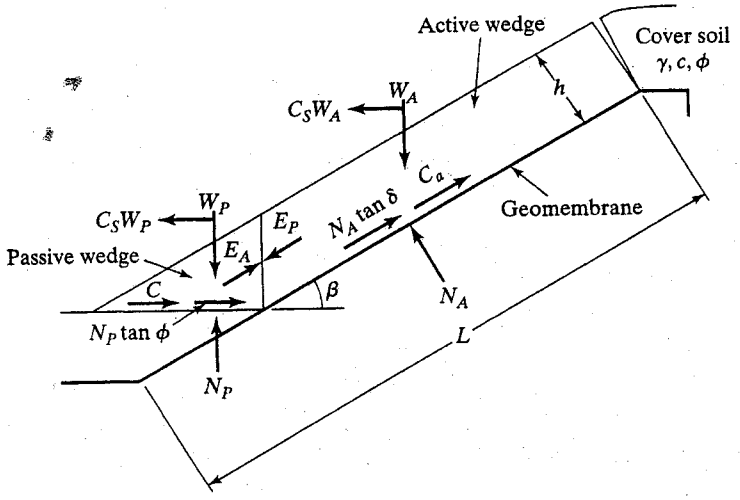

FIGURE 13.17 Limit Equilibrium Forces Involved in Pseudostatic Analysis Using a Average Seismic Coefficient.

Using Figure 13.17, the additional seismic force is $C_S \cdot W_A$ acting horizontally on the active wedge. All additional symbols used in Figure 13.17 have been previously defined, and the expression for finding the *FS*-value is derived next.

Considering the active wedge, by balancing the forces in the horizontal direction, the resulting formulation is

$$E_A \cdot \cos\beta + \frac{(N_A \cdot \tan\delta + C_a) \cdot \cos\beta}{FS} = C_S \cdot W_A + N_A \cdot \sin\beta$$

Hence, the interwedge force acting on the active wedge is

$$E_A = \frac{(FS)(C_S \cdot W_A + N_A \cdot \sin\beta) - (N_A \cdot \tan\delta + C_a) \cdot \cos\beta}{(FS) \cdot \cos\beta}$$

The passive wedge can be considered in a similar manner, and the following formulation results:

$$E_P \cdot \cos\beta + C_S \cdot W_P = \frac{C + N_P \cdot \tan\delta}{FS}$$

Hence, the interwedge force acting on the passive wedge is

$$E_P = \frac{C + W_P \cdot \tan\phi - C_S \cdot W_P \cdot (FS)}{(FS) \cdot \cos\beta - \sin\beta \cdot \tan\phi}$$

Again, by setting $E_A = E_P$, the equation can be arranged in the form of $ax^2 + bx + c = 0$, which in this case is

$$a \cdot FS^2 + b \cdot FS + c = 0$$

The resulting *FS* can be expressed as

$$FS = \frac{-b \pm (b^2 - 4 \cdot a \cdot c)^{0.5}}{2 \cdot a} \tag{13.44}$$

where $a = (C_S \cdot W_A + N_A \cdot \sin\beta) \cdot \cos\beta + C_S \cdot W_P \cdot \cos\beta$

$b = -[(C_S \cdot W_A + N_A \cdot \sin\beta) \cdot \sin\beta \cdot \tan\phi + N_A \cdot \tan\delta + C_a) \cdot \cos^2\beta + (C + W_P \cdot \tan\phi) \cdot \cos\beta]$

$c = (N_A \cdot \tan\delta + C_a) \cdot \sin\beta \cdot \cos\beta \cdot \tan\phi$

Using these concepts, a design curve for the general problem under consideration as a function of seismic coefficient can be developed. (See Figure 13.18.) Note that the curve is developed specifically for the variables stated in the legend. Example 13.6 illustrates the use of the equations and of the curve.

EXAMPLE 13.6

The following are given: a-30-m-long slope with uniform thickness cover soil of 300 mm at a unit weight of 18 kN/m^3. The soil has a friction angle of 30° and zero cohesion (i.e., it is a sand). The cover soil is on a geomembrane as shown in Figure 13.17. Direct shear testing has resulted in an interface friction angle of 22° with zero adhesion. The slope angle is 3(H)-to-1(V)

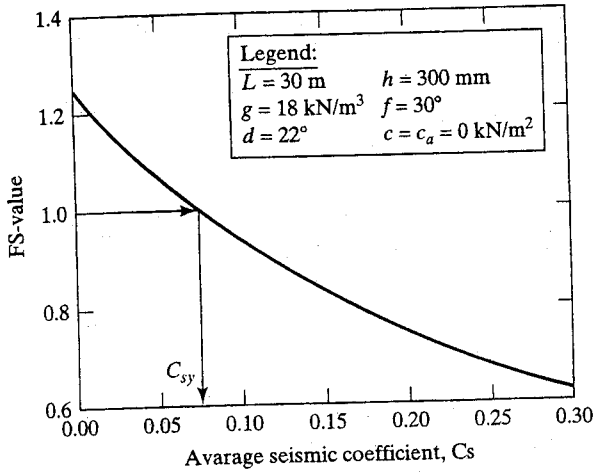

FIGURE 13.18 Design Curve for an Uniformly Thick Cover Soil Pseudostatic Seismic Analysis with Varying Average Seismic Coefficients.

(i.e., 18.4°). A design earthquake appropriately transferred to the site's cover soil results in an average seismic coefficient of 0.10. What is the *FS*-value?

Solution Solving Equation 13.44 for the values

$$a = 59.6 \text{ kN/m}$$
$$b = -66.9 \text{ kN/m}$$
$$c = 10.4 \text{ kN/m}$$

results in $FS = 0.94$

Note that the value of $FS = 0.94$ agrees with the design curve of Figure 13.18 at a seismic coefficient of 0.10.

Comment Had the above *FS*-value been greater than 1.0, the analysis would have been complete. The assumption is that cover soil stability can withstand the short-term excitation of an earthquake and still not slide. However, since the value in this example is less than 1.0, a second part of the analysis is required.

The *second part* of the analysis is directed toward calculating the estimated deformation of the lowest shear-strength interface in the cross section under consideration. The deformation is then assessed in light of the potential damage that may be imposed on the system.

To begin the permanent deformation analysis, a yield acceleration C_{sy} is obtained from a pseudostatic analysis under an assumed $FS = 1.0$. Figure 13.18 illustrates this procedure for the assumptions stated in the legend. It results in a value of $C_{sy} = 0.075$. Coupling this value with the time history response obtained for the actual site location and cross section results in a comparison as shown in Figure 13.19(a). If the earthquake time history response never exceeds the value of C_{sy}, there is no anticipated permanent deformation. However, whenever any part of the time history exceeds the value of C_{sy},

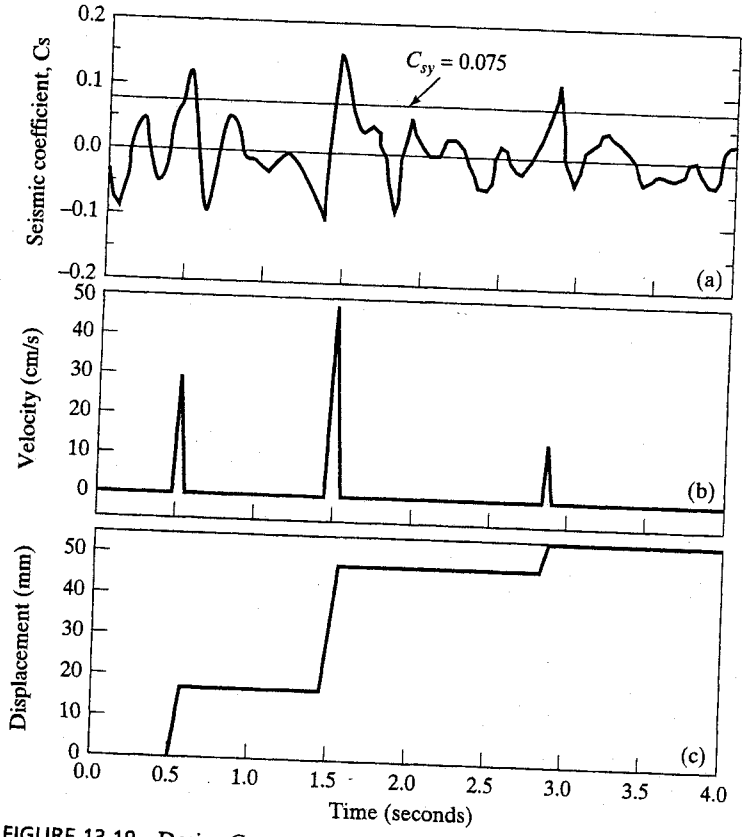

FIGURE 13.19 Design Curves to Obtain Permanent Deformation Utilizing
(a) Acceleration,
(b) Velocity, and
(c) Displacement curves.

permanent deformation is expected. By double integration of the acceleration time history curve to velocity [Figure 13.19(b)], and then to displacement [Figure 13.19(c)], the anticipated value of deformation can be obtained. This value is considered to be permanent deformation and is then assessed based on the site-specific implications of damage to the final cover system. Empirical charts (e.g., Makdisi and Seed, 1978) also can be used to estimate the permanent deformation. Example 13.7 continues the previous pseudostatic analysis into the deformation calculation.

EXAMPLE 13.7

Continue Example 13.6 and determine the anticipated permanent deformation of the weakest interface in the cover soil system. The site-specific seismic time-history diagram is given in Figure 13.19(a).

Solution The interface of concern is the cover soil-to-geomembrane ratio for this particular example. With a yield acceleration of 0.075 from Figure 13.18, and the site-specific design time history shown in Figures 13.19(a), integration produces Figure 13.19(b) and then 13.19(c). The three peaks exceeding the yield acceleration value of 0.075 produce a cumulative deformation of approximately 54 mm (2.1 inches). This value is now viewed in light of the deformation capability of the cover soil above the particular interface used at the site. Note that some references limit the deformation to either 100 or 300 mm (4 to 12 inches), depending on site-specific situations. (See Richardson et al., 1995.)

Comments An assessment of the implications of deformation [in this example it is 54 mm (2.1 inches)] is very subjective. For example, this problem could easily have been framed to produce much higher permanent deformation. Such deformation can readily be envisioned in high seismic-prone areas. (See Anderson and Kavazajian, 1995, and Matasovic et al., 1995.) Discussion is ongoing in this regard. In addition to an assessment of cover soil stability, the concerns for appurtenances and ancillary piping must also be addressed.

13.4.5 General Remarks

As seen from the previous analytic development and examples in this section, veneer slope failures are fully capable of being evaluated and, as such, of being avoided. Unfortunately, many failures of this type exist and the literature is abundantly clear in this regard (e.g., Thiel and Steward, 1993; McKelvey, 1994; Giroud et al., 1995a and 1995b).

Whatever analysis is selected by the designer (the foregoing followed that of Koerner and Soong, 1998; and Qian, 1997), the following items are overriding considerations:

(i) Proper assessment of interface shear strengths is critically necessary.

(ii) The designer must make a reasonable estimate of the equipment and the contractor's practice used to construct the system.

(iii) The designer must make a proper assessment of the design storm event.

(iv) A proper assessment of the design seismic event is necessary assuming that the site is in a potentially seismically active area.

It should also be noted that the designer has a number of alternatives with which to make a given slope stable. A higher factor of safety can result by modifying the geometry, adding downslope soil berms, or including veneer reinforcement. See Koerner and Soong (1998) for an extension of the methodology of this section into these various stabilizing considerations.

13.5 SUBSOIL FOUNDATION FAILURES

Designers regularly perform calculations to verify the safety of natural slopes, excavated slopes, and constructed embankments. These procedures are directly applicable to the design and analysis of solid waste materials that are placed in landfills [recall Figures 13.1(c), (d) and (e)]. Such calculations serve as a basis for choosing either

waste slope angles and waste slope lengths with specified factor-of-safety (*FS*) values before waste placement, or for the redesign after obtaining an unacceptable value or analyzing a failure. The procedure involves determining the shear stresses developed along the most critical failure surface and comparing them with the shearing resistances of the materials through which the surface passes. The entire procedure is called a slope stability analysis and it is well developed in the geotechnical engineering literature (e.g., see Sherard et al., 1963; Hirschfield and Poulos, 1973; and others).

13.5.1 Method of Analysis

By far, the majority of slope stability procedures that are performed are based on two-dimensional (2-D) cross sections and analyses. Using such procedures, there are many analysis methods, but all assume that the critical cross section resulting in the lowest *FS*-value can be identified. Since numerous iterations are invariably required, computer codes are commonplace in order to identify the critical cross section. A cross section of a circular arc failure is shown in Figure 13.20(a). In the conventional manner, it is subdivided into n-slices where the i^{th} slice is shown in Figure 13.20(b). From this point, a number of different calculation methods can be followed.

For the analysis of the case histories to follow which failed along a circular arc, the simplified Bishop method was used, see Koerner and Soong (2000). The derivation is readily available and leads to the following equation for the FS-value:

$$FS = \frac{\sum_{i=1}^{n} [c \cdot \Delta b_i + (W_i - u_i \cdot \Delta b_i) \cdot \tan\phi]/m_i}{\sum_{i=1}^{n} W_i \cdot \sin\theta_i} \tag{13.45}$$

Here,

$$m_i = \cos\theta_i \cdot (1 + \tan\phi \cdot \tan\theta_i / FS) \tag{13.46}$$

See Figure 13.20 for definitions of the terms.

13.5.2 Case Histories

To illustrate the importance of assessing the subgrade soil upon which the waste mass is to be placed, three case histories of failures are presented next. All were circular-arc-type failures initiating in the soft foundation soils beneath the solid waste and then propagating up through the waste mass itself.

Case History R-1

Case history R-1 is a municipal solid waste landfill that failed in 1984. The failure was rotational and involved approximately 110,000 m^3 of solid waste. Divinoff and Munion (1986) and Erdogan et al., (1986) have reported on this case history.

Background. The municipal solid waste (MSW) landfill site in this case history covered 22 ha. It was bounded on three sides by a tidal marsh. The landfill was in operation for approximately 15 years and rose 44 m above the marsh at its highest location. The side

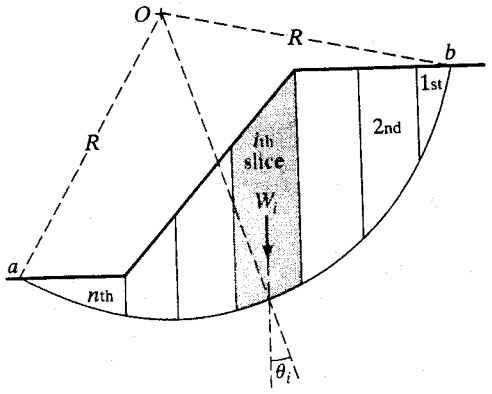

(a) Cross section

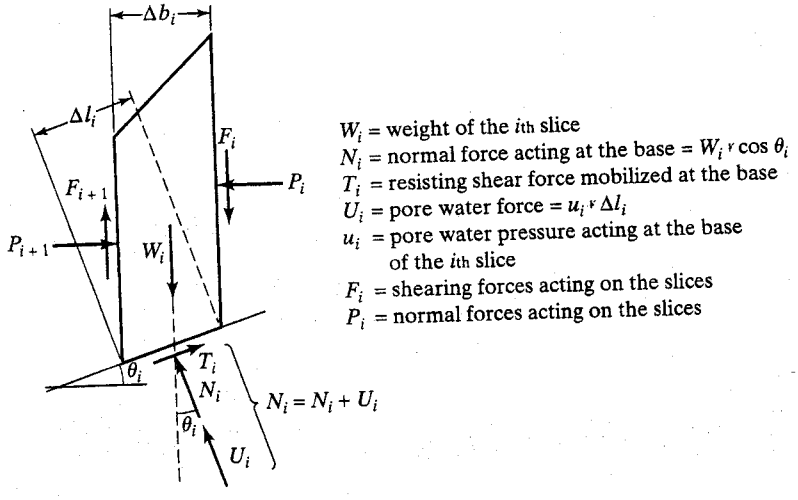

(b) Force acting on the ith slice

FIGURE 13.20 Procedure Showing Circular Arc Subdivided into Slices and Analysis of the i^{th} Slice

slopes were generally 4(H)-to-1(V) and a small toe berm was constructed around the edge of the slope. The development of a particular portion of the site was such that waste placement was temporarily postponed because a small stream entered the landfill at this location. Eventually, this area was filled and waste was placed quite rapidly (in 4 or 5 months) just before the failure occurred; it was the eventual location of the failure.

Description of Failure. Approximately 70 mm of rain fell for three days prior to the failure, which caused the water level of the adjacent marsh to rise approximately 3.2 m. A near-vertical crack opened at the top of the waste, eventually measuring 12-m deep, 18-m wide, and 180-m long(see Figure 13.21). The opening was crescent-shaped in plan view conforming closely to the ground contours before waste was placed at the

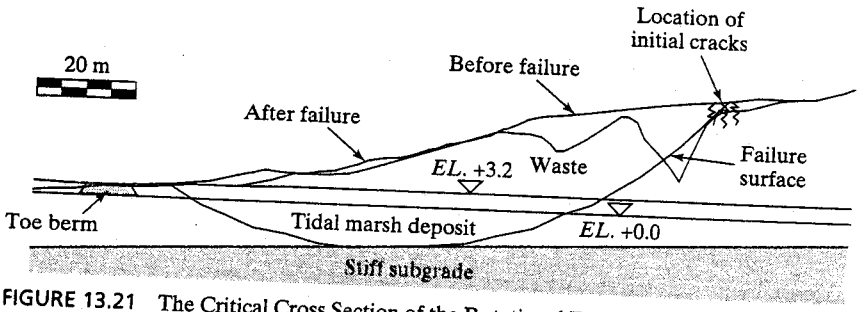

FIGURE 13.21 The Critical Cross Section of the Rotational Failure Surface (after Divinoff and Munion, 1986)

location. Subsidiary cracks opened down-slope in the moving waste mass as failure occurred. The toe berm was lifted several meters and was severely distorted as it moved in front of the failing waste mass, which extended for approximately 60 m. The critical cross section is shown in Figure 13.21. Note the difference in liquid level within the waste mass as just described.

Foundation Soil Conditions. The thickness of the tidal marsh beneath the waste was variable, but it can be described as having a 3-m surface crust (called "meadow mat") consisting of fine sand, silt, brick fragments, roots and decomposed solid waste. Some 7 to 12 m of silty clay/clayey silt with water content of 88% to 117% and undrained shear strength of 4.3 to 12.5 kPa was beneath the meadow mat. Stiff, dense silty fine sand was beneath the tidal marsh and its upper surface eventually formed the tangent point for the circular arc failure in the overlying tidal marsh and waste mass.

Waste Condition. The waste was placed directly on the meadow mat. There was neither a liner nor a leachate collection system in use at this landfill. Compaction of the waste was only nominal and a relatively low unit weight of 10.2 kN/m^3 was estimated. The shear strength of the waste was unknown, although Divinoff and Munion (1986) found by back analysis that an undrained strength of 37 kPa resulted in an $FS = 1.0$. The waste mass during its time of placement and before the failure was acting as a surcharge on the tidal marsh, which resulted in some (unknown) amount of consolidation.

Case History R-2

Case history R-2 is a municipal waste landfill that failed in 1989. The failure was multirotational in nature and involved approximately 500,000 m^3 of solid waste. Reynolds (1991) and Richardson and Reynolds (1990) have reported on the case history.

Background. The operation of the landfill site in this case history began in the 1970's. It was started as a relatively small, commercially-operated, municipal solid waste disposal site. Over the years, the facility was expanded and incorporated additional waste piles of ash/sludge and asbestos. The landfill was an above-grade landfill and was underlain with a thick deposit of clayey soil.

To the west of the site, work was starting on an expansion to the existing landfill. The expanded area was to be lined with a composite liner system consisting of a geomembrane overlying a 0.6-m-thick layer of recompacted clay. In order to facilitate

the liner system construction and to increase the capacity of the future landfill, the plans called for the removal of up to 3 m of the upper stiff clay in the expansion area. Such excavation activity eventually became the triggering mechanism of the landfill failure.

Description of Failure. On August 14, 1989, after approximately 120 mm of rain fell for 10 days prior to the incident, a multirotational slope failure occurred toward and into the proposed landfill expansion area west of the existing landfill. During the movement, six large crevasses (one after the other) opened up in the waste mass. Figure 13.22(a) shows the critical cross section of the failed landfill. The entire movement lasted about 15 seconds. Analysis of the failure indicated that a single rotational failure first occurred under the original landfill slope as in Figure 13.22(a). This initial failure left a steep, unsupported slope within the remaining waste pile and the underlying clay. This directly led to five sequential slides of similar types progressing eastward into the existing landfill mass. Blocks of waste and clay followed the direction of the initial movement. As seen in Figure 13.22(b), the blocks formed progressively from the west to the east and moved horizontally as much as 50 m. Some of the crevasses were approximately 15-m wide and up to 10-m deep. Traces of remolded clay were discovered up to 120 m beyond the original toe of the landfill. Due to the remolding, the clay lost 80 to 90% of its original undrained shear strength.

Foundation Soil Conditions. The landfill in this case history is underlain by 15 to 21 m of clayey soil. The top 3 m of the thick clay deposit is weathered and fissured and is designated as a stiff clay. Below the stiff clay, there is the soft clay zone with thickness

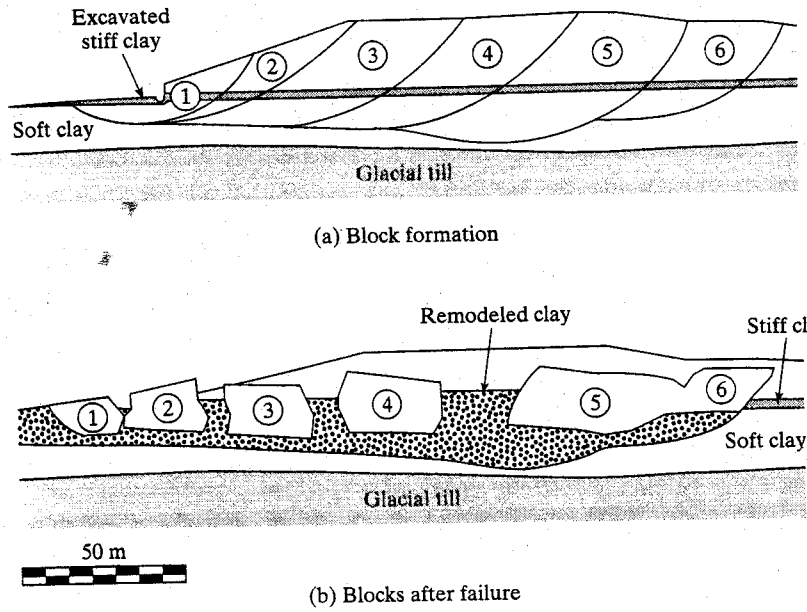

FIGURE 13.22 Critical Cross Section of Landfill R-2 Showing the "Block" Formation (after Reynold, 1991)

varying from 12 to 18 meters. The vertical permeability of this zone is in the range of 10^{-7} to 10^{-8} cm/sec. Laboratory tests conducted prior to the failure indicated undrained shear strength (cohesion) of approximately 20 kPa for the underlying soft clayey soil. (See Reynolds, 1991; and Richardson and Reynolds, 1990.)

Waste Condition and Placement. Based on an estimated unit weight of waste of 5.8 kN/m^3, a height limitation of 16.8 m was originally set on the existing MSW landfill in mid-1986. By mid-1987, the landfill reached a height of approximately 12.2 m. Data obtained at that point indicated a waste unit weight of 12.2 kN/m^3. This is probably due to a higher compactive effort and the heavy (sand and gravel) daily cover material. While the increased unit weight of the waste worked against the slope stability, the strength gain due to the consolidation of the clayey soil permitted a gradual increase in the height of the landfill. As a result, by early 1989, the MSW landfill actually exceeded the height limitation to a value of 18.3 m. After the occurrence of the failure, several large pits of undisturbed waste were excavated and the removed material was weighed. The pit dimensions were also measured to determine the actual volumes for calculating the actual unit weight of the waste. The average of ten such tests produced a value of 14.7 kN/m^3. As to the shear strength parameters of the municipal solid waste, values of 17 kPa for cohesion and 20° for friction angle were determined, Reynolds (1991).

Case History R-3

Case History R-3 is a contaminated soil landfill expansion that failed in 1995 and involved approximately 110,000 m^3. De Santayana and Pinto (1998) have reported on the case history.

Background. The site is adjacent to a major river and was first used for soil disposal beginning in 1970. Disposal was directly on top of the in-situ estuarine and alluvial soft clay deposit. Landfilling commenced in 1985 and then ceased in 1990. The area was 17 ha in area and the height was approximately 15 m. A lateral expansion was then necessary consisting of an additional 7.5 ha. This was the eventual area that failed.

The foundation soil profile at the expansion site consisted of (from top to bottom); (i) a 4- to 5-m-thick, silty-clay fill layer, (ii) a 20- to 25-m-thick estuarine and alluvial soft clay deposit, (iii) a thin, irregular, sometimes absent, basal sand and gravel deposit, and (iv) bedrock, consisting of alternating layers mainly of sandy limestone and calcareous sandstone.

The Lining System. Due to the nature of the contaminated soils being placed in the landfill, a lining system with leachate collection capability was designed and constructed. A perimeter berm surrounding the three-cell area was first constructed and then the lining system was constructed. The lining system consisted of (from bottom to top) (i) a granular drainage layer for collection of consolidation water, (ii) a geotextile filter, (iii) a 0.5-m-thick compacted clay liner, (iv) a geosynthetic clay liner, (v) a 1.5-mm-thick, high-density polyethylene liner, and (vi) a leachate collection layer composed of a geonet drainage layer, a geotextile filter, and 0.3 m of a granular protective layer.

Description of the Failure. After two minor indications of instability were observed (as evidenced by tension cracks on top of the waste), a major failure occurred on June 25,

1995. About 110,000 m^3 failed with a front length of about 270 m, affecting the area loaded with contaminated soils. (See Figure 13.23.) The area within the tension cracks suddenly sank several meters and moved towards the river. At the top of the slide mass, two main scarps appeared several meters apart. The failure surface was clearly visible at the scarps and was almost vertical. It resulted in a settlement of about 4 m and a horizontal movement of several meters toward the river. The geosynthetic materials were visibly torn at the scarps. There were numerous minor cracks, particularly at both sides of the area affected by the slide, and they were mostly parallel arranged, with opening widths of about a few centimeters to several decimeters.

The slide extended well into the river, propagating before it an undulating shape of mud waves and depressions. The east berm of the cells, situated approximately in the middle zone of the slide mass, underwent little vertical movement, but significant horizontal displacement towards the river occured. The berm was clearly displaced at the south side of the slide, and consequently, the pipes installed under the berm (underdrain pipes) and in the berm (leachate force main) were also broken.

Analysis of the Failure. According to de Santayna and Pinto (1998), the strength of the soft clay was overestimated in the original design. The soft clay layer was considered to

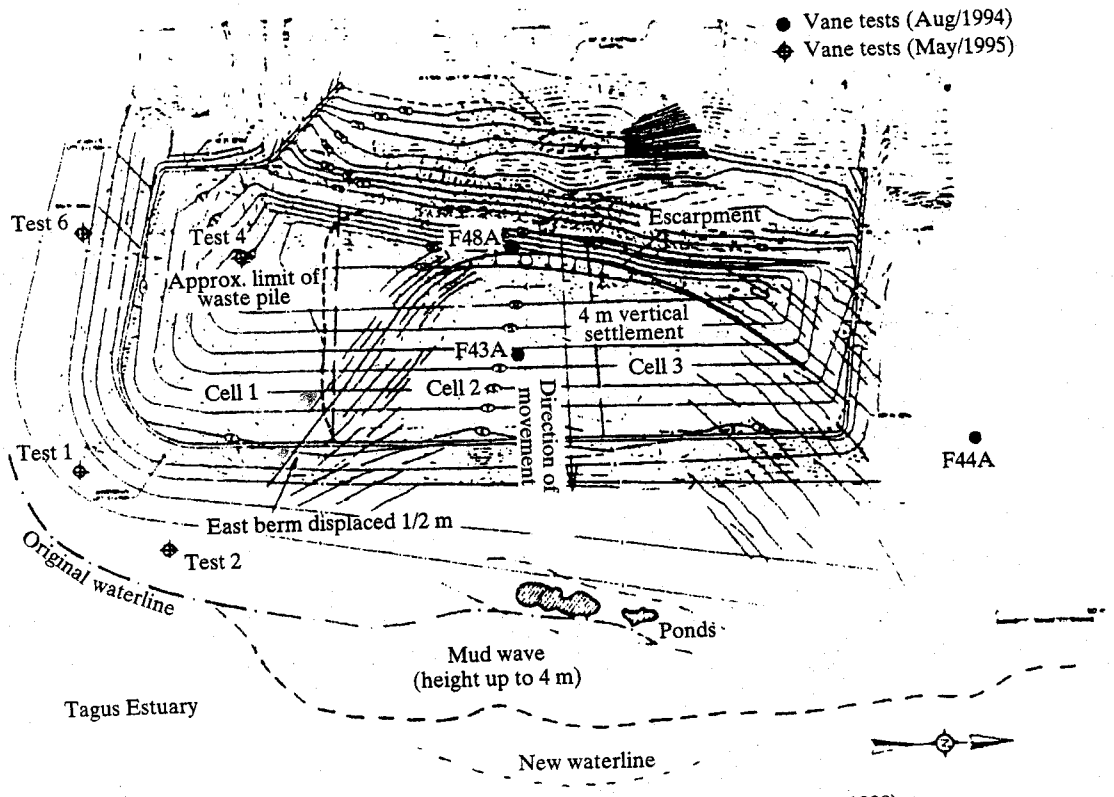

FIGURE 13.23 Plan View of Case History R-3 (after de Santayana and Pinto, 1998)

be normally consolidated under the surcharge of about 4 m of fill. The soft clay layer, however, was underconsolidated below the fill layer. The excess pore pressures caused by the placement of the fill in the 1970s and 1980s had experienced very little dissipation—particularly between elevations of −10 and −20 m—at the time waste placement started. In the middle zone of the soft clay layer, the difference between the actual undrained strength and the one used in the stability analyses was of the order of 10 kN/m^2. The original short-term stability analysis did not consider the possibility of failure surfaces extending to the river (like the one that actually happened), where there was no fill layer over the soft clay, and, hence, the soft clay did not have the undrained strength assumed in the stability calculations.

As noted, this case history had a geosynthetic lining system that failed along with the rotational movement. However, the lining system could not (and was not) a contributing issue to the failure. The little reinforcement benefit that may have been provided by the geosynthetic layer is negligible in the context of this large of a waste mass. This, as with the previous two case histories, was completely a geotechnical-related failure of the classical rotational failure mode except now a portion of the failure surface passes through waste materials.

13.5.3 General Remarks

It should be obvious from these three case histories that proper site characterization during the design stage and well before waste placement is critical. Irrespective of the high shear strength of waste materials, if the soil foundation fails, it will eventually propagate through the waste mass and cause the entire system to fail. Once a crack is observed on the surface of the waste mass, the entire failure surface beneath it has been mobilized. Failure of the mass is then imminent.

The situation is obviously important when dealing with soft, fine-grained soils. Typically, but certainly not always, such soils are near rivers, harbors, and estuaries. Best available geotechnical practice must be followed (recall Section 13.3.3). Even beyond site investigation, laboratory testing, and design which lead to site-specific plans and specifications, one should consider field instrumentation. Piezometers placed in the subsoil and inclinometers placed at the toe of the waste slope (and beyond) could be most valuable in providing an instantaneous assessment of the landfill as waste is being placed. Unfortunately, such instrumentation is rarely provided, even for sensitive site situations.

13.6 WASTE MASS FAILURES

The relatively low interface shear strengths of components within liner systems can lead to translational failures of the type shown in Figure 13.1(f). However, failure can only occur if the toe of the waste mass is unsupported by an opposing slope or large soil berm. Unfortunately, unsupported toe conditions are often the case. Canyon landfills are very common in areas of mountainous or rolling topography. Even when an excavation is dug for a landfill, the waste mass during filling is generally left unsupported at its toe. This section deals with the instability of such situations.

13.6.1 Translational Failure Analysis

While the approach to translational failures is generally similar to that described in Section 13.5.1, the failure surface is not circular, but usually piecewise linear. Thus, the simplified Bishop method is not applicable. A translational (or two-wedge) failure analysis is used to calculate the factor of safety for the landfill against possible mass movement of the type of "translational (or wedge) failure along liner" [Figure 13.1(f)] in the interim filling condition.

The waste mass shown in Figure 13.24(a) can be divided into two discrete parts, one active wedge lying on the side slope and tending to cause failure, and another passive wedge lying on the cell bottom floor and tending to resist failure. The forces acting on the active and passive wedges are shown in Figure 13.24(a). The individual forces, friction angles, and slope angles involved in the analysis are listed as follows:

W_P = weight of the passive wedge;
N_P = normal force acting on the bottom of the passive wedge;
F_P = frictional force acting on the bottom of the passive wedge (parallel to the bottom of the passive wedge);
E_{HP} = normal force from the active wedge acting on the passive wedge (unknown in magnitude, but with the direction perpendicular to the interface of the active and passive wedges);

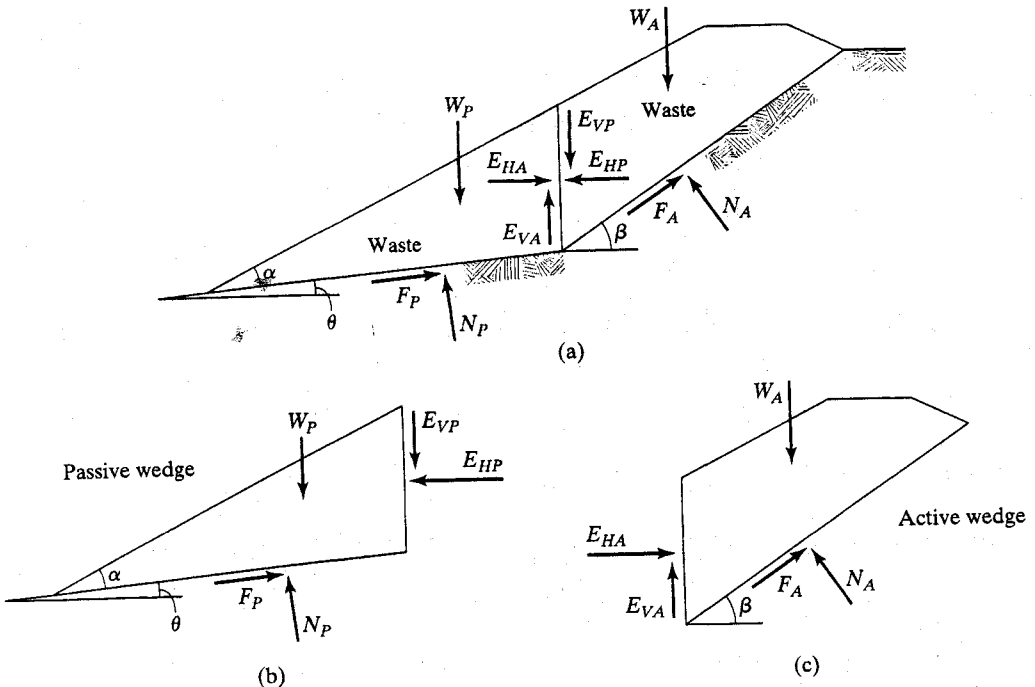

FIGURE 13.24 Forces Acting on Two adjacent Wedges for Solid Waste Filled in Landfill

E_{VP} = frictional force acting on the side of the passive wedge (unknown in magnitude, but with the direction parallel to the interface of the active and passive wedges);
FS_P = factor of safety for the passive wedge;
δ_P = minimum interface friction angle of multi-layer liner components beneath the passive wedge;
ϕ_s = friction angle of the solid waste;
α = angle of the solid waste slope, measured from horizontal, degrees;
θ = angle of the landfill cell subgrade, measured from horizontal, degrees;
W_A = weight of the active wedge;
W_T = total weight of the active and passive wedges;
N_A = normal force acting on the bottom of the active wedge;
F_A = frictional force acting on the bottom of the active wedge (parallel to the bottom of the active wedge);
E_{HA} = normal force from passive wedge acting on the active wedge (unknown in magnitude, but with the direction perpendicular to the interface of the active and passive wedges), $E_{HA} = E_{HP}$;
E_{VA} = frictional force acting on the side of the active wedge (unknown in magnitude, but with the direction parallel to the interface of the active and passive wedges), $E_{VA} = E_{VP}$;
FS_A = factor of safety for the active wedge;
δ_A = minimum interface friction angle of multi-layer liner components beneath the active wedge;
β = angle of the side slope, measured from horizontal, degrees;
FS = factor of safety for the entire solid waste mass.

Considering the force equilibrium of the passive wedge [Figure 13.24(b)], the forces acting on it are

$\Sigma F_Y = 0$:

$$W_P + E_{VP} = N_P \cdot \cos\theta + F_P \cdot \sin\theta \tag{13.47}$$

$$F_P = N_P \cdot \tan\delta_P / FS_P \tag{13.48}$$

$$E_{VP} = E_{HP} \cdot \tan\phi_s / FS_P \tag{13.49}$$

Substituting Equations 13.48 and 13.49 into Equation 13.47 gives

$$W_P + E_{HP} \cdot \tan\phi_s / FS_P = N_P \cdot (\cos\theta + \sin\theta \cdot \tan\delta_P / FS_P), \text{ and} \tag{13.50}$$

when $\Sigma F_X = 0$,

$$F_P \cdot \cos\theta = E_{HP} + N_P \cdot \sin\theta \tag{13.51}$$

Substituting Equation (13.48) into Equation (13.51) gives

$$N_P \cdot \cos\theta \cdot \tan\delta_P / FS_P = E_{HP} + N_P \cdot \sin\theta$$

$$N_P \cdot (\cos\theta \cdot \tan\delta_P / FS_P - \sin\theta) = E_{HP}$$

$$N_P = \frac{E_{HP}}{\cos\theta \cdot \tan\delta_P/FS_P - \sin\theta} \tag{13.52}$$

Substituting Equation 13.52 into Equation 13.50 gives

$$W_P + E_{HP} \cdot \tan\phi_s/FS_P = \frac{E_{HP} \cdot (\cos\theta + \sin\theta \cdot \tan\delta_P/FS_P)}{\cos\theta \cdot \tan\delta_P/FS_P - \sin\theta}$$

$$E_{HP} \cdot (\cos\theta + \sin\theta \cdot \tan\delta_P/FS_P) = W_P \cdot (\cos\theta \cdot \tan\delta_P/FS_P - \sin\theta) + E_{HP} \cdot (\cos\theta \cdot \tan\delta_P/FS_P - \sin\theta) \cdot \tan\phi_s/FS_P$$

$$E_{HP} \cdot (\cos\theta + \sin\theta \cdot \tan\delta_P/FS_P - \cos\theta \cdot \tan\delta_P \cdot \tan\phi_s/FS_P^2 + \sin\theta \cdot \tan\phi_s/FS_P) = W_P \cdot (\cos\theta \cdot \tan\delta_P/FS_P - \sin\theta)$$

$$E_{HP} = \frac{W_P \cdot (\cos\theta \cdot \tan\delta_P/FS_P - \sin\theta)}{\cos\theta + (\tan\delta_P + \tan\phi_s) \cdot \sin\theta/FS_P - \cos\theta \cdot \tan\delta_P \cdot \tan\phi_s/FS_P^2} \tag{13.53}$$

Considering the force equilibrium of the active wedge [Figure 13.12(c)] yields

$\Sigma F_Y = 0$:

$$W_A = F_A \cdot \sin\beta + N_A \cdot \cos\beta + E_{VA} \tag{13.54}$$

$$F_A = N_A \cdot \tan\delta_A/FS_A \tag{13.55}$$

$$E_{VA} = E_{HA} \cdot \tan\phi_s/FS_A \tag{13.56}$$

Substituting Equations 13.55 and 13.56 into Equation 13.54 gives

$$W_A = N_A \cdot (\cos\beta + \sin\beta \cdot \tan\delta_A/FS_A) + E_{HA} \cdot \tan\phi_s/FS_A \tag{13.57}$$

$\Sigma F_X = 0$:

$$F_A \cdot \cos\beta + E_{HA} = N_A \cdot \sin\beta \tag{13.58}$$

Substituting Equation 13.55 into Equation 13.58 gives

$$E_{HA} = N_A \cdot (\sin\beta - \cos\beta \cdot \tan\delta_A/FS_A)$$

$$N_A = \frac{E_{HA}}{\sin\beta - \cos\beta \cdot \tan\delta_A/FS_A} \tag{13.59}$$

Substituting Equation 13.59 into Equation 13.57 gives

$$W_A = E_{HA} \cdot \frac{\cos\beta + \sin\beta \cdot \tan\delta_A/FS_A}{\sin\beta - \cos\beta \cdot \tan\delta_A/FS_A} + E_{HA} \cdot \tan\phi_S/FS_A$$

$$E_{HA} \cdot \frac{\cos\beta + \sin\beta \cdot \tan\delta_A/FS_A + \sin\beta \cdot \tan\phi_s/FS_A - \cos\beta \cdot \tan\delta_A \cdot \tan\phi_s/FS_A^2}{\sin\beta - \cos\beta \cdot \tan\delta_A/FS_A} = W_A$$

$$E_{HA} = \frac{W_A \cdot (\sin\beta - \cos\beta \cdot \tan\delta_A/FS_A)}{\cos\beta + (\tan\delta_A + \tan\phi_s) \cdot \sin\beta/FS_A - \cos\beta \cdot \tan\delta_A \cdot \tan\phi_s/FS_A^2} \tag{13.60}$$

Because $E_{HA} = E_{HP}$ and $FS_A = FS_P = FS$, Equation 13.60 must equal Equation 13.53, giving

$$\frac{W_A \cdot (\sin\beta - \cos\beta \cdot \tan\delta_A / FS)}{\cos\beta + (\tan\delta_A + \tan\phi_s) \cdot \sin\beta / FS - \cos\beta \cdot \tan\delta_A \cdot \tan\phi_s / FS^2} = \frac{W_P \cdot (\cos\theta \cdot \tan\delta_P / FS - \sin\theta)}{\cos\theta + (\tan\delta_P + \tan\phi_s) \cdot \sin\theta / FS - \cos\theta \cdot \tan\delta_P \cdot \tan\phi_s / FS^2}$$

$$W_A \cdot (\sin\beta - \cos\beta \cdot \tan\delta_A / FS)[\cos\theta + (\tan\delta_P + \tan\phi_s) \cdot \sin\theta / FS - \cos\theta \cdot \tan\delta_P \cdot \tan\phi_s / FS^2]$$
$$= W_P \cdot (\cos\theta \cdot \tan\delta_P / FS - \sin\theta)[\cos\beta + (\tan\delta_A + \tan\phi_s) \cdot \sin\beta / FS - \cos\beta \cdot \tan\delta_A \cdot \tan\phi_s / FS^2]$$

$$(W_A \cdot \sin\beta - W_A \cdot \cos\beta \cdot \tan\delta_A / FS)[\cos\theta + (\tan\delta_P + \tan\phi_s) \cdot \sin\theta / FS - \cos\theta \cdot \tan\delta_P \cdot \tan\phi_s / FS^2]$$
$$= (W_P \cdot \cos\theta \cdot \tan\delta_P / FS - W_P \cdot \sin\theta)[\cos\beta + (\tan\delta_A + \tan\phi_s) \cdot \sin\beta / FS - \cos\beta \cdot \tan\delta_A \cdot \tan\phi_s / FS^2]$$

$$W_A \cdot \sin\beta \cdot \cos\theta + W_A \cdot (\tan\delta_P + \tan\phi_s) \cdot \sin\beta \cdot \sin\theta / FS - W_A \cdot \sin\beta \cdot \cos\theta \cdot \tan\delta_P \cdot \tan\phi_s / FS^2$$
$$- W_A \cdot \cos\beta \cdot \cos\theta \cdot \tan\delta_A / FS - W_A \cdot (\tan\delta_P + \tan\phi_s) \cdot \cos\beta \cdot \sin\theta \cdot \tan\delta_A / FS^2$$
$$+ W_A \cdot \cos\beta \cdot \cos\theta \cdot \tan\delta_A \cdot \tan\delta_P \cdot \tan\phi_s / FS^3 = W_P \cdot \cos\beta \cdot \cos\theta \cdot \tan\delta_P / FS$$
$$+ W_P \cdot (\tan\delta_A + \tan\phi_s) \cdot \sin\beta \cdot \cos\theta \cdot \tan\delta_P / FS^2 - W_P \cdot \cos\beta \cdot \cos\theta \cdot \tan\delta_A \cdot \tan\delta_P \cdot \tan\phi_s / FS^3$$
$$- W_P \cdot \cos\beta \cdot \sin\theta - W_P \cdot (\tan\delta_A + \tan\phi_s) \cdot \sin\beta \cdot \sin\theta / FS + W_P \cdot \cos\beta \cdot \sin\theta \cdot \tan\delta_A \cdot \tan\phi_s / FS^2$$

$$(W_A \cdot \sin\beta \cdot \cos\theta + W_P \cdot \cos\beta \cdot \sin\theta) \cdot FS^3 + [W_A \cdot (\tan\delta_P + \tan\phi_s) \cdot \sin\beta \cdot \sin\theta$$
$$+ W_P \cdot (\tan\delta_P + \tan\phi_s) \cdot \sin\beta \cdot \sin\theta - W_A \cdot \cos\beta \cdot \cos\theta \cdot \tan\delta_A - W_P \cdot \cos\beta \cdot \cos\theta \cdot \tan\delta_P] \cdot FS^2$$
$$- [W_A \cdot (\tan\delta_P + \tan\phi_s) \cdot \cos\beta \cdot \sin\theta \cdot \tan\delta_A + W_P \cdot (\tan\delta_A + \tan\phi_s) \cdot \sin\beta \cdot \cos\theta \cdot \tan\delta_P$$
$$+ W_A \cdot \sin\beta \cdot \cos\theta \cdot \tan\delta_P \cdot \tan\phi_S + W_P \cdot \cos\beta \cdot \sin\theta \cdot \tan\delta_A \cdot \tan\phi_s] \cdot FS$$
$$+ (W_A \cdot \cos\beta \cdot \cos\theta \cdot \tan\delta_A \cdot \tan\delta_P \cdot \tan\phi_s + W_P \cdot \cos\beta \cdot \cos\theta \cdot \tan\delta_A \cdot \tan\delta_P \cdot \tan\phi_s) = 0$$

$$(W_A \cdot \sin\beta \cdot \cos\theta + W_P \cdot \cos\beta \cdot \sin\theta) \cdot FS^3 + [(W_A \cdot \tan\delta_P + W_P \cdot \tan\delta_A + W_T \cdot \tan\phi_s) \cdot \sin\beta \cdot \sin\theta$$
$$- (W_A \cdot \tan\delta_A + W_P \cdot \tan\delta_P) \cdot \cos\beta \cdot \cos\theta] \cdot FS^2 - [W_T \cdot \tan\phi_s \cdot (\sin\beta \cdot \cos\theta \cdot \tan\delta_P$$
$$+ \cos\beta \cdot \sin\theta \cdot \tan\delta_A) + (W_A \cdot \cos\beta \cdot \sin\theta + W_P \cdot \sin\beta \cdot \cos\theta) \cdot \tan\delta_A \cdot \tan\delta_P] \cdot FS$$
$$+ W_T \cdot \cos\beta \cdot \cos\theta \cdot \tan\delta_A \cdot \tan\delta_P \cdot \tan\phi_s = 0 \tag{13.61}$$

Equation 13.61 is now solved as follows:

$$a \cdot FS^3 + b \cdot FS^2 + c \cdot FS + d = 0 \tag{13.62}$$

$$a = W_A \cdot \sin\beta \cdot \cos\theta + W_P \cdot \cos\beta \cdot \sin\theta$$
$$b = (W_A \cdot \tan\delta_P + W_P \cdot \tan\delta_A + W_T \cdot \tan\phi_s) \cdot \sin\beta \cdot \sin\theta - (W_A \cdot \tan\delta_A + W_P \cdot \tan\delta_P) \cdot \cos\beta \cdot \cos\theta$$
$$c = -[W_T \cdot \tan\phi_s \cdot (\sin\beta \cdot \cos\theta \cdot \tan\delta_P + \cos\beta \cdot \sin\theta \cdot \tan\delta_A) + (W_A \cdot \cos\beta \cdot \sin\theta + W_P \cdot \sin\beta \cdot \cos\theta) \cdot \tan\delta_A \cdot \tan\delta_P]$$
$$d = W_T \cdot \cos\beta \cdot \cos\theta \cdot \tan\delta_A \cdot \tan\delta_P \cdot \tan\phi_s$$

When the cell subgrade is very small (i.e., $\theta \approx 0$), $\sin\theta \approx 0$, and $\cos\theta \approx 1$, Equation 13.62 then becomes

$$a \cdot FS^3 + b \cdot FS^2 + c \cdot FS + d = 0 \tag{13.63}$$

where $a = W_A \cdot \sin\beta$
$b = -(W_A \cdot \tan\delta_A + W_P \cdot \tan\delta_P) \cdot \cos\beta$

$$c = -(W_T \cdot \tan\phi_s + W_P \cdot \tan\delta_A) \cdot \sin\beta \cdot \tan\delta_P$$
$$d = W_T \cdot \cos\beta \cdot \tan\delta_A \cdot \tan\delta_P \cdot \tan\phi_s$$

In the conventional translational (or two-wedge) failure analysis method, the direction of the resultant force E_P of E_{HP} and E_{VP} (or the resultant force E_A of E_{HA} and E_{VA}), which acts on the interface between the passive wedge and active wedge, is usually assumed to be parallel to waste filling slope. The effect of the waste property of the interface between the active and passive wedges (i.e., shear strength of the waste) on the stability is not considered for this assumption. Actually, the real direction of the resultant force E_A of E_{HA} and E_{VA} (or the direction of the interwedge force) should be calculated as

$$\begin{aligned} \tan\omega &= E_{VP}/E_{HP} \\ &= (E_{HP} \cdot \tan\phi_s/FS)/E_{HP} \\ &= \tan\phi_s/FS \\ \omega &= \tan^{-1}(\tan\phi_s/FS) \end{aligned} \tag{13.64}$$

where ω = inclination angle of the interwedge force (i.e., the resultant force of E_{HP} and E_{VP}), measured from horizontal, degrees;
ϕ_s = friction angle of solid waste;
FS = factor of safety for the entire solid waste mass.

Municipal solid waste usually settles a considerable amount during the filling operation. Review of field settlements from several landfills indicates that municipal solid waste landfills usually settle approximately 15 to 30% of the initial height because of placement and decomposition. The large settlement of the waste fill induces shear stresses in the liner system on the side slope, all of which tends to displace the liner downslope. The large settlement of the waste fill also causes the large deformation of the landfill cover to induce shear stresses in the final cover system. These shear stresses induce shear displacements along specific interfaces in the liner and cover systems that may lead to the mobilization of a residual interface strength. In addition, thermal expansion and contraction of the side slope liner and cover systems during construction and filling may also contribute to the accumulation of shear displacements and the mobilization of a residual interface shear strength in the liner system (Qian, 1994; Stark and Poeppel, 1994).

Earthquake loading can provide permanent displacements along landfill liner interfaces, resulting in a permanent reduction in their available shear resistance following the completion of the dynamic loading. Post-earthquake static stability must therefore be evaluated using shear strengths that are compatible with the shear displacements predicted to be experienced during the earthquake. In areas of high seismicity, this probably implies that the static stability of the final configuration of the landfill should be assured assuming the mobilization of full residual strength conditions (Byrne, 1994).

Landfill stability should be considered not only during construction and operation periods, but also for the duration of the closure period. Land development of closed landfills should be also considered in the future. Thus, the shear strengths (e.g., δ_P, δ_A, and ϕ_s) used in stability analysis must be carefully selected based on actual site-specific conditions.

EXAMPLE 13.8

Calculate the factor of safety for a landfill filling shown in Figure 13.25. Use a translational failure analysis and the following information:

Minimum interface friction angle of bottom liner system, $\delta_P = 20°$;
Minimum interface residual friction angle of side slope liner system, $\delta_A = 14°$;
Friction angle of solid waste, $\phi_s = 33°$;
Waste unit weight $= 10.2\ kN/m^3$;
Landfill subgrade is 2% [50(H):1(V)];
Waste filling slope is 25% [4(H):1(V)];
Side slope angle, $\beta = 18.4°$;
Height of side slope is 30 m;
Distance between the top edge of waste and the top edge of side slope is 20 m.

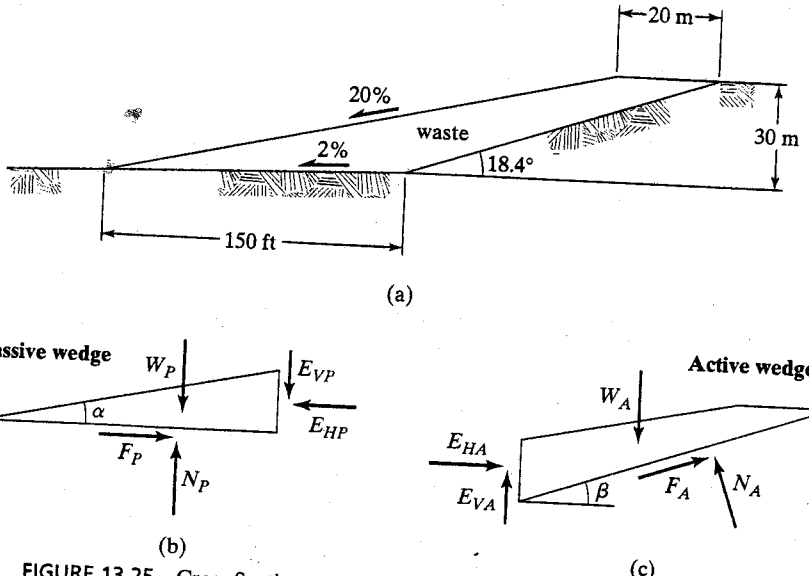

FIGURE 13.25 Cross Section of a Solid Waste Landfill during Filling Condition

Solution The forces acting on the solid waste mass are shown in Figure 13.25. The side slope angle is at 18.4° and the slope angle of cell subgrade is 1.15° according to a 2% slope; hence,

$$\sin\beta = \sin(18.4°) = 0.3162, \cos\beta = \cos(18.4°) = 0.9487,$$
$$\sin\theta = \sin(1.15°) = 0.0200, \cos\theta = \cos(1.15°) = 0.9998$$
$$\tan\delta_A = \tan(14°) = 0.2493, \tan\delta_P = \tan(20°) = 0.3640,$$
$$\tan\phi_s = \tan(33°) = 0.6494.$$

The total weight of solid waste mass is

$$W_T = 10{,}987 \text{ kN/m}$$

The weight of the passive wedge is

$$W_P = 3{,}465 \text{ kN/m}$$

The weight of the active wedge is

$$W_A = W_T - W_P = 10{,}987 - 3{,}465 = 7{,}522 \text{ kN/m}$$

Use Equation 13.62 to calculate *FS*.

Calculate the coefficients of a, b, c, and d in Equation 13.62:

$$\begin{aligned}
a &= W_A \cdot \sin\beta \cdot \cos\theta + W_P \cdot \cos\beta \cdot \sin\theta \\
&= 7{,}522 \times 0.3162 \times 0.9998 + 3{,}465 \times 0.9487 \times 0.0200 \\
&= 2{,}444 \text{ kN/m} \\
b &= (W_A \cdot \tan\delta_P + W_P \cdot \tan\delta_A + W_T \cdot \tan\phi_s) \cdot \sin\phi \cdot \sin\theta - (W_A \cdot \tan\delta_A + W_P \cdot \tan\delta_P) \cdot \cos\beta \cdot \cos\theta \\
&= (7{,}522 \times 0.3640 + 3.465 \times 0.2493 + 10{,}987 \times 0.6494) \times 0.3162 \times 0.0200 - \\
&\quad (7{,}522 \times 0.2493 + 3{,}465 \times 0.3640 \times 0.9487 \times 0.9998 \\
&= -2{,}907 \text{ kN/m} \\
c &= -[W_T \cdot \tan\phi_s \cdot (\sin\beta \cdot \cos\theta \cdot \tan\delta_P + \cos\beta \cdot \sin\theta \cdot \tan\delta_A) + \\
&\quad (W_A \cdot \cos\beta \cdot \sin\theta \cdot W_P \cdot \sin\beta \cdot \cos\theta) \cdot \tan\delta_A \cdot \tan\delta_P] \\
&= -[10{,}987 \times 0.6494 \times (0.3162 \times 0.9998 \times 0.3640 + 0.9487 \times 0.0200 \times 0.2493) + \\
&\quad (7{,}522 \times 0.9487 \times 0.0200 + 3{,}465 \times 0.3162 \times 0.9998) \times 0.2493 \times 0.3640] \\
&= -967 \text{ kN/m} \\
d &= W_T \cdot \cos\beta \cdot \cos\theta \cdot \tan\delta_A \cdot \tan\delta_P \cdot \tan\phi_s \\
&= 10{,}987 \times 0.9487 \times 0.9998 \times 0.2493 \times 0.3640 \times 0.6494 \\
&= 614 \text{ kN/m}
\end{aligned}$$

(13.62)

$$a \cdot FS^3 + b \cdot FS^2 + c \cdot FS + d = 0$$
$$2{,}444 \cdot FS^3 - 2{,}907 \cdot FS^2 - 967 \cdot FS + 614 = 0$$
$$FS^3 - 1.189 \cdot FS^2 - 0.396 \cdot FS + 0.251 = 0$$
$$FS^3 + 0.251 = 1.189 \cdot FS^2 + 0.396 \cdot FS$$

which is solved by trial and error as in the following table:

Assumed FS	$FS^3 + 0.251$	$1.189 \cdot FS^2 + 0.396 \cdot FS$	Closure
(1)	(2)	(3)	(2) − (3)
1.5	3.626	3.269	0.357
1.4	2.995	2.885	0.110
1.3	2.448	2.524	−0.076
1.35	2.711	2.702	0.009
1.34	2.657	2.666	−0.009
1.345	2.684	2.684	0

Thus, $FS = 1.345$.

The direction of the resultant force of E_{HP} and E_{VP} (i.e., direction of the interwedge force) can be calculated from Equation 13.34 as

$$\begin{aligned} \tan\omega &= \tan\phi_s/FS \\ &= \tan(33°)/1.345 \\ &= 0.649/1.345 \\ &= 0.483 \\ \omega &= 25.8° \end{aligned} \tag{13.64}$$

Recall that the inclination of waste filling slope is 20%, which is only 11.3°. Thus, the direction of the resultant force of E_{HP} and E_{VP} is definitely not parallel to the waste filling slope as is often assumed in these types of calculations (Corps of Engineers, 1960).

13.6.2 Case Histories

Alternatively, for the analysis of the case histories that follow, which failed in a translational manner, the simplified Janbu method was used. (See Koerner and Soong, 2000.) This derivation is also readily available in the literature and leads to a similar equation for the FS-value, but it is now modified with an f_o-value. The resulting equation is

$$FS = (f_o) \cdot \frac{\sum_{i=1}^{n} [c \cdot \Delta b_i + (W_i - u_i \cdot \Delta b_i) \cdot \tan\phi]/m_i}{\sum_{i=1}^{n} W_i \cdot \sin\theta_i} \tag{13.65}$$

where m_i is defined in Equation 13.31, and f_o is a function of the curvature ratio of the failure surface and the type of soil. Since these surfaces are linear, however, the depth-to-length ratio is zero and the value of $f_o = 1.0$. The analysis becomes quite straightforward. (See Schuster and Krizek, 1978.)

To illustrate the seriousness of translational failures (they have represented the largest waste mass failures to date), three case histories are presented next.

Case History T-1

Case history T-1 is a municipal solid waste landfill that experienced a major failure in 1993. The failure was translational in nature and involved approximately 470,000 m^3 of solid waste. The sliding waste mass buried numerous homes in its path and resulted in the loss of 27 lives. The only reference to our knowledge is the consultants report to the municipality owner/operator (Anonymous, 1994).

Background. The operation of the landfill in this case history began in 1972. There was neither a liner nor leachate collection system present. The waste was apparently placed directly on the native ground surface. In the subsequent years, the facility was receiving approximately 1,500 metric tons of municipal solid waste daily. The landfill site is situated within the upper portion of a southward sloping valley that discharges runoff into a local stream. As shown in Figure 13.26(a), a village is located on the south side of the stream directly opposite the valley at an elevation significantly below the landfill. Figure 13.26(b) gives the critical 2-D cross section of the landfill prior to the failure. Of necessity, the scales are significantly distorted. The landfill had been built up into a relatively level plateau at a surface elevation of approximately 150 m. The southern side slope of the landfill, which faced the stream, was very steep, approximately 35 to 40°, which averages to 1(V)-to-1.3(H).

Waste Placement. The sequence of the municipal solid waste placement began at a location approximately 250 m from the landfill entrance [i.e., at the southern end of the landfill, as shown in Figure 13.26(a)]. The landfilling activities took place at this location for approximately 11 years until 1983. At that point, the waste mass had been built up into a level plateau at an average elevation of 130 m. The waste mass was not covered with soil when the landfilling operation was terminated at this particular location. Waste in this area rapidly decomposed over the years and turned black in color. A subsequent landfilling operation was started in the northern and eastern part of the site at a location near the entrance of the landfill. It was continued until 1990 when the waste mass reached an elevation of 140. Again, no cover soil was placed above the waste mass. The final phase of the landfilling activity was initiated in 1990 and continued until the time of failure. This phase initially took place over the top of the second phase waste mass (near the landfill entrance) and continued over the top of the original waste mass at the south portion of the landfill. By early 1993, the existing decomposed waste was entirely covered by an additional 20 to 25 m of waste that brought the surface of the landfill to an elevation of approximately 150 m. Note that several portions of the waste mass partially blocked the drainage route of storm water that ran into the tributary valley. This blockage created water ponds on both the eastern and western sites of the landfill [see Figure 13.26(a)]. The average elevation of these water ponds was approximately 130 m.

Description of Failure. On April 28, 1993, a sudden and massive waste failure occurred in this 50-m high landfill. The decomposed waste mass moved down the valley at high speed for approximately 500 m into the stream and continued up-gradient into the northern portion of a nearby village [see Figure 13.26(a)]. Slide debris, approximately 15- to 20-m in thickness, buried a number of homes and resulted in the loss of 27 lives.

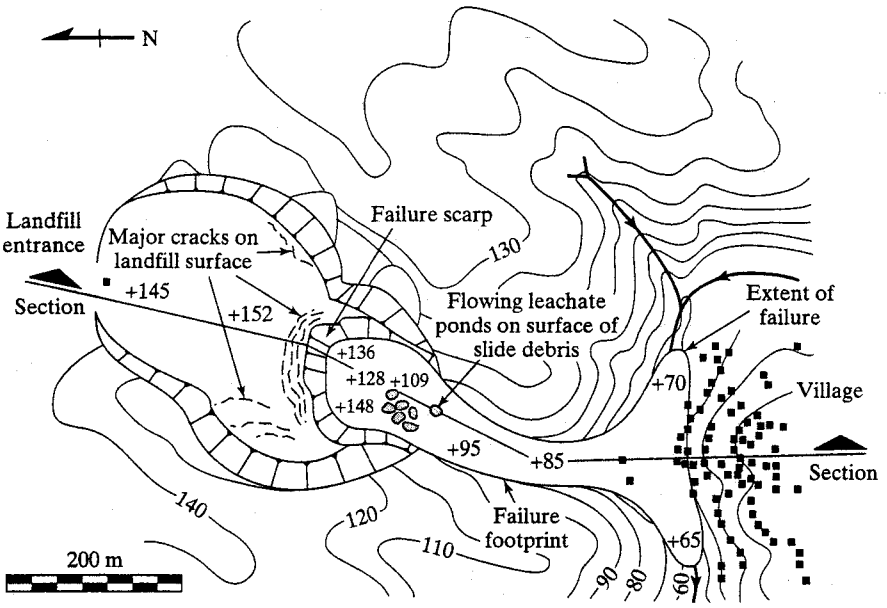

(a) Plan view of the site after failure

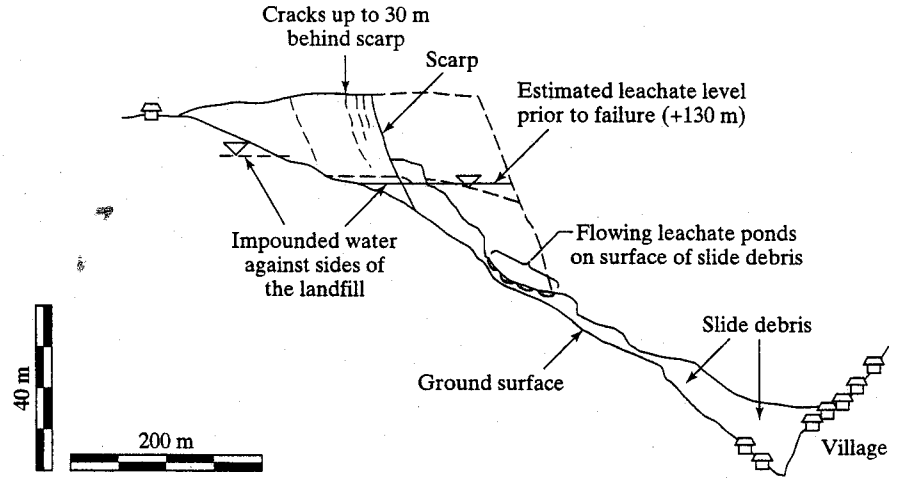

(b) Critical cross section after the failure

FIGURE 13.26 Plan View and Critical Cross Section of Case History T-1 after the Failure

The failure involved approximately 470,000 m^3 of solid waste. The investigation concluded that the failure surfaces passed through the waste mass at about 110-m behind the crest of the waste slope and to the base of the decomposed waste adjacent to the natural ground surface [see Figure 13.26(b)]. Although many factors could have contributed to the failure (i.e., over-built steep slopes or even gas uplift pressures), the triggering mechanism of the failure was likely an excessive leachate level within the old, decomposed waste caused by continued water infiltrating from the adjacent surface water ponds. The flowing leachate ponds observed on surface of the slide debris tend to support this conclusion.

Case History T-2

Case history T-2 is a municipal solid waste landfill in which a major section failed in 1997. The failure was translational in nature and involved approximately 1,100,000 m^3 of solid waste. Kenter et al. (1996), Stark et al. (1997), Stark and Evans (1997), Schmucker and Hendron (1997), Schmucker (1998), and Stark et al. (2000b) have reported on this case history.

Background. The landfill began as an outgrowth of farm waste storage in 1945 and transitioned into one that accepted mixed wastes shortly thereafter. Over the intervening years, the facility grew in both area and height as it continued to accept residential solid waste, commercial solid waste, industrial waste, and asbestos. The majority of the overall site was developed prior to the existence of requirements for engineered environmental control. The older areas of the landfill have neither liners nor leachate collection systems. These areas were, however, constructed over low permeability colluvium soils that overlie interbedded shales and limestones, all of which tend to act as a natural liner. Beginning in 1988, a clay liner was required and this was further upgraded to a composite liner in 1994. Thus, the initial phase consisted of a clay liner for its initial 5.7 ha and a composite liner was intended for the remaining 1.5 ha. As the northern portion of this phase (i.e., the 1.5 ha area) was being prepared for composite liner placement, excavation of the next phase was ongoing. It should be noted that both of these areas were at a significantly lower elevation than the existing landfill. Rock (shale) blasting was used to reach the lower elevation and was ongoing at the time of the failure.

Description of Failure. At about noon on March 9, 1996, five days after the first crack appeared on the top of the existing landfill, the landfill began to move as a large mass northward into the open excavation areas. A waste mass of approximately 1,100,000-m^3 translated some 50 to 60 m in less than five minutes. Figure 13.27(a) shows an aerial photograph taken after the failure. Based on field observations and the results of a subsequent subsurface investigation, the failure surface passed through the solid waste at a very steep inclination down to the underlying colluvium soil [see Figure 13.27(b)]. From this point, the failure plane extended within the colluvium soil until it exited at the toe of the slope. The leachate head within the waste mass prior to failure was estimated at the level shown in Figure 13.27(b), with a maximum depth of approximately 13 m, Schmucker and Hendron (1997). It is concluded by Schmucker and Hendron (1997) and Schmucker (1998) that the likely triggering mechanism for the failure was the additional buildup of leachate head in the landfill due to ice forma-

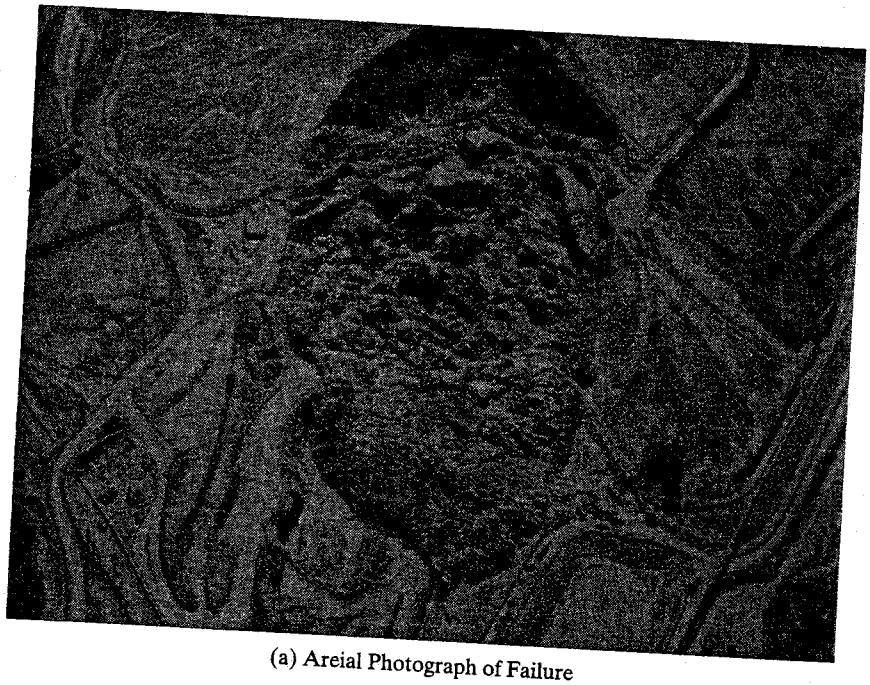

(a) Areial Photograph of Failure

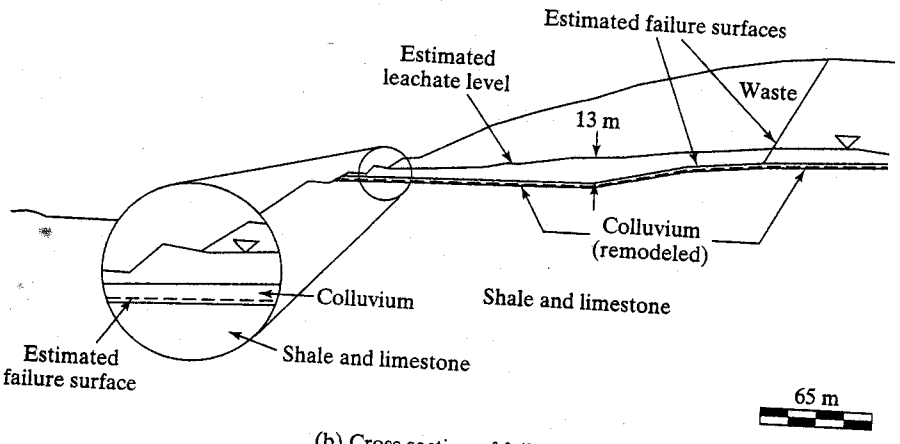

(b) Cross section of failure

FIGURE 13.27 Details of Case History T-2

tion at the exposed waste face near the toe of the slope. However, this hypothesis is contested by Stark et al. (2000b), who claim that the excessive height was the main contributing factor.

Foundation Soil Conditions. The existing landfill in this case history was placed immediately above the in-situ colluvium soils. Such soils are commonly found in this

geographic area with thickness up to 10 m, although at the site the layer was approximately 3 to 4 m thick. It was postulated by Stark et al. (2000a) that the colluvium deposit was marginally stable because it was in a residual shear strength state due to the constant down-slope deformation caused by waste placement and its gravitational stresses. While this is uncertain, it is possible that dynamic stresses caused by blasting at the toe of the slope may have been an additional destabilizing factor.

Case History T-3

Case History T-3 is a hazardous waste landfill that failed in 1988. It was translational in that the entire waste body of approximately 490,000 m^3 moved as a mass within a period of seven hours. The failure resulted in 10.7 m of lateral displacement and 4.3 m of vertical settlement at the top of the solid waste as it moved downgradient. Seed et al. (1990), Mitchell et al. (1990), Byrne et al. (1992), and Stark and Poepple (1994) have reported on this case history.

Background. The landfill site in this case history occupied 15 ha. The configuration consisted of a large oval-shaped bowl excavated into the ground to a depth of about 30 m. The bowl had a nearly horizontal base and side slopes of either 2 (H)-to-1 (V) or 3 (H)-to-1 (V) inclination, but was open-sided on its southeast side. Figure 13.28 shows the general configuration. Both the base and side slopes of the excavation were lined with a very complex multilayered geomembrane, compacted clay liner, and leachate drainage system.

The northern portion of the facility was completed first. The placement of hazardous solid waste was initiated in this section of the facility in early 1987, while the liner system for the future phase was being constructed southward. The waste mass placed in the southerly cell eventually was to provide a buttress against the previously placed waste.

Liner System. The liner system at the base of the landfill consisted of the following layers, from the top to the bottom:

- protective soil layer;
- leachate collection and removal system (consisting of a geotextile filter/separator, a 0.3-m-thick, granular soil layer, another geotextile filter/separator, and a geonet);
- primary composite liner (consisting of a 1.5-mm-thick, smooth HDPE geomembrane and a 0.5-m-thick compacted clay liner);
- leak detection, collection, and removal system (consisting of a geotextile filter/separator, a 0.3-m-thick, granular soil layer, and another geotextile filter/separator);
- secondary composite liner (consisting of a 1.5-mm-thick, smooth HDPE geomembrane and a 1.1-m-thick compacted clay liner);
- vadose zone de-watering system (consisting of a geotextile filter/separator, a 0.3-m-thick, granular soil layer and another geotextile filter/separator);
- 2.0-mm-thick, smooth HDPE geomembrane; and
- in-situ compacted soil subgrade.

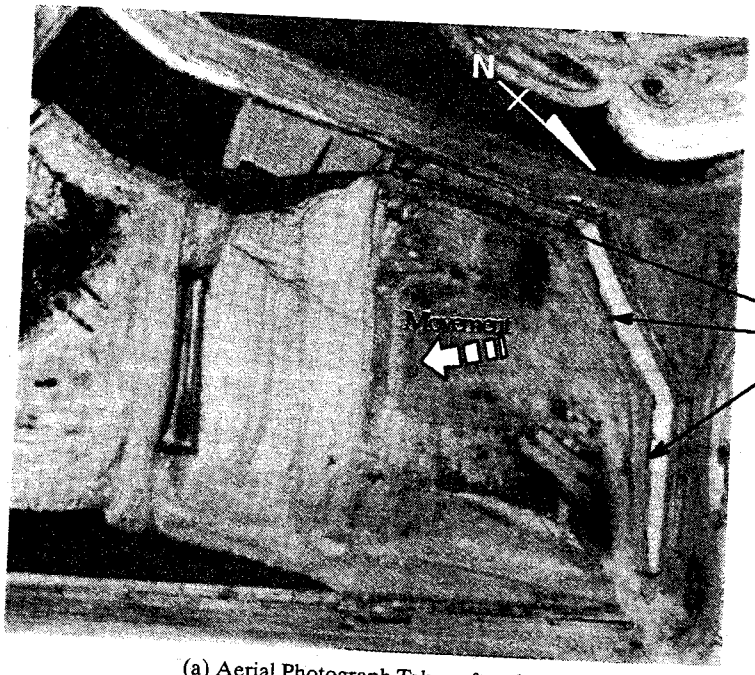

(a) Aerial Photograph Taken after the Failure of Landfill T-3

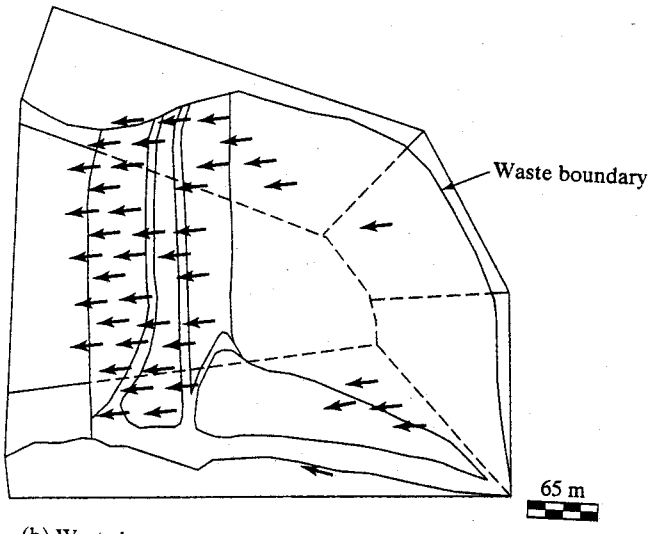

(b) Waste boundary after failure showing displacement vectors

FIGURE 13.28 Landfill T-3 after Failure (after Seed et al., 1990) Used with permission of ASCE.

The liner system on the side slopes of the landfill consisted of the following layers, from the top to the bottom:

- protective soil layer;
- leachate collection and removal system (consisting of a geotextile filter/separator and a geonet);
- primary 1.5-mm-thick, smooth HDPE geomembrane liner;
- leak detection, collection, and removal system (consisting of a geotextile filter/separator and a geonet);
- secondary composite liner (consisting of a 1.5-mm-thick, smooth HDPE geomembrane and a 1.1-m-thick compacted clay liner); and
- in-situ compacted soil subgrade.

Waste Properties. The waste material was estimated to have a unit weight of 17.3 kN/m^3. This relatively high value is indicative of a large amount of soil surrounding the containers of hazardous waste and the nature of the solid waste itself. The shear strength of the waste was not relevant to the analysis since the failure surfaces did not pass through any of the waste material.

Description of the Failure. On March 19, 1988, a slope-stability failure occurred at this particular landfill. The first sign of failure was a 12-mm-wide crack across a truck ramp at the northeast corner of the landfill. It was observed at about 6:30 AM. Since it was Saturday, few personnel were at the site, and its seriousness was neither suspected nor communicated to others. At approximately 9:30 AM, 75- to 100-mm-wide cracks with 150- to 200-mm vertical offsets were observed along the crests of the 2(H)-to-1(V) slopes. The main failure, which was quite abrupt, was reported to have occurred at 1:30 PM. Approximately 490,000 m^3 of waste was involved in the abrupt translational slide that occurred subsequently. Surface cracking was clearly visible, as were major tears and displacements on the exposed portions of the liner system along all three of the side slopes. The direction of the waste movement is shown in Figure 13.28(b) using displacement vectors. The maximum fill height was approximately 27 m at the time of the failure.

Failure Surfaces. As described by Mitchell et al. (1990) and Seed et al. (1990), the actual failure surfaces were the geomembrane-to-CCL interface of the secondary composite liner along the base, and the primary geomembrane-to-underlying geotextile interface on the side slopes of the landfill. As noted, all of the geomembranes were smooth, since textured liners were not available at the time of the failure. The triggering mechanism that led to the waste failure, however, was likely to have been the excessive wetness of the geomembrane-to-compacted clay liner interface at the base of the landfill. Rainfall during construction and waste placement, as well as the consolidation water expelled from the CCL, was felt to have caused an excessively wetted clay interface with the overlying geomembrane.

13.6.3 General Remarks

Translational failures of the type presented in these three case histories represent the largest landfill failures that have occurred insofar as waste volumes are concerned. As

was seen, such failures can be life-threatening as well. As was the situation for rotational failures, the analysis is straightforward and many computer codes are available. The critical issue is the proper assessment of interface shear strengths. Both product-specific materials and site-specific conditions must be properly determined (recall Section 13.3.1).

As pointed out by Koerner and Soong (2000), excessive moisture was invariably the triggering mechanism in the failures that they evaluated. In their study of 10 landfill failures (5 of which are included in this section), all were due, at least in part, to excessive liquids. There were three locations of the excess liquids:

(i) Leachate buildup within the waste mass, resulting in the failure surfaces to be above the liner system that was at the base of the landfill.

(ii) Extremely wet compacted clay liners beneath the geomembrane in composite liner systems, resulting in failure surfaces immediately beneath the geomembrane and above, or nominally within, the excessively wet clay.

(iii) Wet foundation or soft backfill soils resulting in failure surfaces within the subgrade soil beneath the waste mass.

Additional information on these three situations, and the particular triggering mechanism involved in each of the failures is given in Table 13.1.

Clearly, excessive liquids above, below, or within the failure surfaces were involved in the failures in all 10 case histories presented and analyzed by Koerner and Soong (2000).

TABLE 13.1 Summary of Triggering Mechanisms Involved in the Case Histories Presented by Koerner and Soong (2000)

Case History	Reason for low initial FS-value	Triggering mechanism
U-3	Leachate buildup within waste mass	Excessive buildup of leachate level due to ponding
U-4		Excessive buildup of leachate level due to ice formation
L-4		Excessive buildup of leachate level due to liquid waste
L-5		Excessive buildup of leachate level due to leachate injection
L-1	Wet clay beneath geomembrane (i.e., GM/CCL composite)	Excessive wetness of the GM/CCL interface
L-2		Excessive wetness of the GM/CCL interface
L-3		Excessive wetness of the bentonite in an unreinforced GCL
U-1	Wet foundation or soft backfill soil	Rapid rise in leachate level within the waste mass
U-2		Foundation soil excavation exposing soft clay
U-5		Excessive buildup of perched leachate level on clay liner

U = unlined (or clay lined) sites
L = geomembrane or composite (GM/CCL) lined sites
Used with permission of ASCE.

13.7 CONCLUDING REMARKS

The general concept of a waste containment system is to prevent leakage of leachate (and escape of gases) from a landfill. As such, most past efforts have rightly been focused on these issues. What particular liner system is best for a given site and given waste from a leakage perspective is obviously important and has been the focus of much of this text.

However, when one compares leakage from a waste containment system (even relatively large leakage) with the massive failures given in this chapter, the message is obvious. Waste failures simply are not acceptable. Nevertheless, some have occurred. Table 13.2 offers a glimpse of the magnitude and seriousness that such situations can engender.

Of major importance is that all of the failures in Table 13.2 were straightforwardly analyzed in light of current geotechnical and geosynthetics practice. That being said, it is necessary that we not only do the forensic analysis after the failures, but also that we do the proper design initially to avoid such failures in the first place. This requires that a knowledgeable design consultant be utilized throughout the process for each of the following stages:

(i) the liner system beneath the waste,

(ii) the waste placement at all critical stages, and

(iii) the cover system above the waste.

While liner and cover systems have generally been designed and constructed with carefully controlled CQC and CQA, waste placement has rarely been designed, and even more rarely has it been controlled. This latter issue is invariably left to the landfill operator. Since many of the failures in Table 13.1 were during waste filling, the operations of waste placement must be carefully planned and then executed accordingly.

TABLE 13.2 Summary of Waste Failures Analyzed by Koerner and Soong (2000)

Identification	Year	Location	Type of Failure	Quantity of Waste Involved in Failure (m^3)
Unlined Sites				
U-1	1984	N. America	Single Rotational	110,000
U-2	1989	N. America	Multiple Rotational	500,000
U-3	1993	Europe	Translational	470,000
U-4	1997	N. America	Translational	1,100,000
U-5	1997	N. America	Single Rotational	100,000
Lined Sites				
L-1	1988	N. America	Translational	490,000
L-2	1994	Europe	Translational	100,000
L-3	1997	N. America	Translational	300,000
L-4	1997	Africa	Translational	300,000
L-5	1997	S. America	Translational	1,200,000

Used with permission of ASCE.

This necessitates construction quality assurance (CQA) personnel being on the site during landfill placement operations on challenging sites where a failure might occur. Obviously, not all sites require such scrutiny, but certainly some do.

In general, the stability of a landfill should be evaluated by performing stability analyses for conditions that will exist at different stages of excavation, construction, operation, and closure of the facility. The analyses should address the following five conditions:

(i) Side slope stability during excavation;
(ii) Liner system stability during construction;
(iii) Waste mass stability during filling stage;
(iv) Final cover system stability; and
(v) Landfill postclosure stability.

With proper design and construction, it is hoped that the failures illustrated in this chapter will cease to exist.

PROBLEMS

13.1 Rank the seriousness of the six potential landfill instability situations described in Section 13.1 and illustrated in Figure 13.1.

13.2 Describe the general remedies for the six potential landfill instability situations described in Section 13.1 and illustrated in Figure 13.1.

13.3 The three materials that are possibly involved in landfill failures are geosynthetics, natural soils, and solid waste. (Recall Section 13.3.) What other types of materials might be involved under less common situations?

13.4 In the laboratory, determination of shear strength of geosynthetics, natural soils, and solid waste (recall Section 3.3), (a) What are the appropriate ASTM test methods in current use? and (b) How does the size of the test device possibly influence the results?

13.5 In the direct shear testing of geosynthetics, a strength intercept (i.e., an adhesion value) at zero normal stress is sometimes observed. For what types of materials can this value be justifiably used in stability analyses?

13.6 How does the shear strength of a compacted clay liner (CCL) vary with moisture content? Illustrate your answer on a graph of moisture content versus dry density.

13.7 What is the difference between peak shear strength, high-deformation shear strength, and residual shear strength? Illustrate your answer on a shear deformation versus shear strength graph.

13.8 Regarding Example 13.1, recalculate the *FS*-values for the following variations and plot your response curves. (Other variables than listed below remain the same as in the example).

(a) Slope lengths from 10 to 100 m.
(b) Cover soil thickness from 200 to 1000 mm.
(c) Slope angles from 2(H)-to-1(V) to 5(H)-to-1(V).
(d) Cover soil friction angles from 15 to 40°.
(e) Interface friction angles from 10 to 35°.

13.9 Regarding Example 13.2, recalculate the *FS*-values for the following variations and plot your response curves. (Variables not given in the list that follows remain the same as in the example).

(a) Bulldozer ground pressure from 20 to 150 kN/m^2.

(b) Bulldozer tracks from 2.0 to 5.0 m long.

(c) Bulldozer tracks from 0.4 to 1.0 m wide.

13.10 Regarding Example 13.3, recalculate the *FS*-values for the bulldozer time to reach 20 km/hour from 1 to 10 seconds and plot your response curves. (Other variables than those listed remain the same as in the example).

13.11 Two seepage force scenarios were presented in Section 13.3.3: horizontal and parallel. Give situations where each could occur by filling the the following:

Seepage Scenario	Leachate Collection System	Final Cover System
Horizontal		
Parallel		

13.12 A 36-ft- (10.8-m)-high and 3(H):1(V) slope has cover sand with a uniform thickness of 2 ft (0.6 m) and a unit weight of 115 lb/ft^3 (18 kN/m^3). The cover sand has a friction angle of 30° and zero cohesion. Seepage occurs parallel to the slope and the seepage water head in the sand layer is 5.2 inches (0.13 m). The saturated unit weight of the sand is 120 lb/ft^3 (19 kN/m^3). The interface friction angle between the sand drainage layer and geomembrane is 20° with zero adhesion. Calculate the factor of safety for the cover soil on the side slope. If the factor of safety is less than 1.2, use the incremental method to achieve a factor of safety no less than 1.2 for the cover sand resting on the sideslope.

13.13 Regarding Example 13.6, recalculate the *FS*-values for the seismic coefficient from 0.0 to 0.30 and plot your response curves. (Other variables than those listed remain the same as in the example).

13.14 For the above problem, what are the implications (i.e., regarding further analysis) if the *FS*-value is above or below 1.0?

13.15 In assessing the results of a permanent deformation analysis, as in Example 13.7, what factors influence the establishment of an allowable deformation value?

13.16 Three case histories of subsoil foundation failures were presented in Section 13.5. Assemble them in table form (e.g., height, slope, area, soils involved, waste involved, failure mass, and failure triggering action) and provide commentary. Also, include what possible preventative measures could have been taken to avoid the failures.

13.17 Calculate the factor of safety for a filling landfill like that shown in Figure 13.25 against possible mass movement. Use a two-wedge analysis and the following information:

Interface friction angle of bottom liner, $\delta_P = 18°$;
Interface residual friction angle of side slope liner, $\delta_A = 10°$;
Friction angle of solid waste, $\phi_s = 33°$;
Waste unit weight = 70 lb/ft^3;
Landfill subgrade is 2% [50 (H):1(V)], $\theta = 1.15°$;
Side slope angle, $\beta = 18.4°$ [3(H):1(V)];
Waste filling slope is 25% [4(H:1(V)];
Height of side slope is 50 feet;
Distance between the top edge of waste and the top edge of side slope is 50 feet.

If the waste filling slope is changed to 33% [3(H):1(V)], recalculate the factor of safety.

13.18 Calculate the factor of safety for a filling landfill like the one shown in Figure 13.25 against possible mass movement. Use a two-wedge analysis and the following information:

Interface friction angle of bottom liner, $\delta_P = 18°$;
Interface residual friction angle of side slope liner, $\delta_A = 10°$;
Friction angle of solid waste, $\phi_s = 33°$;
Waste unit weight = 70 lb/ft^3;
Landfill subgrade is 15%, $\theta = 8.5°$;
Side slope angle, $\beta = 18.4°$ [3(H):1(V)];
Waste filling slope is 25% [4(H):1(V)];
Height of side slope is 50 feet;
Distance between the top edge of waste and the top edge of side slope is 50 feet.

13.19 Three case histories of waste mass failure were presented in Section 13.6. Assemble them in table form (e.g., height, slope, area, geosynthetics involved, waste involved, failure mass, and failure triggering mechanism) and provide commentary. Also, include what possible preventative measures could have been taken to avoid the failures.

13.20 The six landfill failures of Section 13.5 and 13.6 were all serious and involved many organizations and individuals. Interestingly, none of them had any instrumentation. What types of instrumentation could have been used in such situations and what information could have been generated to foreworn of such incidents?

REFERENCES

Algermissen, S. T., (1969) "Seismic Risk Studies in the United States," *Proc. 4th World Conference on Earthquake Engineering,* Vol. 1, Santiago, Chile, pp. A1-14–27.

Anderson, D. G. and Kavazajian, E. Jr., (1995) "Performance of Landfills Under Seismic Loading," *Proceedings of Third International Conference on Recent Advances in Geotechnical Earthquake Engineering and Soil Dynamics,* University of Missouri, Rolla, MO, April, Vol. 3, pp. 2–7.

Anonymous (1994), "Emergency Consulting Engineering and Design Services to Stabilize the Ümbaniye Dump Site and Evaluation of Potential Safety Problem at Other Solid Wate Dumps in Istanbul," Prepared for the Municipality of Greater Istanbul, Turkey, CH2M Hill International, Ltd.

Byrne, R. J., Kendall, J., and Brown, S., (1992) "Cause and Mechanism of Failure of Kettleman Hills Landfill," *Proceedings of ASCE Specialty Conference on Stability and Performance of Slope and Embankments—II,* Berkeley, CA, June 28–July 1, pp. 1–23.

Byrne, R. J., (1994) "Design Issues with Strain-Softening Interfaces in Landfill Liners," *Waste Tech '94,* Landfill Technology, Technical Proceedings, Charleston, SC, January 13–14.

Cancelli, A. and Rimoldi, P., (1989) "Design Criteria for Geosynthetic Drainage Systems in Waste Disposal," *Proc. of Sardinia '89,* 2nd Intl. Landfill Symposium, Porto Conte, Sassari, Italy.

Concoran, G. T. and McKelvy, J. A., (1995) "Stability of Soil Layers on Compound Geosynthetic Slopes," *Proc. Waste Tech '95,* New Orleans, LA, Environ Industry Assoc., pp. 301–304.

Corps of Engineers, (1960) "Manual EM 1110—1902," U.S. Army, Washington DC, 195 pages.

Daniel, D. E., Shan, H.-Y., and Anderson, J. D., (1993) "Effects of Partial Wetting on the Performance of the Bentonite Component of a Geosynthetic Clay Liner," *Proc. Geosynthetics '93,* IFAI, St. Paul, MN, pp. 1483–1496.

de Santayana, F. P. and Pinto, A. A. V., (1998) "The Bierolos Landfill Eastern Expansion Landslide," *Proc. Environmental Geotechnics,* S. e. Pinto (Ed.), Balkema Publ. Co., Rotterdam, pp. 905–910.

Divinoff, A. H. and Munion, D. W., (1986) "Stability Failure of a Sanitary Landfill," Proc. Intl. Symp. on Environmental Geotechnology, H.-Y. Fang, Ed., Envo Publ. Co., Inc. pp. 25–35.

Erdogan, H., Sadat, M. M., and Hsieh, N. N., (1986) "Stability Analysis of Slope Failures in Landfills: A Case Study," *Proc. of 9th Annual Madison Waste Conference,* Univ. of Wisconson-Madison, pp. 168–177.

Giroud, J. P. and Beech, J. F., (1989) "Stability of Soil Layers on Geosynthetic Lining Systems," *Geosynthetics '89 Proceedings,* Vol. 1, pp. 35–46.

Giroud, J. P., Williams, N. D., Pelte, T., and Beech, J. F., (1995a) "Stability of Geosynthetic-Soil Layered Systems on Slopes," *Geosynthetic International,* Vol. 2, No. 6, pp. 1115–1148.

Giroud, J. P., Bachus, R. C., and Bonaparte, R., (1995b) "Influence of Water Flow on the Stability of Geosynthetic-Soil Layered Systems on Slopes," *Geosynthetic International,* Vol. 2, No. 6, pp. 1149–1180.

Hassini, S., (1992) "Some Aspects of Landfill Design," *Environmental Geotechnology,* Proceedings of the Mediterranean Conference on Environmental Geotechnology, A. A. Balkema Publishers, pp. 137–144.

Hirshfield, R. C. and Poulos, S. J., Eds., (1973) *Embankment—Dam Engineering,* John Wiley and Sons, New York, NY 454 pgs.

Humphrey, D. N. and Leonards, G. A., (1986) "Slide Upstream Slope of Lake Shelbyville Dam," *Journal of Geotechnical Engineering,* ASCE, Volume 112, No. 5, pp. 564–577.

Idriss, I. M., (1990) "Response of Soft Soil Sites During Earthquake," *Proc. Symposium to Honor Professor H. B. Seed,* Berkeley, California.

Kenter, R. J., Schmucker, B. O., and Miller, K. R., (1996) "The Day the Earth Didn't Stand Still: The Rumpke Landslide," *Waste Age,* Atlanta, GA, March, pp. 36–41.

Koerner, R. M., (1994) *Designing with Geosynthetics,* 3rd Ed., Prentice Hall Book Co., Englewood Cliffs, NJ, 783 pgs.

Koerner, R. M. and Hwu, B. -L., (1991) "Stability and Tension Considerations Regarding Cover Soils on Geomembrane Lined Slopes," *Journal. of Geotextiles and Geomembranes,* Vol. 10, No. 4, pp. 335–355.

Koerner, R. M. and Soong, T. -Y., (1998) "Analysis and Design of Veneer Cover Soils," *Proc. 6th IGS,* IFAI, Roseville, MN, pp. 1–26.

Koerner, R. M. and Soong, T. -Y., (2000) "Stability Assessment of Ten Large Landfill Failures," *Advances in Transportation and Geoenvironmental Systems Using Geosynthetics, Proceedings of Sessions of GeoDenver 2000,* ASCE Geotechnical Special Publication No. 103, pp. 1–38.

Ling, H. I. and Leschinsky, D., (1997) "Seismic Stability and Permanent Displacement of Landfill Cover Systems," *Journal of Geotechnical and Geoenvironmental Engineering,* ASCE, Vol. 123, No. 2, pp. 113–122.

Makdisi, F. I. and Seed, H. B., (1978) "Simplified Procedure for Estimating Dam and Embankment Earthquake-Induced Deformations," *Journal of Geotechnical Engineering,* ASCE, Vol. 104, No. GT7, pp. 849–867.

Matasovic, N., Kavazanjian, E., Jr., Augello, A. J., Bray, J. D., and Seed, R. B., (1995) "Solid Waste Landfill Damage Caused by January 17, 1994 Northridge Earthquake," In: Woods, M.C. and Seiple, R. W., Eds., *The Northridge, California, Earthquake of 17 January 1994,* California Department of Conservation, Division of Mines, and Geology Special Publication 116, Sacramento, California, pp. 43–101.

Matasovic, N., Kavazanjian E. Jr., and Yan, L., (1997) "Newmark Deformation Analysis with Degrading Yield Acceleration," Proc. Geosynthetics '97, IFAI, St. Paul, MN, pp. 989–1000.

McKelvey, J. A. and Deutsch, W. L., (1991) "The Effect of Equipment Loading and Tapered Cover Soil Layers on Geosynthetic Lined Landfill Slopes, " *Proceedings of the 14th Annual Madison Avenyue Conference,* Madison, WI, University of Wisconsin, pp. 395–411.

McKelvey, J. A., (1994) "Consideration of Equipment Loadings in Geosynthetic Lined Slope Design," *Proc. 8th Intl. Conf. of the Intl. Assoc. for Computer Methods and Advancement in Geomechanics,* Morgantown, WV, Blakema, pp. 1371–1377.

Mitchell, J. K., Seed, R. B., and Seed, H. B., (1990) "Kettleman Hills Waste Landfill Slope Failure I: Liner System Properties," *J. of Geotech. Engrg.,* ASCE, Vol. 116, No. 4, pp. 647–668.

Mitchell, R. A. and Mitchell, J. K., (1992) "Stability Evaluation of Waste Landfills," *Proceedings of ASCE Specialty Conference on Stability and Performance of Slope and Embankments—II,* Berkeley, CA, June 28–July 1, pp. 1152–1187.

Mitchell, J. K., Seed, R. B., and Seed, H. B., (1990) "Kettleman Hills Waste Landfill Slope Failure I: Liner System Properties," *Journal of Geotechnical Engineering,* ASCE, Volume 116, No. 4, pp. 647–668.

Qian, Xuede, (1994) "Stability Analyses for Vertical and Lateral Expansions of Landfill," Michigan Department of Environmental Quality, Waste Management Division, Lansing, MI.

Qian, Xuede, (1997) "Stability Analysis of Cover Soil over Geosynthetic Layered Slope with Seepage Force," Michigan Department of Environmental Quality, Waste Management Division, Lansing, MI.

Reynolds, R. T., (1991) "Geotechnical Field Techniques Used in Monitoring Slope Stability at a Landfill," *Field Measurements in Geotechnics,* Sorum (ed.), Balkema, Rotterdam, ISBN 90 5410 0257.

Richardson, G. N., Kavazanjian, E. Jr., and Matasovic, N., (1995) "RCRA Subtitle D (258) Seismic Design Guidance for Municipal Solid Waste Landfill Facilities," EPA/600/R-95/051, U. S. Environmental Protection Agency, Cincinnati, OH, 143 pgs.

Richardson, G. N. and Reynolds, R. T., (1990) "Landslide at a Naturally Lined Landfill," ASCE Materials Conf., Denver, CO, 25 pgs.

Schmucker, B. O., (1998) "The Rumpke Waste Failure," *Waste Age,* March, pp. 30–38.

Schmucker, B. O. and Hendron, D. M., (1997) "Forensic Analysis of 9 March 1996 Landslide at the Rumpke Sanitary Landfill, Hamilton County, Ohio," *Proc. Seminar on Slope Stability in Waste Systems,* ASCE Central Ohio, Cincinnati and Toledo Sections.

Schnabel, P. B., Lysmer, J., and Seed, H. B., (1972) "SHAKE: A Computer Program for Earthquake Response Analysis of Horizontally Layered sites," Report No EERC 72–12, Earthquake Engineering Research Center, University of California, Berkeley, CA.

Schuster, R. L. and Krezik, R. J., (1978) *Landslides: Analyses and Control,* Natl. Academy of Sciences, Washington, DC, 427 pages.

Seed, H. B. and Idriss, I. M., (1982) "*Ground Motions and Soil Liquefaction During Earthquakes,*" Monographs No. 5, Earthquake Engineering Research Center, University of California, Berkeley, CA, 134 pgs.

Seed, R. B., Mitchell, J. K., and Seed, H. B., (1990) "Kettleman Hills Waste Landfill Slope Failure II: Stability Analyses," *Journal of Geotechnical Engineering,* ASCE, Volume 116, No. 4, pp. 669–690.

Sherard, J. L., Woodward, R. J., Gizienski, S. F., and Clevenger, W. A., (1963) *Earth and Earth-Rock Dams,* John Wiley & Sons, New York, 727 pgs.

Singh, S. and Murphy, P., (1990) "Evaluation of the Stability of Sanitary Landfills, ASTM STP 1070, ASTM, W. Conshohocken, PA, pp. 240–258.

Soong, T. -Y. and Koerner, R. M., (1996) *Cover Soil Slope Stability Involving Geosynthetic Interfaces,* Geosynthetic Research Institute Report 18, Philadelphia, PA, 87 pages.

Soong, T. -Y., Hungr, O., and Koerner, R. M., (1998) "Analysis of Selected Landfill Failures by 2-D and 3-D Stability Methods," *Proc. 12 GRI Conference,* GII Publications, Folsom, PA (in print).

Soong, T. -Y. and Koerner, R. M., (1999) "Stability Analysis (2-D and 3-D) and Assessment of Ten Lined Landfills," GRI Report #21, 250 pgs.

Soong, T. -Y. and Koerner, R. M., (1996) "Seepage Induced Slope Instability," *Journal of Geotextiles and Geomembranes,* Vol. 14, No. 7/8, pp. 425–445.

Stark, T. D., Eid, H. T., Evans, W. D., and Sherry, P. E., (2000a) "Municipal Solid Waste Slope Failure: Part I–Waste and Foundation Soil Properties," *Journal Geotechnical and Geoenvironmental Engineering,* ASCE, Vol. 126, No. 5, pp. 397–407.

Stark, T. D., Eid, H. T., Evans, W. D., and Sherry, P. E., (2000b) "Municipal Solid Waste Slope Failure: Part II–Stability Analyses," *Journal of Geotechnical and Geoenvironmental Engineering,* ASCE, Vol. 126, No. 5, pp. 408–419.

Stark, T. D. and Evans, W. D. (1997), "Balancing Act," Civil Engineering, ASCE, August, pp. 8A–11A.

Stark, T. D. and Poeppel, A. R., (1994) "Landfill Liner Interface Strengths from Torsional Ring Stress Tests," *Journal of Geotechnical Engineering,* ASCE, Vol. 120, No. 3, pp. 597–617.

Terzaghi, K., (1943) *Theoretical Soil Mechanics,* John Wiley & Sons, New York.

Thiel, R. S. and Stewart, M. G., (1993) "Geosynthetic Landfill Cover Design Methodology and Construction Experience in the Pacific Northwest," Proc. Geosynthetics '93, IFAI, St. Paul, MN, pp. 1131–1144.

CHAPTER 14

Vertical Landfill Expansions

The acquisition and permitting of new landfill sites poses several difficulties. An attractive alternative to landfill owners is to consider expansions to existing landfills. This option may entail the design and permitting of a vertical expansion over old landfill areas. The advantages of vertical landfill expansion include (1) optimal use of landfill area, (2) high waste volume filled per unit area, (3) low construction cost, (4) less public opposition, and (5) easier permitting. Expansion can occur by vertical and/or lateral expansion in which the old landfill is encapsulated by the new (vertical and lateral expansion), or by placement of new landfill atop the old (piggyback expansion). Figure 14.1 shows a cross-section of a vertical and lateral expansion landfill; Figure 14.2 shows a cross section of a piggyback vertical expansion landfill.

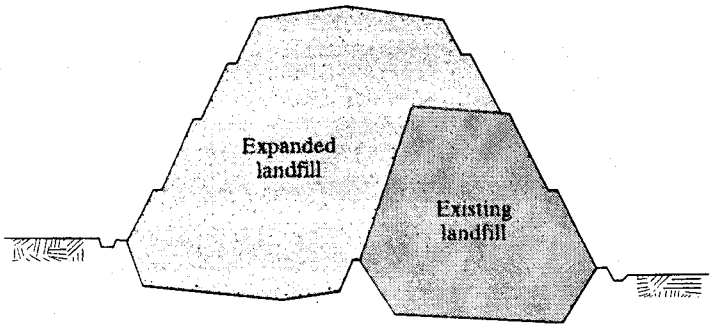

FIGURE 14.1 Cross Section of a Vertical and Lateral Expansion Landfill

14.1 CONSIDERATIONS INVOLVED IN VERTICAL EXPANSIONS

The additional waste fill from a vertical landfill expansion will cause settlement of the existing landfill and result in liner system and slope stability problems for both existing and expanded landfills. A gas collection system in the existing landfill may also be of concern due to the large deformation of the solid waste surrounding gas collection pipes. A liner and leachate collection system constructed on an existing landfill may experience large differential settlements. The long-term performance of these systems is thus a major design consideration.

Large differential settlements within existing refuse may occur because of the collapse or degradation of large objects, which have been deposited in old landfills. These settlements could result in tensile strains in a liner system placed on the top of an old landfill. If the tensile strain within the liner exceeds the tensile capacity of the material, whether it is a soil or a geosynthetic, tension cracks or tensile failure will develop. The tension cracks will reduce the effectiveness of the liner as a hydraulic barrier by providing a direct flow path through the liner system (Jang and Montero, 1993). Under extreme conditions, large differential settlements could result in the reversal of leachate flow gradients and directions. If grade reversal takes place at the surface of a liner and leachate collection system, leachate will pond on the liner, and increase the potential for infiltration of the leachate into the old landfill.

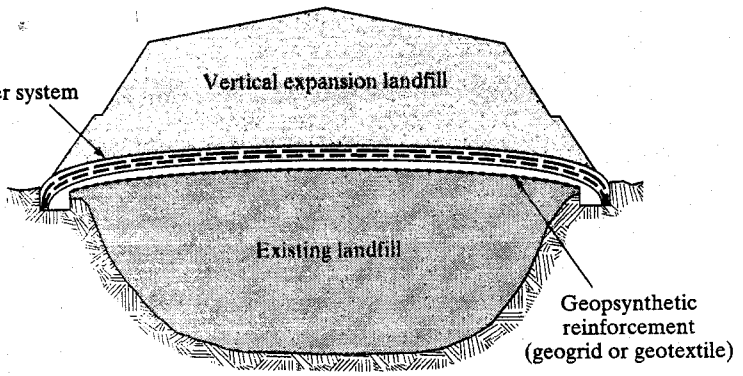

FIGURE 14.2 Cross Section of a Piggyback Vertical Expansion Landfill

The additional waste fill due to the vertical expansion may also affect the bottom topography or subgrade elevations beneath the existing landfill and cause ponding problems on the bottom liner. Almost certainly, this extra load will increase the deflection and wall stress of the leachate and gas collection pipes buried in the existing landfill (if any are present) and may also cause pipe failure or pipe wall stability problems.

Major design steps and considerations for vertical landfill expansion include (Qian, 1996)

(i) Selecting a suitable composite liner system for placement over the existing landfill.

(ii) Estimating the overall total settlement and differential settlement of the existing landfill caused by new waste fill.

(iii) Estimating the differential settlement due to the degradation of large objects in the old landfill, or reinforcing the liner system to minimize this differential settlement.

(iv) Calculating subgrade elevation changes beneath the existing landfill caused by the differential settlements due to both existing and extra waste filling.

(v) Evaluating the deformation and stability conditions of the leachate and gas collection pipes in the existing landfill due to the extra waste fill.

(vi) Evaluating the stability of the soil mass, liner system, waste mass, and final cover system in various conditions (e.g., excavation, construction, operation, and closure conditions).

14.2 LINER SYSTEMS FOR VERTICAL EXPANSION

The existing solid waste mass, which is relatively compressible, must provide the foundation of the liner system for the vertical expansion landfill. Tensile strains and stresses can develop within the various bottom liner components as a result of differential settlements due to the compression of the underlying solid waste landfill. These tensile strains and stresses can adversely affect the integrity of the liner components. If a compacted clay liner is proposed, it must be recognized that it possesses very little tensile strength (allowable tensile strain is less than 1.0 percent) and is susceptible to cracking as a result of differential settlement. Thus, it is likely that the effectiveness of a compacted clay liner as a hydraulic barrier would be seriously compromised in a vertical expansion landfill. As such, compacted clay liners are generally not recommended for vertical or lateral expansions. A geosynthetic clay liner (GCL) can be used as an alternative to a compacted clay liner. Geosynthetic clay liners are considerably more effective as impervious barriers. They can withstand relatively high in-plane tensile strains and stresses induced by differential settlement (recall Section 5.3). The allowable tensile strain of geosynthetic clay liners range from 6 to 20 percent, contrasted to less than 1 percent for a compacted clay liner.

With respect to the geomembrane components of a composite liner system placed over an existing landfill, several different geomembranes can be selected. These include linear low density polyethylene (LLDPE), flexible polypropylene (fPP), and polyvinyl chloride (PVC) geomembranes. It should be noted that

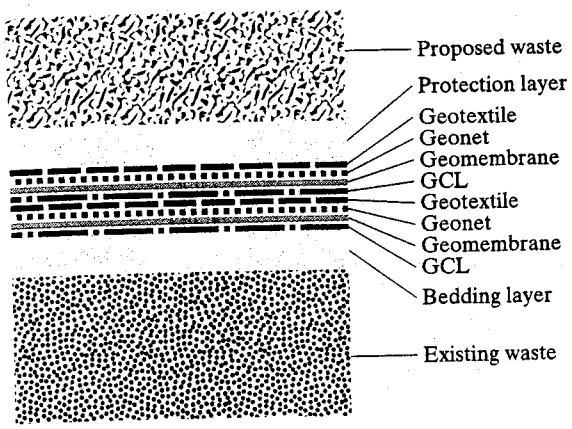

FIGURE 14.3 Double Composite Liner System over Existing Waste

high density polyethylene (HDPE) can also be considered if the tensile strain is mobilized slowly. The reason HDPE is often not used in these situations is that the test method used to simulate differential subsidence (ASTM D5617) applies load very fast in comparison to actual conditions in a landfill. The default pressure rate is 1.0 lb/in^2/min; thus, stress relaxation does not occur and the HDPE fails at relatively low strains of approximately 25%. The other geomembranes cited fail at strains from 75 to 100%. A textured geomembrane should generally be selected to provide a relatively greater interface strength between geomembrane and geosynthetic clay liner or geosynthetic composite drainage layer. Because of the magnitude of the settlements that the liner system will experience and the possibility of "local" liner deformations due to localized subsidence effects, it is important to select a geomembrane with superior extension properties. For a number of reasons (differential settlement, substandard liner under existing waste, etc.) a double liner system is desirable under a vertical expansion.

Cross sections of typical double-composite liner systems used in vertical expansions of landfills are shown in Figures 14.3 and 14.4. A geogrid or high strength geotextile is placed beneath the bottom of the liner system to reinforce the liner system in

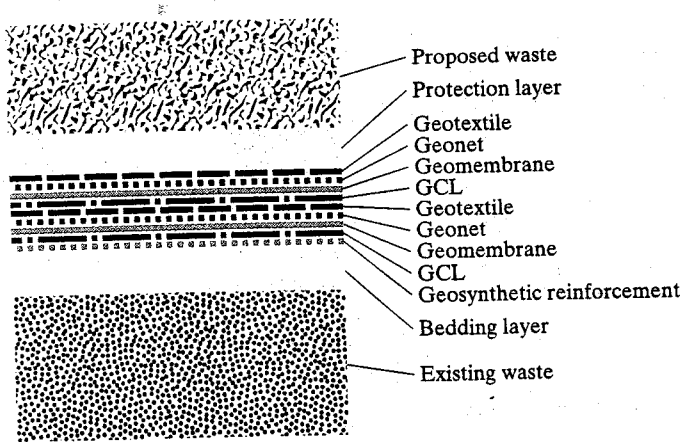

FIGURE 14.4 Double Composite Liner System Reinforced with Geosynthetic Reinforcement over Existing Waste

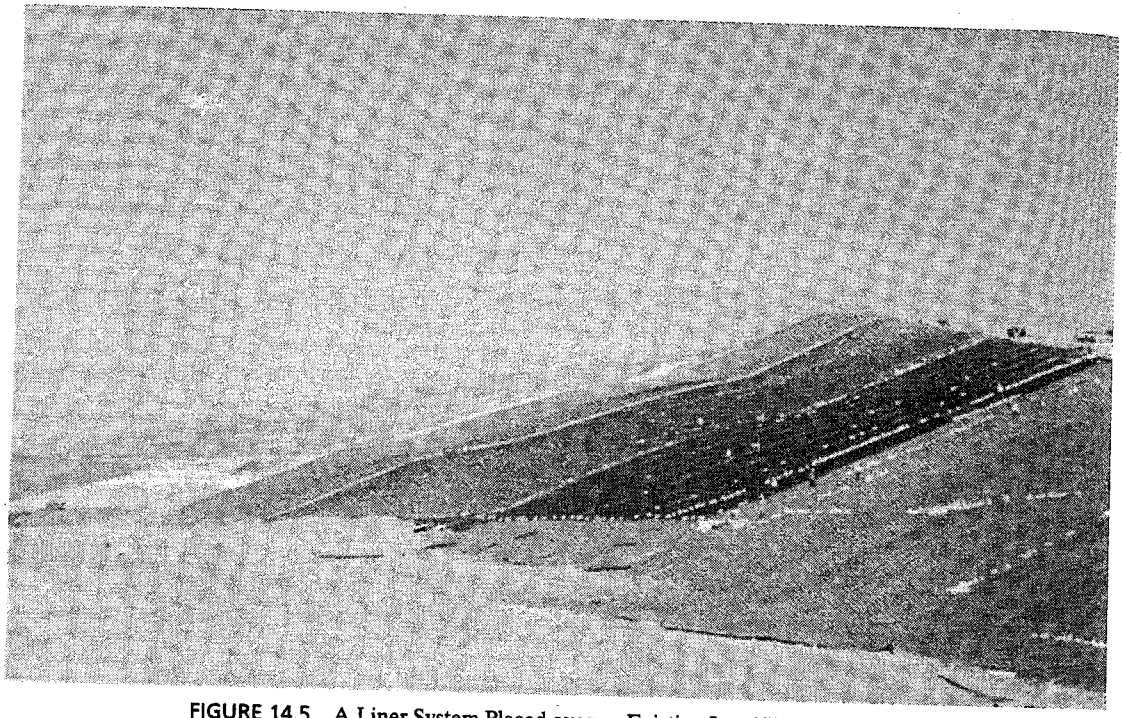

FIGURE 14.5 A Liner System Placed over an Existing Landfill for a Vertical Expansion Project

Figure 14.4. The geosynthetic reinforcement can prevent excessive tensile strain in the liner system over the existing landfill. Figure 14.5 shows a double composite liner system placed over an existing landfill for a vertical expansion project.

14.3 SETTLEMENT OF EXISTING LANDFILL

The area-wide (also the "total") settlement of waste when subjected to an increase in overburden pressure due to the vertical expansion is characterized by two components, a rapid primary settlement and a long-term, time-dependent secondary settlement. The primary and secondary settlements of the existing landfill due to the vertical expansion can be calculated by using the following equations from Chapter 12:

Primary Settlement of Existing Landfill

$$\Delta Z_c = C_c' \cdot H_o \cdot \log \frac{\sigma_o + \Delta\sigma}{\sigma_o} \tag{14.1}$$

where ΔZ_c = primary settlement of existing landfill;
H_o = initial thickness of the waste layer of the existing landfill;
C_c' = modified primary compression index. $C_c' = 0.17 \sim 0.36$;
σ_o = existing overburden pressure acting at the mid level of the waste layer;
$\Delta\sigma$ = increment of overburden pressure due to vertical expansion.

Secondary Settlement of Existing Landfill

$$\Delta Z_\alpha = C'_\alpha \cdot H_o \cdot \log \frac{t_2}{t_1} \tag{14.2}$$

where ΔZ_c = secondary settlement of existing landfill;
H_o = initial thickness of the waste layer before starting secondary settlement;
C'_α = modified secondary compression index. $C'_\alpha = 0.03 \sim 0.1$;
t_1 = starting time of the secondary settlement. It is assumed to be equal to the age of existing landfill for vertical expansion project;
t_2 = ending time of the secondary settlement.

Total Settlement of Existing Landfill

$$\Delta Z = \Delta Z_c + \Delta Z_\alpha \tag{14.3}$$

where ΔZ = total settlement of existing landfill;
ΔZ_c = primary settlement of existing landfill;
ΔZ_α = long-term secondary settlement of existing landfill.

The calculations should be performed at discrete points along several selected settlement lines over the existing landfill. At each point, the thickness of the existing waste in the existing landfill and the thickness of the proposed waste to be placed in the vertical expansion (i.e., the overburden pressure) can be estimated. As an example, see the cross-section, shown in Figure 14.6. The value of the total settlement at each point depends on both the thickness of the existing waste and the load due to the proposed waste fill.

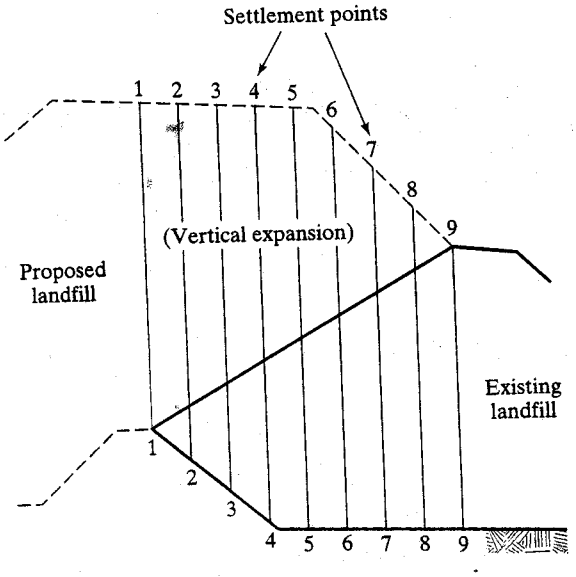

FIGURE 14.6 Cross Section of Existing and Proposed Landfills along Settlement Lines

14.4

The differential settlements resulting in tensile strains of liner system materials and leachate collection pipes over the existing landfill, and final grades between adjacent settlement points after settlement can be evaluated from the calculated values of the total settlements at various settlement points along each settlement line on the landfill subgrade.

The differential settlement between adjacent points can be calculated using the equation

$$\Delta Z_{i,i+1} = Z_{i+1} - Z_i \tag{14.4}$$

where $\Delta Z_{i,i+1}$ = differential settlement between points i and $i + 1$,
Z_i = total settlement of point i,
Z_{i+1} = total settlement of point $i + 1$.

14.4

The final slope angle between adjacent points after settlement can be calculated using the equation

$$\tan\beta_{Fnl} = \frac{X_{i,i+1} \cdot \tan\beta_{Int} - \Delta Z_{i,i+1}}{X_{i,i+1}} \tag{14.5}$$

where $X_{i,i+1}$ = horizontal distance between points i and $i + 1$,
$\Delta Z_{i,i+1}$ = differential settlement between points i and $i + 1$,
β_{Int} = initial slope angle between points i and $i + 1$,
β_{Fnl} = final slope angle between points i and $i + 1$ after settlement.

The landfill subgrade changes along each settlement line due to different settlements can be calculated from the preceding equation.

The tensile strains of the liner system and leachate collection system resulting from the settlements can be estimated using the equation

$$\varepsilon_{i,i+1} = \frac{(L_{i,i+1})_{Fnl} - (L_{i,i+1})_{Int}}{(L_{i,i+1})_{Int}} \times 100\% \tag{14.6}$$

where $\varepsilon_{i,i+1}$ = tensile strain in liner system between points i and $i + 1$,
$(L_{i,i+1})_{Int}$ = distance between points i and $i + 1$ in their initial positions,
$(L_{i,i+1})_{Fnl}$ = distance between points i and $i + 1$ in their post-settlement positions.

The distance between points i and $i + 1$ in their initial positions can be calculated using the equation

$$(L_{i,i+1})_{Int} = [(X_{i,i+1})^2 + (X_{i,i+1} \cdot \tan\beta_{Int})^2]^{1/2} \tag{14.7}$$

The distance between points i and $i + 1$ in their post-settlement positions can be calculated using the equation

$$(L_{i,i+1})_{Fnl} = [(X_{i,i+1})^2 + (X_{i,i+1} \cdot \tan\beta_{Int} - \Delta Z_{i,i+1})^2]^{1/2} \tag{14.8}$$

The maximum acceptable tensile strains (i.e., the elongations at yield) of various liner system and leachate collection system components can be obtained from the product specific laboratory testing.

14.4 ESTIMATION OF DIFFERENTIAL SETTLEMENT DUE TO WASTE HETEROGENEITY

An approach for analyzing the differential settlement at the surface of a liner system caused by the collapse of a void within an existing landfill is outlined in this section. On the basis of this analysis, a new design method is presented and described. Currently available methods to estimate "void-induced" differential settlements are first summarized briefly. One of these methods, which is based on an elastic solution, is further discussed and illustrated by an example.

14.4.1 Current Methods for Estimating Localized Subsidence

To the authors' knowledge there is no specific methodology used to quantify the settlement resulting from the presence of a void within a landfill. However, similar situations are often encountered in mining and other geotechnical applications (e.g., collapse of buried sinkholes). Several methods to analyze "void-induced" settlement have been developed and are documented in mining and geotechnical journals and conference proceedings. The following four methods of analysis are briefly summarized herein based on a review by Jang and Montero (1993):

Mining Subsidence Empirical Methods. A mechanism similar to the collapse of a large object within an existing landfill and the resulting differential settlement at the surface of a liner system exists in mining operations (Brauner, 1973; BNCB, 1975). Mining subsidence occurs in a bowl-shaped pattern. Empirical methods have been developed to analyze the subsidence of "long-wall" mines, an underground mining technique mainly used in rock formations. The method is applied to a specific geographical region and is uniquely based on the geological characteristics of the region. Because there is no generic solution available for all geographical regions, this method is not suitable for the analysis of differential settlement for a landfill in a vertical expansion configuration.

Numerical Methods. Finite element analyses of a void within a soil layer have been conducted in several research fields other than landfill engineering. Wang and Badie (1985) used a finite element analysis and a physical model to analyze the bearing capacity of a shallow footing above a void embedded in clay. The results of Wang's finite element analysis were confirmed by experimental model tests. Drumm et al. (1987) also used finite element analysis to evaluate the deformation of highly plastic soils in contact with cavitose bedrock. The calculated settlements were presented as a function of cavity size.

Displacement Method. "Closed-form" solutions for the strain field in an initially isotropic and homogeneous incompressible soil due to near-surface ground loss were presented by Sagaseta (1987). The differential settlement of a point on a plane is calculated in this method as a function of the displacement of other points. The applications of the closed-form solutions to some typical problems indicate that the calculated movements agree quite well with experimental observations and compare favorably with other commonly used numerical methods.

Elastic Solution. An analytical elastic method to evaluate settlements caused by voids at depth was presented by Tsur-Lavie et al. (1980, 1988). This method can be used to calculate the surface settlement as a function of the dimension of the void, thickness of medium (soil/rock) over the void, and Poisson's ratios. The method presented is based on a solution developed by Golecki (1978, 1979) for stresses and displacements in an infinite homogeneous elastic half space, with discontinuous step-like uniform boundary displacement representing the collapsing of a void. The displacement in the surrounding medium and the resulting differential settlement at the medium surface is then calculated by an elastic method. The results obtained from the analytical elastic method were compared with British National Coal Board (BNCB) mining subsidence field measurement data by Tsur-Lavie et al. and are in close agreement with one another.

Any of the methods discussed previously can be used to calculate differential settlements resulting from the existence of a void at depth. The numerical methods discussed (i.e., the finite element and finite difference methods), are suitable for the analysis of problems with nonhomogeneous, anisotropical materials. On the other hand, the displacement method and the elastic solution method require little or no material properties for the analysis, and therefore they can be applied quite readily to a vertical expansion design. Of these two methods, the elastic solution has several advantages. First, it has been calibrated by field measurements; second, it is amenable to sensitivity analyses based on different soil or waste characteristics. The elastic solution method is much easier to apply than the finite element analysis, and since it neglects arching in the waste, it is conservative.

The section that follows describes how Jang and Montero (1993) employed the elastic solution method developed by Tsur-Lavie et al. to analyze the effect of "void-induced" differential settlement on a liner system constructed underneath a proposed vertical expansion to an existing landfill.

14.4.2 Elastic Solution Method Applied to a Vertical Expansion

14.4.2.1 Differential Settlement Mechanism. Differential settlement in a vertical expansion liner system takes place when the surrounding waste in an existing landfill moves into the voids created by the degradation of a large object such as a large household appliance or unfilled box/container. A model was developed to analyze this mechanism and is shown in Figure 14.7 (Jang and Montero, 1993). In this model, soil and waste are represented by a half-space medium. Surface differential settlements in the model are influenced by the following factors:

(i) Engineering properties of the medium;
(ii) The thickness of the medium over the void, T;
(iii) The containment liner system grade, α;
(iv) The void size, length L_x × width L_y × depth D.

To quantify the influence of these factors on surface deformation, an influence function (Jang and Montero, 1993) is first developed. The differential settlement can then be calculated and evaluated with the influence function.

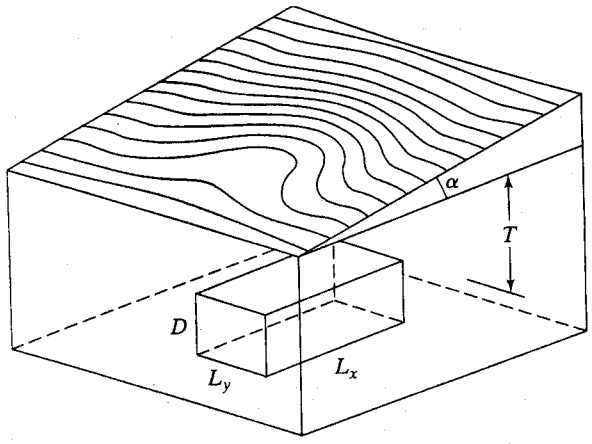

FIGURE 14.7 Differential Settlement Model—Three Dimensional Elastic Solution Model (Jang and Montero, 1993)

14.4.2.2 Approach. A computer program was developed to solve the three-dimensional equations presented in the analytical elasticity solution (Tsur-Lavie et al., 1988). This computer program evaluates the differential settlement caused by voids at depth. The input variables in the program consist of the following:

(i) The void size, defined by $L_x \times L_y \times D$;
(ii) The soil thickness T over the void; and
(iii) Poisson's ratio of the subsiding material.

The computer program was verified by comparing its output with the characteristic curves presented in the paper by Tsur-Lavie et al. (1988).

14.4.2.3 Assumptions. Three basic assumptions were made to model the deformation of a surface due to the presence of a void at depth. These assumptions are as follows:

(i) The liner surface is stress free;
(ii) Differential settlement on a horizontal plane is projected to a graded surface;
(iii) A constant Poisson's ratio.

For further discussion of each of these assumptions and their significance, see Jang and Montero (1993).

14.4.2.4 Example Calculation for the Design of a Sloped Liner System. As noted previously, evaluation of the surface deformation of a sloped liner surface requires an approximation that is made by projecting the differential settlements calculated on a horizontal surface to a sloped surface. This procedure results in a conservative approximation because the distance between the points along the sloping surface and the void are always greater than or equal to those in the horizontal case. Therefore, the differential settlements calculated in the sloped surface will be slightly higher than those in the horizontal case.

Design Problem. A landfill-buried void 3 ft (0.9 m) long by 3 ft (0.9 m) wide by 6 ft (1.8 m) deep is used in the analysis. These dimensions represent a typical household refrigerator—a large object likely to be disposed of at a sanitary landfill.

The analysis of a liner system sloping at a 7% grade is presented as an example (modified from Jang and Montero, 1993). The 7% sloping surface and soil/waste thicknesses of 6, 7.5, 9, and 12 ft (1.8, 2.25, 2.7, and 3.6 m) were analyzed over an area 21 ft (6.4 m) long by 21 ft (6.4 m) wide. The void is assumed to be located in the center of this area.

Presentation and Discussion of Results. In a contour plot, a contour line represents the same elevation along a line. A closed contour therefore indicates either a depression or a mound. The presence of closed contours representing a deep depression is an unacceptable condition in the design of a liner system.

The deformed surface elevations in each grid point are calculated by the computer program. The deformed surface contours on the 7% sloped surface are then plotted for each case, as shown in Figure 14.8 (Jang and Montero, 1993). Where the thickness of the soil/waste layer is 6 ft (1.8 m), as shown in Figure 14.8(a), the presence of the void will create a depression 0.3 ft (90 mm) deep. This depression could trap and accumulate liquids, hindering the free flow of leachate towards a collection point. When the thickness of the soil/waste layer above the void is increased to 7.5 ft (2.25 m), the depression is reduced to less than 0.1 ft (30 mm), as shown in Figure 14.8(b). With a 9-ft- (2.7-m)-thick soil/waste layer over the void, the depression disappears. The disturbance in the liner surface decreases as the depth to the void increases, as seen when the thickness of the soil/waste layer is increased to 12 ft (3.6 m) [Figure 14.8(c) and Figure 14.8(d)].

To evaluate the potential for grade reversal, a characteristic curve of required soil waste thicknesses, T, over a 3-ft- (0.9-m)-deep by 6-ft- (1.8-m)-long void versus liner surface grades, α, is illustrated in Figure 14.9.

For each analysis, the tensile strains were calculated from the deformed spacing between adjacent grid points in the surface against the initial grid spacing. A characteristic curve of the maximum tensile strains versus ratio of void width L_y to controlled fill thickness T was developed from the analyses' results. This curve is presented in Figure 14.10.

The maximum tensile strain generated by the differential settlements was examined to evaluate the integrity of a composite liner, which included a geomembrane and a clay layer (see Figure 14.10). The geomembrane can sustain tensile strains higher than those that the clay component of the composite liner can sustain before tensile failure or tension cracks develop within the clay component. Therefore, the tensile strain limit of the clay component can be used as an acceptable design criterion to evaluate the integrity of composite liners.

From the maximum tensile strains versus soil/waste thickness (T) curve, a soil layer thickness T equal to 9 ft (2.7 m), the maximum tensile strain caused by the 3-ft-(0.9-m)-wide by 3-ft- (0.9-m)-deep by 6-ft- (1.8-m)-long void is 0.2%. This strain is within acceptable limits for a clay layer as shown in Figure 14.11 (after Gilbert and Murphy, 1987).

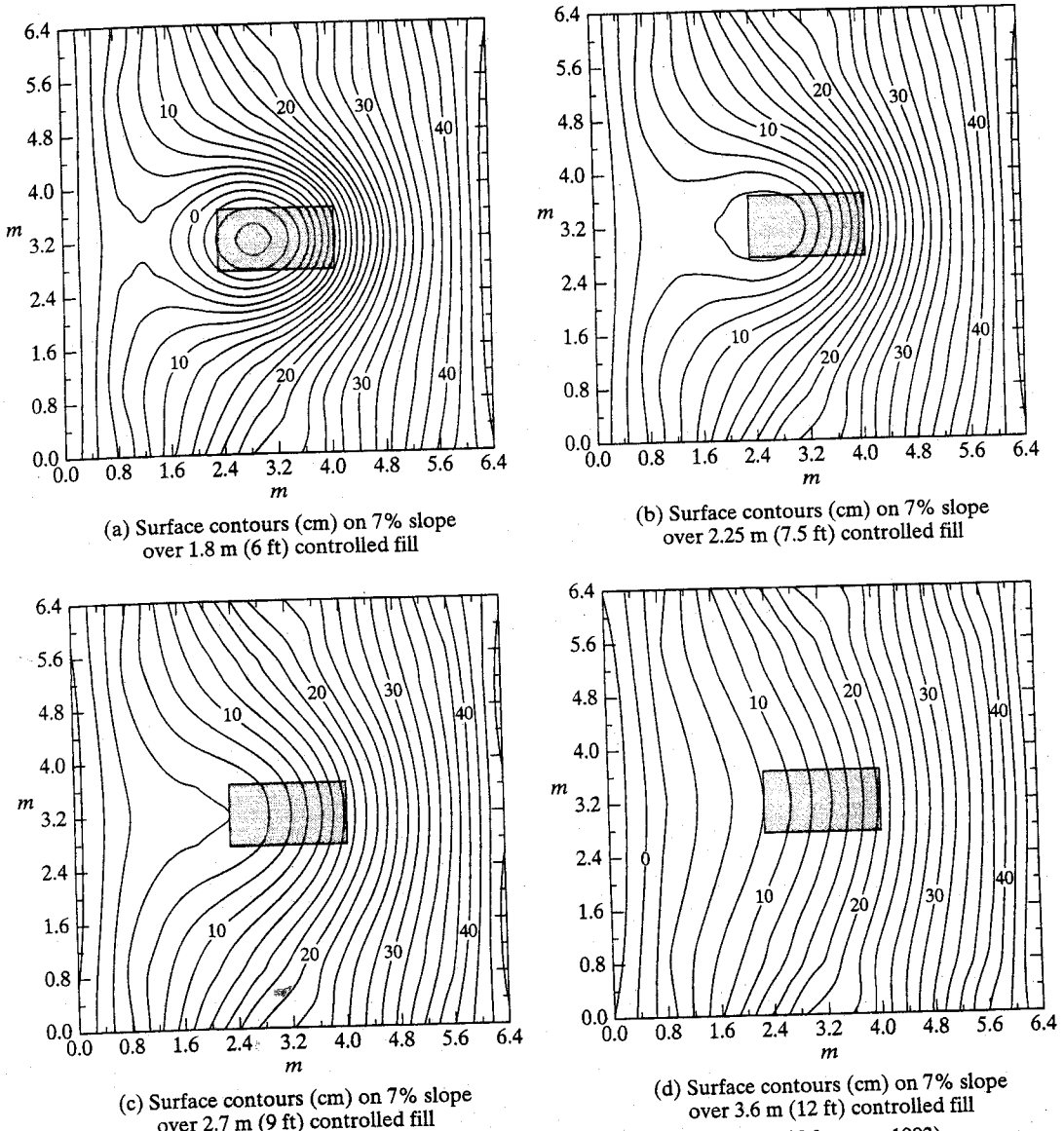

(a) Surface contours (cm) on 7% slope over 1.8 m (6 ft) controlled fill

(b) Surface contours (cm) on 7% slope over 2.25 m (7.5 ft) controlled fill

(c) Surface contours (cm) on 7% slope over 2.7 m (9 ft) controlled fill

(d) Surface contours (cm) on 7% slope over 3.6 m (12 ft) controlled fill

FIGURE 14.8 Deformed Contours on a 7% Sloping Surface (Jang and Montero, 1993)

On the basis of the above example analysis, a 2.7-m- (9-ft)-thick soil/waste layer can serve as a strain transition zone to prevent grade reversal, excessive tensile strains and stresses from developing in a liner system. Therefore, a 9-ft- (2.7-m)-thick layer of soil or "selected" waste should be placed, in this example, before constructing the vertical landfill containment liner.

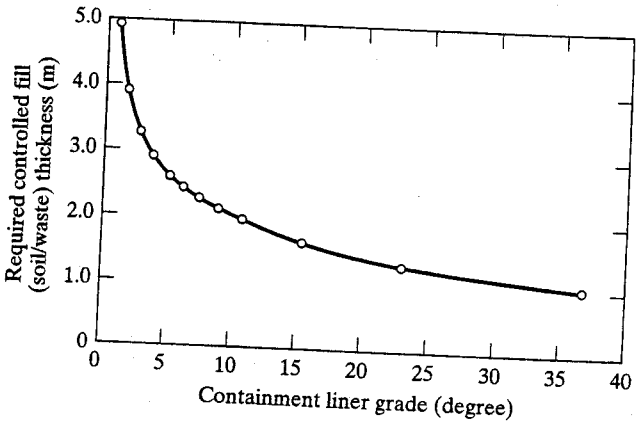

FIGURE 14.9 Required Controlled Fill Thickness to prevent Grade Reversal, T, versus Containment Liner Grade, α, on 0.9 m × 0.9 m × 1.8 m (3 *ft* × 3 *ft* × 6 *ft*) Void (Jang and Montero, 1993)

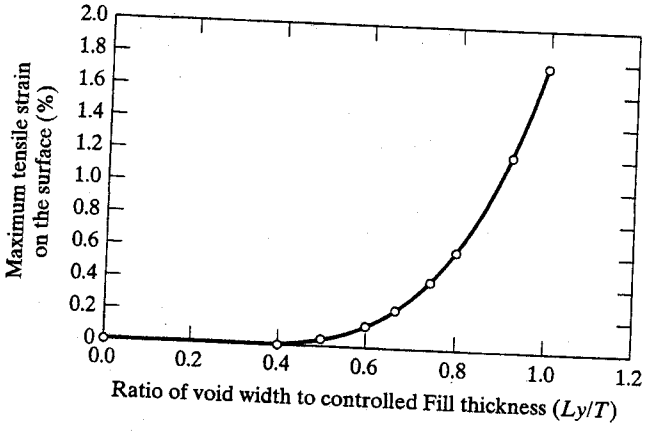

FIGURE 14.10 Maximum Tensile Strain versus Ratio of Void Width to Controlled Fill Thickness on 0.9 m × 0.9 m × 1.8 m (3 *ft* × 3 *ft* × 6 *ft*) Void (Jang and Montero, 1993)

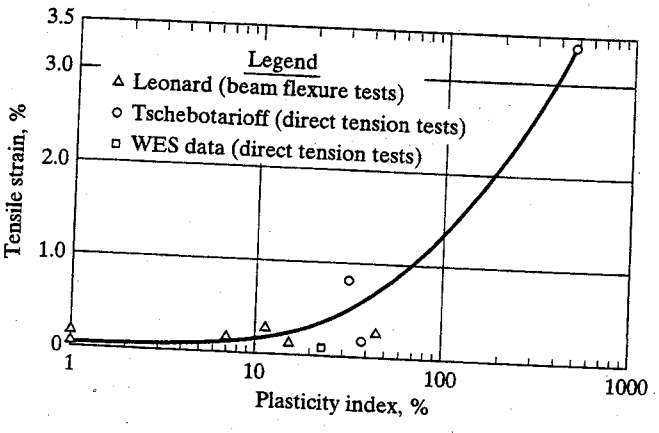

FIGURE 14.11 Tensile Strain versus Plasticity Index (Gilbert and Murphy, 1987)

For slope angles other than the 7% used in the example analysis, the tensile strains and potential for grade reversal on a liner surface can be evaluated (Jang and Montero, 1993) according to the thickness versus maximum tensile strain and thickness versus liner grade characteristic curves, settlement contours and containment liner design criteria. From this evaluation, the required backfill thicknesses in different liner grades and liner systems can be determined and designed to prevent grade reversal and excessive tensile strains on a vertical expansion liner and leachate collection system.

14.5 VERTICAL EXPANSION OVER UNLINED LANDFILLS

The moisture content of solid waste placed in landfills located in semiarid or arid areas are generally below field capacity. In this case leachate will not be released from the waste to impact underlying groundwater even though some of these old landfills lack liners. On the other hand, if the waste is compressed sufficiently, its available moisture-holding capacity will decrease and its moisture content may eventually reach field capacity. In this case, additional compression beyond this point will squeeze leachate from the waste (Zornberg et al., 2000). If a vertical expansion is planned over an unlined landfill located in a semiarid or arid area, a key consideration is to determine the minimum allowable compressed waste thickness beneath the vertical expansion portion of the landfill. This minimum thickness corresponds to a waste saturation or water content at which leachate stored within old waste in an existing unlined landfill can be released upon further compression.

Zornberg et al. (2000) developed a method to estimate the minimum allowable waste thickness without releasing leachate stored within the waste for a 60-m unlined landfill located in southern California. The field capacity, in-situ moisture content, and unit weight profiles of the waste in this selected landfill were all determined by lab and field testing techniques. These experimental data were used to evaluate the ability of the landfill to continue retaining moisture after additional waste placement. Analysis of their data indicated that if the final waste filling depth is kept below the calculated minimum allowable waste thickness, which ranged from 97 m to 109 m, the moisture content of the waste will not reach its field capacity. Therefore, the leachate should still remain within the waste mass and not impact the groundwater after vertical expansion. Details of the analysis procedures can be found in Zornberg et al. (2000).

14.6 DESIGN CONSIDERATIONS FOR LANDFILL STRUCTURES

If the existing landfill has leachate and gas collection systems, it is necessary to evaluate the effects of the vertical expansion on the operational condition of the leachate and gas collection systems of the existing landfill. Large settlements and differential settlements in the existing landfill may cause large deformation or failure of the gas exaction wells and gas collection header pipes of the gas collection system. The pipe deflection and pipe wall bucking of both leachate and gas collection pipes in the existing landfill must be recalculated by adding the extra load caused by the vertical expansion.

The total settlement of the existing landfill subgrade including elastic, primary and secondary settlements must be estimated again by considering the effect of the vertical expansion. The vertical effective load used to calculate the elastic and primary settlement should be equal to the sum of the existing and extra waste filling. Equations 12.19, 12.21, 12.22, and 12.23 can be used to calculate the elastic, primary, secondary, and total settlements, respectively. The final differential settlement, subgrade changes, and tensile strains of liner system and leachate collection system resulting from the settlements should be carefully estimated using Equations 14.4, 14.5, and 14.6, respectively. Grade reversal and ponding of the bottom liner of the existing landfill is not allowable after vertical expansion.

The landfill structures that may be affected by vertical expansion include the following:

(i) Existing and new liner systems,
(ii) Existing and new leachate collection and detection systems,
(iii) Existing gas collection system,
(iv) Existing waste mass,
(v) Foundation of existing waste mass,
(vi) Existing and new final cover systems, and
(vii) Underdrain system.

The structural considerations that affect the design of a vertical expansion landfill are summarized in Table 14.1:

14.7 GEOSYNTHETIC REINFORCEMENT DESIGN FOR VERTICAL EXPANSIONS

Presently, two methods are being applied to liner systems to minimize the deformation of a liner and leachate collection system constructed between an existing landfill and a proposed vertical expansion. These methods consist of either reinforcing the liner system with a geogrid or high strength geotextile or evaluating the potential differential settlement caused by a void within an existing landfill and allowing the liner system to deform. In the latter method, a required backfill thickness adjustment is calculated to prevent grade reversal and excessive tensile strains on a vertical expansion liner and leachate collection system. The design procedure for reinforcing the liner system with a geosynthetic will be described in this section. The next section describes how to use an elastic solution model to evaluate the potential differential settlement caused by a void within an existing landfill and how to determine the required backfill thickness adjustment to prevent grade reversal.

Liners and collection systems overlying existing landfill areas may require some type of reinforcement. The purpose of the reinforcement is to minimize the tensile strains in the overlying liner and leachate collection systems assuming that a void occurs. Voids are created by progressive degradation and collapse of large objects buried in the old landfill areas.

TABLE 14.1 Structural Considerations for Vertical Expansions

Structure	Design Considerations
Liner [geomembrane, compacted clay liner (NR), and geosynthetic clay liner]	• Tensile strain of new liners over the existing waste, • Stability of new liner system over the existing waste, • Slope changes of the existing liner system.
Pipe (leachate, riser, gas, and underdrain pipes)	• Strength and stability (bucking, crushing, and deflection), • Slope changes.
Geosynthetic Drainage Layer (geocomposite and geonet used in the existing leachate collection and detection system and underdrain system)	• Drainage capacity of geonet and geocomposite will be reduced due to extra waste fill.
Vertical Structures in the Existing Landfill (manholes, riser pipes and gas extraction pipes)	• Negative skin friction force due to waste settlement, • Bearing capacity and stability of the vertical manhole and riser pipe foundations due to negative skin friction force and extra waste fill.
Final Cover [geomembrane, compacted clay liner (NR), and geosynthetic clay liner]	• Tensile strain for the elements of the existing landfill cover caused by the extra settlement of the existing waste due to the extra waste fill, • Stability of new final cover.
Landfill Subgrade	• Subgrade changes of the existing landfill caused by foundation soil settlement due to extra waste fill, • Subgrade changes of the new landfill cause by the settlement of the existing waste.
Landfill and Foundation Stability	• Stability of the existing waste during the new waste filling, • Stability of the soil foundation due to extra loading, • Stability of combination of the existing and new landfills in various conditions.

NR = not recommended for liner systems of vertical expansions

Geogrid reinforcement is often used in vertical landfill expansion on the top of existing landfills (Figure 14.4), although high-strength geotextiles can function in this application as well. The design of the geosynthetic reinforcement is based on a worst-case scenario assumption that a void is located immediately underneath the liner. The liner is then treated as a plate bridging over the void and carrying the load from the proposed overlying waste. Geosynthetics are placed to support and protect the integrity of the liner system. The design methodology used in geosynthetic reinforcement is based on the tensioned membrane theory. When differential settlement takes place, the geosynthetic deflects into the depression as tensile stresses develop in the reinforced material.

The use of uniaxially oriented, high polyethylene (HDPE) geogrids to support a landfill lining for a vertical expansion and cover system over either a circular or a long narrow depression is described in a stepwise fashion as follows (modified from TENSAR, 1989). A similar approach is used with high-strength geotextiles as well as with other types of geogrids.

14.7.1 Theoretical Background for Geosynthetic Reinforcement

When a depression forms below a layer of geosynthetic reinforcement supporting a landfill lining or cover system, the reinforcement deflects into the depression. This deflection has two effects: bending of the fill materials overlying the reinforcement; and tensioning of the reinforcement (Figure 14.12). The bending of the fill materials generates arching inside the material, which transfers part of the applied load away from the depression. As a result, the vertical stress, σ_{v1}, acting on the reinforcement over the depression is smaller than the vertical stress, σ_{v2}, due to the applied load, which is equal to the weight of the overlying fill materials plus any applied surcharge, q, as shown in Figure 14.12(b). The tensioning of the reinforcement mobilizes a portion of the materials' tensile strength [Figure 14.12(a)]. As a result, the reinforcement acts as a "tensioned membrane" and normally can carry a load applied to the surface. The reinforcement will deflect until the resistance generated by arching of the fill materials and tensioning of the reinforcement balances the applied load.

The method described herein for the design of a geosynthetic to support a landfill lining system was developed by combining arching theory for the fill materials overlying the reinforcement with tensioned membrane theory for the reinforcement. This method has been successively developed by Giroud (1982), Bonaparte and Berg (1987a), and Giroud et al. (1988).

14.7

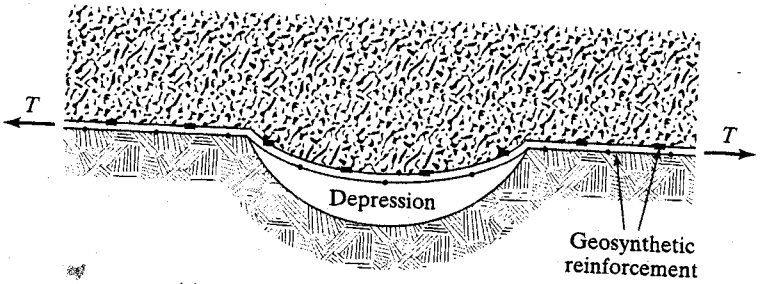

(a) Arching of fill material and tensioning of geosynthetic reinforcement

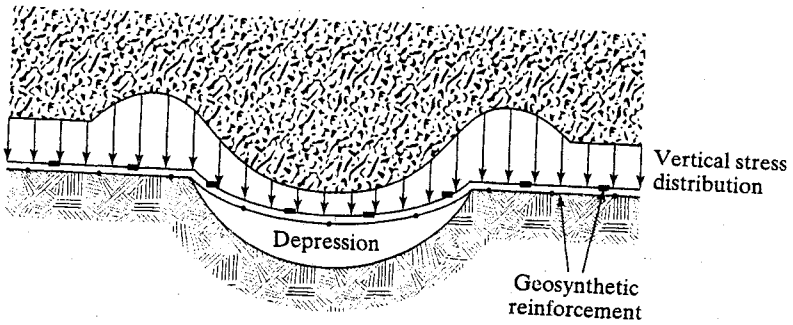

(b) Effect of fill material arching on vertical stress distribution

FIGURE 14.12 Load Carrying Mechanism (after TENSAR, 1989)

Arching of the materials overlying a layer of geosynthetic is dependent on the effective stress friction angles of the materials, the thickness of the materials, and the size of the depression. Materials with effective stress friction angles less than 25° may not develop a significant arch; therefore, it is assumed that the minimum effective stress friction angle of the materials overlying the geosynthetic is at least 25°. Arching will not be fully developed unless the total thickness of the materials overlying the geosynthetic is approximately six times greater than the radius of a circular depression or the half-width of a long, narrow depression. This approximation is for soils, whereas it is felt that the value is lower for municipal solid waste. The exact value awaits further investigation. Because of this, arching is usually developed in the materials above the reinforcement supporting a landfill lining system, but it is usually not developed above the reinforcement supporting a cover system if the size of the depression is greater than one-sixth of the thickness of the cover system.

14.7.2 Assumptions for Geosynthetic Reinforcement Design

The step-by-step design method described herein is directly applicable to geogrid or high strength geotextile support of lining systems under the following assumptions:

(i) The cross-section of the depression is circular. (Long and narrow depressions are addressed in Section 14.7.9.)

(ii) The depression is spanned by two layers of uniaxially oriented geogrid placed in perpendicular directions or by a geogrid or geotextile with equal tensile properties in its machine and cross directions wherein seam strength could well be the limiting parameter.

(iii) The depth of the depression is equal to or greater than the deflection of the reinforcement (i.e., none of the pressure on the reinforcement over the depression is transferred to the bottom of the depression).

(iv) Surcharge loads act uniformly on top of the waste placed above the lining system.

(v) Uniform material properties exist within each distinct zone (soil components of the lining or cover system, and waste placed above the lining system).

(vi) The soil components of the lining or cover system and the waste placed above the lining system have a minimum effective stress friction angle of 25° and effective stress cohesion of zero.

(vii) The bedding soil, if placed above the reinforcement is a granular soil with a minimum effective stress friction angle of 25° and effective stress cohesion of zero.

(viii) There are no hydrostatic (static or excess pore water) pressures within the lining system.

(ix) The long-term (e.g., 120 years) stress-strain characteristics of the reinforcement are accurately defined.

(x) The geogrids interlock with the bedding soil or the friction of the geotextile is adequate to mobilize the stresses that are generated.

(xi) Arching of the fill materials directly above the reinforcement is not affected by the synthetic components of the lining or cover system (i.e., geomembrane, geonet, and geotextile).

14.7.3 Selection of Material Properties

This design method (modified from TENSAR, 1989) assumes that the minimum effective stress friction angle of waste (for design of lining system support), soil components of lining and cover systems, and bedding soil is 25°. As shown in Table 14.2, this assumption is met by most soils. The equations given subsequently in this section were derived by Giroud et al. (1988) and incorporate a minimum effective stress friction angle of 20°. Accordingly, to be conservative, a minimum value of 25° has been recommended.

Bedding Soil. The bedding soil placed above or below the reinforcement is typically a well-compacted sandy soil. The moist unit weight of the bedding soil, γ_b (lb/ft^3 or kN/m^3), and the effective stress friction angle, ϕ'_b (degrees), should be measured or estimated using correlations with published values. For preliminary design purposes, assume that the moist unit weight of the bedding soil is 120 lb/ft^3 (19 kN/m^3) and the effective stress friction angle is at least 25° (see Table 14.2). However, these assumed values should be verified prior to final design.

Municipal Solid Waste. The moist unit weight, γ_{sw} (lb/ft^3 or kN/m^3), and the effective stress friction angle, ϕ'_{sw} (degrees), of the material contained above the lining system should be measured or estimated. The discussion below assumes that this material is municipal solid waste (MSW). For preliminary design purpose, assume that the average moist unit weight of the municipal solid waste (including daily cover) is 60 lb/ft^3 (9.4 kN/m^3) and the effective stress friction angle of the municipal solid waste is at least 25°. However, it is important that a site-specific evaluation of these properties be made. The project engineer should verify the values of ϕ'_{sw} and γ_{sw} used in the final design.

Lining Components. The lining components can consist of geomembranes, geosynthetic clay layers, geonet drainage layers, granular drainage layers, geotextiles, and protective soil cover layers. The material properties of the lining system that must be determined are the moist unit weights of soil components (e.g., granular drainage layers), γ_l (lb/ft^3 or kN/m^3), the effective stress friction angles of the soil components of the lining system, ϕ'_l (degrees), and the minimum yield strain, ε_y, of the lining system components.

TABLE 14.2 Representative Range of Effective Stress Friction Angle Values (Bowles, 1982)

Soil	Effective Stress Friction Angle
Gravel	
Medium Size	40° to 50°
Sandy	35° to 50°
Sand	
Loose Dry	28° to 35°
Dense Dry	35° to 46°
Silt or Silt sand	
Loose	27° to 30°
Dense	30° to 35°
Clay	20° to 30°

The moist unit weight of the soil components must be determined so that overburden stress on the reinforcement due to the lining system can be calculated. For preliminary design purposes, the moist unit weight of the soil component can be taken as 120 lb/ft^3 (19 kN/m^3), and the effective stress friction angle of the soil components of the lining system can be assumed to be at least 25°. (See Table 14.2.) However, the designer should verify these values prior to final design.

The minimum yield strain, ε_y, of the lining system components must be determined so that the allowable strain of the lining system, ε_l, can be calculated. The minimum yield strain of a lining system will be the yield strain of the compacted clay component, if one is present. Otherwise, the yield strain of the geomembrane or GCL is likely to be critical. In any event, the yield strains of all components should be considered. For HDPE geomembranes, an acceptable yield strain for preliminary design is 10%. This criterion is also applicable to polyester geogrids and geotextiles, and to polypropylene geotextiles. A factor of safety is applied to this value to calculate the allowable strain. (See discussion in Section 14.7.5.) The actual yield strain of the geosynthetic should be verified prior to the final design.

14.7.4 Determination of Geometric and Loading Parameters

Geometric Parameters. Simplified geometrical models for a geosynthetic supporting a lining system spanning a depression are shown in Figure 14.13. All the geometrical parameters shown must be defined to determine the required long-term reinforcement

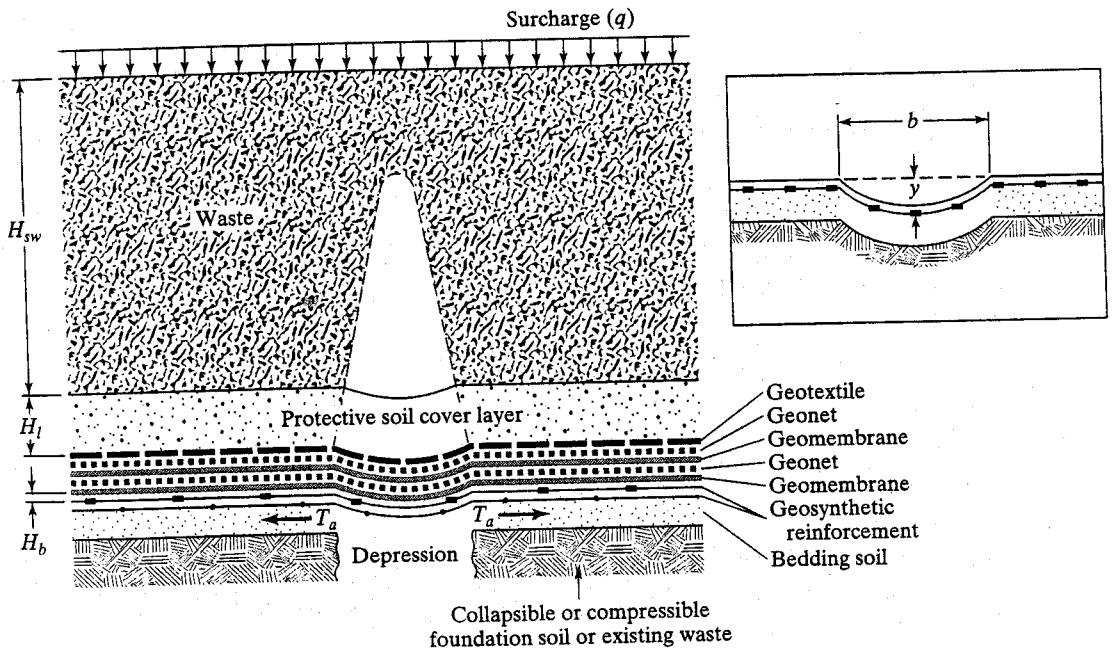

FIGURE 14.13 Simplified Model for Analysis of Stresses in Geosynthetic Reinforcement Supporting a Landfill Lining System Spanning a Depression (TENSAR, 1989)
(Note: Only deflected portion of fill materials exerts pressure on the reinforcement)

tensile load. Selection of the radius of the design depression, r (ft or m), and the allowable deflection of the geogrids, y (ft or m), are discussed in Section 14.7.5.

Loading Parameters. A uniformly distributed surcharge, q (lb/ft^2 or kN/m^2), may be incorporated into the design. This surcharge load is assumed to act on top of the waste contained above the lining system or on top of the cover system. 14.7.6

14.7.5 Design Criteria

Criteria to be used in designing the lining system must be specified. These include such considerations as the size of the depression, allowable deflection into the depression, and factor of safety. These are described next.

Size of Depression. The lining system underlying the reinforcement is assumed to rest initially on a firm subgrade. At some point in time, a circular depression of radius, r (ft or m), is assumed to develop directly below the support. (Long, narrow depressions are addressed in Section 14.7.9.) Subsidence of the underlying subgrade is assumed to be caused by localized collapse of the subgrade soil into depression below the support. Conditions causing subsidence include collapse of a karstic subgrade beneath a lining system or collapse of waste with large voids, such as barrels, household appliances, or furniture, beneath a lining or cover system. The "rusted refrigerator" assumption is commonly used to analyze lining and cover systems placed over municipal solid waste. For this case, the design depression is usually assumed to have a radius of 3 ft (0.9 m), which is the approximate radius of the depression created by a refrigerator that rusts and collapses in the underlying subgrade. 14.7.7

Allowable Deflection. The allowable deflection into a depression, y (ft or m), of the reinforcement is governed by the following criteria:

(i) Allowable strain of the lining system components (discussed in Section 14.7.3) and allowable strain of the reinforcement (discussed in Section 14.7.6).

(ii) Allowable depth of ponding of liquid in the lining system.

Strain Criteria: The reinforcement must be designed to support the lining system at a strain less than or equal to the allowable strain of the system, ε_l. (The allowable strain of a lining or cover system is equal to the minimum yield strain of the system, ε_y, divided by a factor of safety against rupture, F_R, as described in this section and given by Equation 14.11.) The reinforcement must also be designed to function at a strain less than its allowable strain, ε_g (Section 14.7.6).

Drainage Criteria: The deflection into a depression of the drainage layer of a lining system could impede drainage. The change in slope of a lining system drainage layer is dependent not only on the vertical deflection and radius of the depression, but also on the initial slope of the drainage layer. Furthermore, the effect of a depression on the hydraulic performance of a lining system is dependent on the allowable design head for that system. The designer should consider the drainage criterion once specific information regarding drainage layer slopes and allowable hydraulic heads are available.

Factor of Safety. A factor of safety F_R against rupture is incorporated into the design and applied both to the minimum long-term yield strain ε_y of the lining or cover system

and to the rupture strain ε_r of the reinforcement. A factor of safety against yield or rupture of 1.5 is recommended.

14.7.6 Selection of Allowable Reinforcement Strain

The material properties of the reinforcement that should be determined are the allowable strain of the material, ε_g, and the long-term allowable design tensile load of the material, T_a. The selection of the allowable strain is discussed in this subsection; the long-term allowable design tensile load is discussed next in Section 14.7.7.

The allowable strain of geosynthetic reinforcement is equal to the rupture strain of the material divided by a factor of safety against rupture, F_R. Wrigley (1987) reported rupture strain values, ε_r, for HDPE geogrids of at least 15%. Since a factor of safety against rupture of 1.5 is recommended here (Section 14.7.5), the calculated allowable strain, ε_g, of HDPE geogrids is at least 10%, because of the following relationship:

$$\varepsilon_g = \varepsilon_r / F_R \tag{14.9}$$

For this method, the allowable strain of HDPE geogrids is conservatively set at $\varepsilon_g = 10\%$. This agrees very well with polyester geogrids and polyester geotextiles. Thus, a 10% strain criterion can be used for all types of currently available geosynthetic reinforcement materials.

14.7.7 Selection of Long Term Allowable Design Tensile Load

Methodology. The short-term, wide-width tensile strength is readily available for all types of geosynthetic reinforcement. It is performed using the ASTM D4595 testing procedure. The maximum stress is referred to as the ultimate strength, or "T_{ult}". In order to obtain the long-term allowable tensile strength, "T_{allow}", the ultimate value must be modified using reduction factors. Typically, these reduction factors are established for creep, installation damage, and chemical/biological degradation. The formulation is given by Equation 14.10 as.

$$T_{allow} = \frac{T_{ult}}{RF_{CR} \times RF_{ID} \times RF_{CBD}} \tag{14.10}$$

where T_{allow} = long-term allowable design tensile load (lb/ft or kN/m);
T_{ult} = short-term ultimate load from tensile tests (lb/ft or kN/m);
RF_{CR} = reduction factor which accounts for creep;
RF_{ID} = reduction factor which accounts for installation damage.
RF_{CBD} = reduction factor which accounts for chemical/biological degradation;

Other reduction factors (e.g., to account for seams or holes) can be included on a site-specific and product-specific basis. Some discussion on the various reduction factors follows. For additional commentary, see Koerner (1998).

Long Term Deformation (Creep). Since the wide width test is conducted quickly in comparison to field situations, a reduction factor for long-term creep is necessary. The customary procedure is covered in ASTM D5262. The tests usually take 10,000 hours

TABLE 14.5 Assumed Properties of Candidate Reinforcement Products

Product	T_{ult}		Reduction Factors			T_{allow}	
	lb/ft	kN/m	RF_{CR}	RF_{CR}	RF_{ID}	lb/ft	kN/m
GG1	3,300	48	2.5	1.1	1.2	1,000	15
GG2	4,860	71	2.0	1.1	1.3	1,700	25
GG3	8,460	123	2.5	1.1	1.3	2,350	34

14.8 STABILITY ANALYSIS FOR VERTICAL EXPANSIONS

The stability of the whole landfill including both the existing and new filling portions should be evaluated by performing slope stability analyses for conditions in effect at different stages of construction and operation of the facility. The analyses should address the following conditions:

(i) Stability of the soil mass of the side slopes during excavation (during excavation condition).

(ii) Stability of the liner system of the vertical expansion portion on the side slopes prior to waste placement (post construction condition).

(iii) Stability of the proposed new portion during waste placement (interim configuration or during filling condition).

(iv) Stability of the proposed new portion after filling when the landfill is in its final configuration. The evaluation of final configuration stability considering potential slip surface through the waste mass, along liner system interface, and through the landfill foundation (final configuration or post filling condition).

(v) Stability of the final cover system (after closure condition).

The slope stability analysis methods for these conditions have been described in detail in Chapter 13. Values of the factor of safety of at least 1.5 are generally accepted by regulatory agencies as representing a long-term stable condition.

Experience has shown that potential slip surfaces in landfills having the lowest factors of safety are often along soil-geosynthetic or geosynthetic-geosynthetic interfaces within the liner system and cover system. Therefore, shear strength parameters for interfaces within the following systems are required for slope stability analyses:

(i) Liner system over natural ground;

(ii) Liner system on landfill side slope;

(iii) Liner system in the portions of the landfill that have previously been constructed;

(iv) Final cover system.

Each system contains several interfaces and materials along which (or in which) shear failure could potentially occur. The shear strength of each system is characterized by the shear parameters of the weakest material or interface in the system. These

parameters are called the *critical shear strength* parameters. In addition, evaluation of the shear strength parameters for the waste itself are required to perform slope stability analyses for final and interim landfill configurations.

Municipal solid waste usually settles a considerable amount during the filling operation (recall Figure 12.1). Here it can be seen that municipal solid waste landfills settle approximately 10 to 30% of their initial height. The large settlement of the waste fill induces shear stresses in the liner system on the side slope, which tends to displace the liner downslope. The large settlement of the waste fill and the large deformation of the landfill cover tend to induce shear stresses in the final cover system. These shear stresses induce large shear displacements along specific interfaces in the liner and cover systems that may lead to the mobilization of a reduced or residual interface strength. In addition, thermal expansion and contraction of the side slope liner and cover systems during construction and filling may also contribute to the accumulation of shear displacements and the mobilization of a residual interface strength (Qian, 1994; Stark and Poeppel, 1994; Qian, 1996).

A landfill should be designed for long-term performance. Accordingly, landfill safety should be considered not only during the relatively brief construction and operation periods, but also during a closure period lasting potentially hundreds of years. The potential for development of other uses for closed landfills should be also considered. Therefore, residual interface strengths should be assessed and considered for all side slopes for design purposes to make a landfill stable and safe even after being subjected to large settlements.

PROBLEMS

14.1 What are advantages of a vertical landfill expansion?

14.2 Explain why a vertical landfill expansion project is more complicated than a normal landfill project.

14.3 What are main considerations for design of a vertical landfill expansion? What are the principal differences compared to the design of a normal landfill?

14.4 What type of liner system would you select over an existing landfill for a vertical expansion project? Explain the reasons for your selection.

14.5 What two types of differential settlement should be considered during design of a vertical landfill expansion? What causes these two types of differential settlement?

14.6 Explain how to minimize differential settlement caused by waste heterogeneity without having to reinforce the liner.

14.7 List the internal landfill structures that may be impacted by vertical landfill expansion. Explain what causes these impacts.

14.8 How can a liner system be designed to minimize potential damage to a liner and leachate collection system constructed over an existing landfill?

14.9 What assumptions are used for designing geogrids or high strength geotextiles to reinforce a liner system over an existing landfill?

14.10 Explain what are the design criteria for using geogrids or high strength geotextiles to reinforce the liner system over an existing landfill?

14.11 How many different conditions should be considered for stability analysis of proposed vertical expansion designs?